

IN-PLANE SHEAR PERFORMANCE OF PARTIALLY
GROUTED MASONRY SHEAR WALLS

By

SHAWN MARK NOLPH

A thesis submitted in partial fulfillment of
the requirements for the degree of

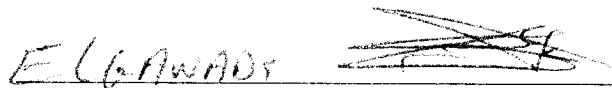
MASTERS IN SCIENCE IN CIVIL ENGINEERING

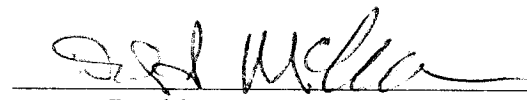
WASHINGTON STATE UNIVERSITY
Department of Civil and Environmental Engineering

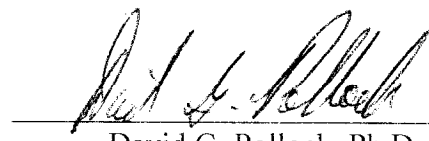
AUGUST 2010

To the Faculty of Washington State University:

The members of the Committee appointed to examine the thesis of SHAWN MARK NOLPH find it satisfactory and recommend that it be accepted.


Mohamed ElGawady, Ph.D., Chair


David I. McLean, Ph.D.


David G. Pollock, Ph.D.

ACKNOWLEDGEMENTS

I would like to offer my sincere thanks to Dr. Mohamed ElGawady for serving as chair of my committee. Your guidance and patience is greatly appreciated. Thank you Dr. David McLean and Dr. David Pollock for serving on my committee. My sincere thanks to the National Concrete Masonry Association, the Northwest Concrete Masonry Association, and the Eastern Washington Masonry Promotion Group for funding.

Thank you Bob Duncan and Scott Lewis, your advice and help were essential throughout this endeavor. Thank you Christophe de Vial for help over several very long and late nights at the lab testing specimens. Tim Vaughan, Jon Thomle, Jamal Elmapruk, and Dr. Dan Dolan - thank you for the help in the lab. Thank you Haitham Mousad for modeling help in SAP. Thank you Lola Gillespie, Cyndi Whitmore, Vicki Ruddick, Glenda Rogers, and Maureen Clausen for making my time in grad school run much smoother than it would have otherwise.

Thank you Jenny Howell, Natalie Vander Hulst, Erika Kemp, Garth Nelson, Ann Summerson, and the crew at Concordia Lutheran LSF for helping me keep some perspective. A very special thank you goes to Nicolle Bladow for lessons on what is truly important in life and the perspective that comes with that knowledge - you are a very special lady and will always have a place in my heart and prayers. Loving thanks are due Aziza Talia Dar, Mighty Charming, and Ilumanora - there is no better reminder that there *is* life outside of grad school than the wonderful company of an Arabian horse!

Last, and most importantly, I would like to thank my family. Without their support I would not have been able to pursue this endeavor and I certainly would not have made it through grad school. Dad - thank you for far more than I can ever express, I wish you had been able to see me finish. Mom and Karl - thank you for the incredible support.

IN-PLANE SHEAR PERFORMANCE OF PARTIALLY GROUTED MASONRY SHEAR WALLS

Abstract

by Shawn Mark Nolph, M.S.
Washington State University
August 2010

Committee Chair: Mohamed ElGawady

This research investigated the effectiveness of the current MSJC (2008) Strength Design shear strength equations for predicting the shear strength of partially grouted masonry walls. Six concrete masonry walls, five partially grouted and one fully grouted, were constructed and subjected to in-plane cyclical loading using a displacement based protocol. Variables investigated included grout horizontal spacing and horizontal (shear) reinforcement ratio. The effects of grout horizontal spacing and horizontal reinforcement ratio were analyzed.

The MSJC (2008) shear equations were found to significantly overestimate the shear strength of specimens with 48 in (1219 mm) grout horizontal spacing (errors between -16% to -43%) and the fully grouted specimen (error of -34%). Specimens with 32 in. (813 mm) and 24 in. (610 mm) grout horizontal spacing were predicted with a -6% and +1% error, respectively.

The experimental results point to a maximum effective shear reinforcement ratio in the range of 0.085% to 0.100% for specimens with a 48 in. (1219 mm) grout horizontal spacing. A shear reinforcement anchorage problem was encountered with two specimens with some suggestion of a developing anchorage problem in other specimens. This suggests the code-compliant 180° hooks may be inadequate or there may need to be a limit placed on shear reinforcement bar diameter for a given masonry unit width. Based on the experimental results,

recommendations were made for modifications to the MSJC (2008) shear equations.

Recommendations for future research were also made.

TABLE OF CONTENTS

	Page
ACKNOWLEDGEMENTS	iii
ABSTRACT	iv
LIST OF FIGURES	ix
LIST OF TABLES	xv

CHAPTERS

1. CHAPTER 1: INTRODUCTION	1
1.1 Background	1
1.2 Scope and Objectives	1
1.3 Previous Work	2
1.4 Current MSJC (2008) Strength Design Equation	2
1.5 Thesis Organization	4
2. CHAPTER 2: EXPERIMENTAL PROGRAM	5
2.1 Introduction	5
2.2 Wall Specimens	5
2.3 Wall Testing	9
2.3.1 Test Setup	9
2.3.2 Test Protocol	11
2.4 Instrumentation	13
3. CHAPTER 3: RESULTS	15
3.1 Introduction	15
3.2 Wall Test Results	15

3.2.1	General Behavior Of Partially Grouted Specimens.....	15
3.2.2	Specimen PG085-48.....	17
3.2.3	Specimen PG120-48.....	20
3.2.4	Specimen PG169-48.....	23
3.2.5	Specimen PG085-32.....	26
3.2.6	Specimen PG085-24.....	29
3.2.7	Specimen FG085-00.....	34
3.2.8	Hysteretic Performance Of The Test Specimens.....	37
3.2.9	Lateral Load vs. Steel Strains.....	41
4.	CHAPTER 4: ANALYSIS AND DISCUSSION OF TEST RESULTS.....	46
4.1	Introduction.....	46
4.2	Test Parameter Evaluation.....	48
4.2.1	Effects Of Grout Horizontal Spacing.....	48
4.2.2	Effects Of Horizontal Reinforcement Ratio.....	53
4.3	Measured vs. Predicted Shear Strength Using MSJC (2008) Shear Equations.....	58
4.4	Modification To The MSJC (2008) Shear Equation.....	63
4.5	Shear Displacement vs Sliding, Rocking and Flexural Displacement.....	68
4.6	Deformations Of Plane Sections.....	70
4.7	Strut And Tie Model.....	72
4.7.1	General Model Outline.....	72
4.7.2	Model for Specimens PG085-48, PG120-48, and PG169-48.....	75
4.7.3	Model for Specimen FG085-00.....	77
4.7.4	Models for Specimen PG085-32.....	78

4.7.5	Models for Specimen PG085-24.....	80
4.7.6	Strut And Tie vs. Experimental Results.....	82
4.8	Other Codes And Methods.....	83
4.8.1	Equations By Fattal.....	83
4.8.2	New Zealand Code.....	85
4.8.3	MSJC (2008) ASD.....	90
5.	CHAPTER 5: CONCLUSIONS.....	91
5.1	Summary.....	91
5.2	Conclusions.....	91
5.3	Modifications To MSJC (2008) Strength Design Equations.....	94
5.4	Future Research.....	95
	REFERENCES.....	96
	NOTATION.....	98
 APPENDICES 		
	Appendix A: Construction.....	99
	Appendix B: Material Properties Specimens and Testing.....	102
	Appendix C: Coordinates Of Instrumentation.....	108
	Appendix D: Instrumentation.....	115
	Appendix E: Strain Gage Hysteretics.....	118
	Appendix F: Foundation Sliding On Reaction Floor.....	133

LIST OF FIGURES

	Page
Figure 2-1: Dimensions common to all wall specimens, given as in. (mm).....	6
Figure 2-2: Horizontal cross-sections of wall specimens. Dimensions are center-to-center of the flexural (vertical) reinforcement. Grouted cells are indicated with shading. Specimen (a) PG085-48, PG120-48, PG169-48, (b) PG085-32, (c) PG085-24, and (d) FG085-00.....	7
Figure 2-3: PG085-48 after testing in the H-frame using the single knee-brace.....	10
Figure 2-4: H-frame setup using single knee brace.....	11
Figure 2-5: H-frame setup using dual knee brace.....	11
Figure 2-6: Testing protocol showing displacement at each cycle.....	12
Figure 2-7: Typical location of strain gages and typical location and identifier for string pots on specimens PG085-48, PG120-48, PG169-48 and FG085-00.....	14
Figure 3-1: Typical location for (a/b) first stair-step crack and (c/d) second stair-step crack in lower panel and first crack in upper panel, for the indicated direction of force application....	16
Figure 3-2: Specimen PG085-48, location of first crack at a drift of 0.11% (9.0 kips (40.0 kN)), (a) east face, (b) west face. Crack opened with a N = north push, S = south pull.....	18
Figure 3-3: Specimen PG085-48, left/right are east/west faces, respectively, after testing to a drift of: (a/b) 0.65% (34.8 kips (155 kN)), and (c/d) 1.5% (42.7 kips (190 kN)).....	19
Figure 3-4: Specimen PG085-48, south end cracking and damage to CMU courses 3, 4 and 5 during testing, (a) east face and south end, (b) south end close-up, and (c) west face.....	19
Figure 3-5: Specimen PG120-48, location of first crack at a drift of 0.11% (8.7 kips (38.7 kN)), (a) east face, and (b) west face. Crack opened with a N = north push, S = south pull.....	21

Figure 3-6: Specimen PG120-48, left/right are east/west faces, respectively, after testing to a drift of: (a/b) 0.65% (32.1 kips (143 kN)), and (c/d) 1.5% (44.8 kips (199 kN))	22
Figure 3-7: Specimen PG120-48, state of damage to south end at end of test, (a) south end and west face, and (b) south end and east face with detached masonry removed	22
Figure 3-8: Specimen PG169-48, location of first crack at a drift of 0.05% (7.5 kips (33.4 kN)), (a) east face, and (b) west face. Crack opened with a N = north push, S = south pull.	23
Figure 3-9: Specimen PG169-48, left/right are east/west faces, respectively, after testing to a drift of: (a/b) 0.65% (45.7 kips (203 kN)), and (c/d) 0.87% (35.7 kips (159 kN))	25
Figure 3-10: Specimen PG169-48, cracking at south end mid-height, (a) east side, and (b) west side	25
Figure 3-11: Specimen PG085-32, location of first crack at a drift of 0.11% (8.8 kips (39.1 kN)), (a) east face, and (b) west face. Crack opened with a N = north push, S = south pull.	27
Figure 3-12: Specimen PG085-32, left/right are east/west faces, respectively, after testing to a drift of: (a/b) 0.65% (39.7 kips (177 kN)), (c/d) 1.3% (58.5 kips (260 kN)), and (e/f) 1.5% (53.3 kips (237 kN))	28
Figure 3-13: Specimen PG085-32, east face, north end cracking at a drift of 1.5%	29
Figure 3-14: Specimen PG085-24 cracking prior to testing, (a) east face, and (b) west face	30
Figure 3-15: Specimen PG085-24, location of first crack at a drift of 0.05% (4.3 kips (19.1 kN)), (a) east face, and (b) west face. Jagged lines represent pre-test cracks. Crack opened with a N = north push, S = south pull.	30
Figure 3-16: Specimen PG085-24, left/right are east/west faces, respectively, after testing to a drift of: (a/b) 0.65% (38.2 kips (170 kN)), (c/d) 1.3% (60.5 kips (269 kN)), and (e/f) 1.7% (54.2 kips (241 kN))	33

Figure 3-17: Specimen PG085-24 south end damage after testing, (a) south end with east face, and (b) south end with west face	33
Figure 3-18: Specimen FG085-00, location of first crack at a drift of 0.11% (9.0 kips (40.0 kN)), (a) east face, and (b) west face. Crack opened with a N = north push, S = south pull	34
Figure 3-19: Specimen FG085-00, left/right are east/west faces, respectively, after testing to a drift of: (a/b) 0.65% (60.4 kips (269 kN)), and (c/d) 1.3% (69.6 kips (310 kN))	36
Figure 3-20: Specimen FG085-00 cracking in north half of wall after testing, (a) east face, and (b) west face	36
Figure 3-21: Lateral force vs. lateral drift for specimens (a) PG085-48, (b) PG120-48, (c) PG169-48, (d) PG085-32, (e) PG085-24, and (f) FG085-00	39
Figure 3-22: Backbone curve and bilinear idealization for specimens (a) PG085-48, (b) PG120- 48, (c) PG169-48, (d) PG085-32, (e) PG085-24, and (f) FG085-00	40
Figure 3-23: Bilinear approximation of backbone curve	41
Figure 3-24: Lateral load vs. maximum strain in the flexural steel for specimens (a) PG085-48, (b) PG120-48, (c) PG169-48, (d) PG085-32, (e) PG085-24, and (f) FG085-00	44
Figure 3-25: Lateral load vs. maximum strain in the shear steel for specimens (a) PG085-48, (b) PG120-48, (c) PG169-48, (d) PG085-32, (e) PG085-24, and (f) FG085-00	45
Figure 4-1: For all test specimens, (a) backbone curves, and (b) bilinear approximation	47
Figure 4-2: (a) Backbone curves for specimens with the same horizontal reinforcement ratio and differing grout horizontal spacing, and (b) backbone curves normalized to peak strength	50
Figure 4-3: Idealized backbone curves for specimens with the same horizontal reinforcement ratio (0.085%) and differing grout horizontal spacing	50

Figure 4-4: Drift vs. net shear stress for $\rho_h = 0.085\%$, (a) using net area from MSJC equations, and (b) using net area from New Zealand standard.....	51
Figure 4-5: Drift vs. force in shear reinforcement and applied force (backbone curve) for specimens with $\rho_h = 0.085\%$ and varying grout horizontal spacing. Specimen (a) PG085-48, (b) PG085-32, (c) PG085-24, and (d) FG085-00.....	52
Figure 4-6: Backbone curves for specimens with 48 in. (1219 mm) grout horizontal spacing and varying horizontal reinforcement ratios.....	53
Figure 4-7: Idealized backbone curves for specimens with 48 in. (1219 mm) grout horizontal spacing and varying horizontal reinforcement ratios.....	54
Figure 4-8: Effects of ρ_h on shear strength.....	54
Figure 4-9: Shear reinforcement ratio (%) vs. maximum strain in shear reinforcement.....	56
Figure 4-10: Drift vs. force in shear reinforcement and applied force (backbone curve) for specimens with 48 in. (1219 mm) grout spacing and varying horizontal reinforcement ratios. Specimen (a) PG085-48, (b) PG120-48, and (c) PG169-48.....	56
Figure 4-11: Load-drift hysteretics for (a) PG085-48, (b) PG120-48, (c) PG169-48, (d) PG085- 32, (e) PG085-24, and (f) FG085-00.....	61
Figure 4-12: Effects of ρ_h on the predictions using MSJC (2008) shear design equations.....	62
Figure 4-13: Specimens with $\rho_h = 0.085\%$, (a) net area vs. V_{max} and V_n , and (b) grout horizontal spacing vs. V_{max} and V_n , with linear trendline for V_{max}	62
Figure 4-14: Effects of grout horizontal spacing on the % error between predicted and actual shear strength (a) all group specimens, and (b) partially grouted only.....	63
Figure 4-15: 45° shear crack.....	65

Figure 4-16: Sliding, Rocking, Flexural and Shear Displacement components for specimens (a) PG085-48, (b) PG120-48, (c) PG169-48, (d) PG085-32, (e) PG085-24, and (f) FG085-00	69
Figure 4-17: Strains at the 2 nd CMU course under a north push and south pull, left and right respectively, for specimens (a/b) PG085-48, (c/d) PG120-48, (e/f) PG169-48, (g/h) PG085-32, (i/j) PG085-24, and (k/l) FG085-00	72
Figure 4-18: Determination of (a) strut angle, and (b) strut width	74
Figure 4-19: Strut and tie model for partially grouted specimens with 48 in. (1219 mm) grout horizontal spacing (a) member labels, and (b) member forces at yield in kips	76
Figure 4-20: Strut and tie model for specimen FG085-00 at first yield, (a) member labels, and (b) member forces at yield in kips	77
Figure 4-21: Strut and tie model for specimen FG085-00 at failure, member forces in kips	78
Figure 4-22: Most conservative strut and tie model for specimen PG085-32, (a) member labels, and (b) member forces at yield in kips	79
Figure 4-23: Rejected strut and tie model for specimen PG085-32. Dashed lines are compression struts, heavy solid lines are tension ties	80
Figure 4-24: Most conservative strut and tie model for specimen PG085-24, (a) member labels, and (b) member forces at failure in kips	81
Figure 4-25: Rejected strut and tie models for specimen PG085-24, model reached failure at (a) 84.9 kips (378 kN) and (b) 112 kips (498 kN)	82
Figure 5-1: Experimental shear strength and shear strength predictions using MSJC (2008) Strength Design, Fattal equations, New Zealand code, and strut and tie model	93
Figure A-1: Foundation reinforcement	99

Figure A-2: Foundation forms	99
Figure A-3: Freshly poured foundations	100
Figure A-4: Foundation with flexural reinforcement at 48 in. (1219 mm)	100
Figure A-5: Wall specimens at mid-construction	101
Figure A-6: Finished wall specimen	101
Figure B-1: Station for applying gypsum caps	102
Figure B-2: Material properties testing equipment, (a) tension/compression press, and (b) controller and data acquisition system	104
Figure D-1: Location of strain gages and location and identifier for string potentiometers on specimens PG085-48, PG120-48, PG169-48 and FG085-00	115
Figure D-2: Location of strain gages and location and identifier for string potentiometers on specimen PG085-32	116
Figure D-3: Location of strain gages and location and identifier for string potentiometers on specimen PG085-24	117
Figure E-1: Strain gage hysteretics for PG085-48	120
Figure E-2: Strain gage hysteretics for PG120-48	123
Figure E-3: Strain gage hysteretics for PG169-48	125
Figure E-4: Strain gage hysteretics for FG085-00	127
Figure E-5: Strain gage hysteretics for PG085-32	129
Figure E-6: Strain gage hysteretics for PG085-24	132
Figure F-1: Sliding of the foundation on the reaction floor as the test progresses, specimen (a) PG085-48, (b) PG120-48, (c) PG169-48, (d) PG085-32, (e) PG085-24, and (f) FG085-00	134

LIST OF TABLES

	Page
Table 2-1: Wall specimen parameters	7
Table 2-2: Wall specimen identifiers, flexural reinforcement and grout horizontal spacing.....	8
Table 4-1: Summary of test results and MSJC predictions	46
Table 4-2: Strength, initial stiffness and displacement ductility for $\rho_h = 0.085\%$	49
Table 4-3: Yield and ultimate stiffness for $\rho_h = 0.085\%$	49
Table 4-4: Strength, initial stiffness and displacement ductility for grout horizontal spacing = 48 in. (1219 mm)	57
Table 4-5: Yield and ultimate stiffness for grout horizontal spacing = 48 in. (1219 mm)	57
Table 4-6: MSJC predicted shear strength, V_n , experimental shear strength, V_{max} , and % Error	62
Table 4-7: Inputs to Equations 4-2 and 4-3, V_{nm} , V_{nm} and V_n	64
Table 4-8: MSJC (2008) and m1-MSJC vs. the experimental results	66
Table 4-9: MSJC (2008) and m2-MSJC vs. the experimental results	66
Table 4-10: MSJC (2008) and m3-MSJC vs. the experimental results	67
Table 4-11: Parameters for ACI equations and resulting strengths	74
Table 4-12: SI values for the strut and tie model shown in Figure 4-19(b)	76
Table 4-13: SI values for the strut and tie model shown in Figure 4-20(b)	77
Table 4-14: SI values for the strut and tie model shown in Figure 4-21	78
Table 4-15: SI values for the strut and tie model shown in Figure 4-22(b)	79
Table 4-16: SI values for the strut and tie model shown in Figure 4-24(b)	81
Table 4-17: Strut & Tie and MSJC (2008) predictions vs. experimental results	83

Table 4-18: Fattal equation shear stress components and predicted shear capacity.....	85
Table 4-19: Fattal and MSJC predictions as a percentage of the experimental results.....	85
Table 4-20: Shear strengths and shear stress components predicted by New Zealand code, observational type of masonry C.....	89
Table 4-21: NZS 4230:2004 and MSJC predictions as a percentage of the experimental results, observational type of masonry C.....	89
Table 4-22: Shear strengths and shear stress components predicted by New Zealand code, observational type of masonry B.....	90
Table 4-23: NZS 4230:2004 and MSJC predictions as a percentage of the experimental results, observational type of masonry B.....	90
Table B-1: Grout prism dimensions.....	103
Table B-2: UngROUTED prism results.....	106
Table B-3: Grouted prism results.....	106
Table B-4: Grout prism results.....	106
Table B-5: CMU test results.....	107
Table B-6: Rebar coupon results.....	107
Table C-1: Coordinates of string pots on specimen PG085-48.....	109
Table C-2: Coordinates of string pots on specimen PG120-48.....	110
Table C-3: Coordinates of string pots on specimen PG169-48.....	111
Table C-4: Coordinates of string pots on specimen PG085-32.....	112
Table C-5: Coordinates of string pots on specimen PG085-24.....	113
Table C-6: Coordinates of string pots on specimen FG085-00.....	114

CHAPTER 1: INTRODUCTION

1.1 Background

Partially grouted masonry shear walls are allowed by the MSJC and have been used in high seismic zones in the USA. The partially grouted shear walls have advantages over fully grouted shear walls. They use less material in construction, thereby lowering costs and presenting a more eco-friendly presence, and decrease the mass of a structure with corresponding benefits under dynamic loading situations. The current MSJC shear equations were developed for fully grouted masonry shear walls and subsequently extended to partially grouted shear walls through the use of some reduction factors, notably by using the net cross sectional area of masonry in place of the gross cross sectional area.

1.2 Scope and Objectives

The primary goal of this research was to validate either the current MSJC Strength Design shear equations or concerns about the validity of these equations and provide recommendations for modifications to the equations.

This research investigated the in-plane shear strength and failure mechanism of six masonry cantilever shear walls, all tested at Washington State University. Five partially grouted specimens had vertical reinforcement and grout horizontal spacing of 48 in. (1219 mm), 32 in. (813 mm), and 24 in. (610 mm). The sixth specimen was a fully grouted wall with vertical reinforcement at 48 in. The nominal dimensions of the walls were 8 ft. (2438 mm) high by 8 ft. 8 in. (2642 mm) long. The walls were constructed of 8 in. (203 mm) nominal concrete masonry units (CMU) on a heavily reinforced concrete footing approximately 12 ft (3658 mm) long by 25 in. (635 mm) wide by 19 in. (483 mm) high. The walls were subjected to constant vertical

pressure of approximately 14 psi (0.097 MPa) and incrementally increasing lateral loading cycles. The test parameters included horizontal spacing of grouted cells and horizontal reinforcement ratio.

1.3 Previous Work

Elmapruk and ElGawady (2009) compared the measured experimental strength of ninety test specimens from the literature to the predictions using the MSJC (2008). The comparisons show that the MSJC was unconservative in many cases and too conservative in other cases. They concluded that, overall, the current MSJC shear equations consistently overpredict shear strength and the shear design provisions need significant revisions. Davis (2008) examined fifty-six fully grouted masonry shear walls and found the current MSJC strength design shear equations to be reasonable for fully grouted shear walls, although with room for improvement.

The available research raises concerns that, while reasonable for the fully grouted walls, the current MSJC shear equations are not adequate for partially grouted walls.

1.4 Current MSJC (2008) Strength Design Equations

The current MSJC Strength Design shear equations consider shear strength contributed by the masonry plus shear strength contributed by the shear reinforcement steel. The equation for fully grouted shear walls is the same as the equation for partially grouted shear walls. The difference in shear strength between the two construction methods is accounted for in the net cross sectional area term, A_n . No other differentiation between the two methods of construction is made.

V_n is the total nominal shear strength provided by the masonry and reinforcement steel and is given by Equation 1-1 (MSJC Equation 3-19):

$$V_n = V_{nm} + V_{ns} \quad (1-1)$$

V_{nm} is the nominal shear strength contributed by the masonry and is given by Equation 1-2 (MSJC Equation 3-22):

$$V_{nm} = \left[4.0 - 1.75 \left(\frac{M_u}{V_u \cdot d_v} \right) \right] \cdot A_n \cdot \sqrt{f'_m} + 0.25 P_u \quad (1-2)$$

where $[M_u / (V_u \cdot d_v)]$ need not be taken greater than 1.0.

Equation 1-2 may be simplified when moment M_u is due to shear force V_u applied at elevation h_w using the relationship of Equation 1-3:

$$\frac{M_u}{V_u \cdot d_v} = \frac{V_u \cdot h_w}{V_u \cdot d_v} = \frac{h_w}{d_v} \quad (1-3)$$

Equation 1-2 then becomes Equation 1-4, which is the form of Equation 1-2 used in this study:

$$V_{nm} = \left[4.0 - 1.75 \left(\frac{h_w}{d_v} \right) \right] \cdot A_n \cdot \sqrt{f'_m} + 0.25 P_u \quad (1-4)$$

where (h_w / d_v) need not be taken greater than 1.0.

V_{ns} is the nominal shear strength contributed by the reinforcing steel and is given by Equation 1-5 (MSJC Equation 3-23):

$$V_{ns} = 0.5 \cdot \left(\frac{A_v}{s} \right) \cdot f_y \cdot d_v \quad (1-5)$$

Equation 1-5 may be modified to use the horizontal reinforcement ratio, ρ_h , as follows. The horizontal reinforcement ratio, ρ_h , may be expressed as Equation 1-6:

$$\rho_h = \frac{A_v}{s \cdot t} \quad (1-6)$$

By rearranging Equation 1-6 to isolate (A_v / s) , Equation 1-7 is obtained:

$$\frac{A_v}{s} = \rho_h \cdot t \quad (1-7)$$

Substituting Equation 1-7 into Equation 1-5 gives Equation 1-8, which is the form of Equation 1-5 used in this study:

$$V_{ns} = 0.5 \cdot (\rho_h \cdot t) \cdot f_y \cdot d_v \quad (1-8)$$

1.5 Thesis Organization

This thesis is composed of five section and six appendices. Chapter 1 introduced the research and contains a brief literature review. Chapter 2 presents the experimental program. Chapter 3 presents the results of the wall specimen tests. Chapter 4 contains the analysis and discussion of the wall test results. Chapter 5 presents recommendations based on Chapter 4. Appendix A presents information on the wall specimen construction. Appendix B presents the construction, testing, and results of the material properties specimens. Appendix C lists the x,y,z coordinates of the instrumentation on the wall specimens. Appendix D contains figures showing the placement of the instrumentation on the wall specimens. Appendix E contains the hysteretics for all strain gages for all wall specimens. Appendix F presents information concerning wall foundation sliding on the reaction floor.

CHAPTER 2: EXPERIMENTAL PROGRAM

2.1 Introduction

This chapter presents specifications of the shear wall specimens tested, the test setup for the shear walls, the testing protocol for the shear walls, and the typical instrumentation setup. Additional details of wall construction may be found in Appendix A. Information on the material properties tests may be found in Appendix B. Full details of the instrumentation for all walls may be found in Appendices C and D.

2.2 Wall Specimens

Test wall specimens were constructed on heavily reinforced foundations designed to avoid any failures associated with an inadequate foundation. Foundation construction details are covered in Appendix A.

Professional masons constructed the test specimens in a running bond using standard hollow concrete masonry units (CMU) and face shell bedding. All specimens were 14 courses high, six and one half block units in length. Each specimen was nominally 112 in. (2845 mm) high, 104 in. (2642 mm) long, and 8 in. (203 mm) wide. Figure 2-1 shows the typical dimensions of a test specimen. Four different configurations of grout horizontal spacing were used as shown in Figure 2-2.

Continuous vertical flexural reinforcement was provided in all the test specimens, i.e. there was no lap splice for the flexural reinforcement. All specimens had approximately the same total area of flexural reinforcement of 3.60 in.^2 (2323 mm^2), corresponding to a reinforcement ratio of 0.456%. Table 2-1 and Figure 2-2 show the number and distribution of the vertical steel reinforcement. The flexural reinforcement was selected such that the flexural capacity of every

specimen exceeded its predicted shear capacity. Horizontal shear was provided in bond beam knockout blocks placed at a spacing of 48 in. (1219 mm) in the 6th and 12th courses. All specimens except specimens PG-120-48 and PG169-48 had 1#5 as shear reinforcement in every bond beam. Specimens PG-120-48 and PG-169-48 had 1#6 and 2#5 as shear reinforcement in every bond beam, respectively. The shear reinforcement rebars were anchored with MSJC code-compliant 180-degree hooks around the outermost vertical reinforcement.

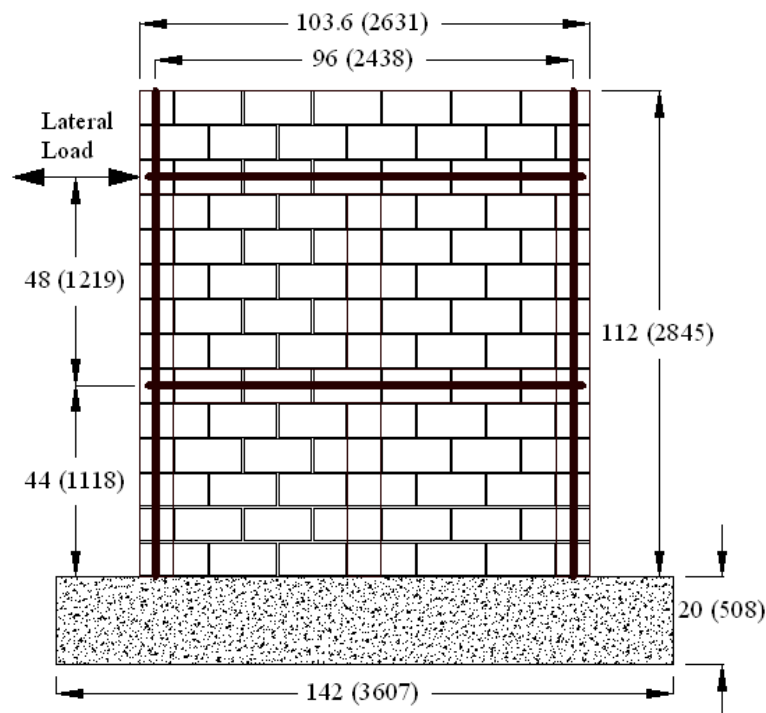


Figure 2-1: Dimensions common to all wall specimens, given as in. (mm)

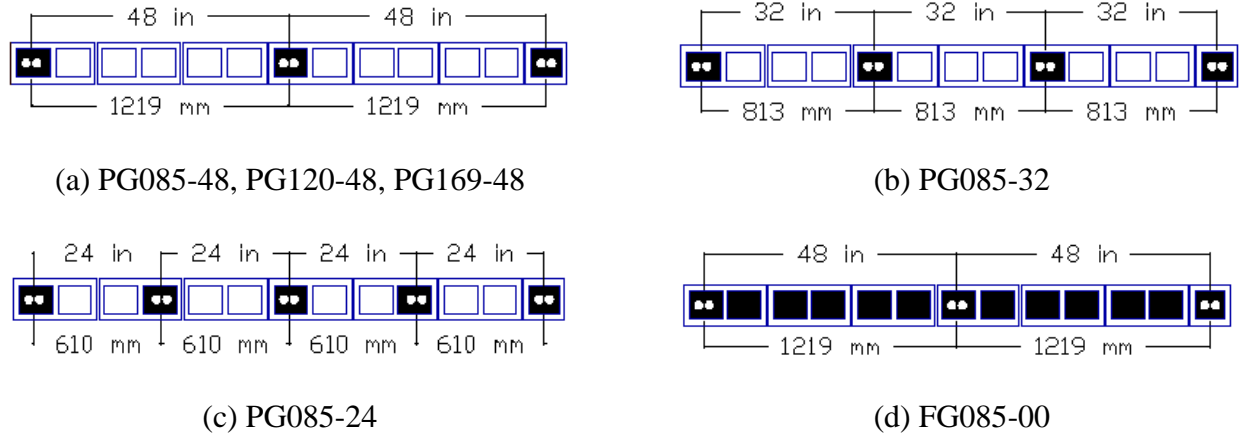


Figure 2-2: Horizontal cross-sections of wall specimens. Dimensions are center-to-center of the flexural (vertical) reinforcement. Grouted cells are indicated with shading. Specimen (a) PG085-48, PG120-48, PG169-48, (b) PG085-32, (c) PG085-24, and (d) FG085-00.

Table 2-1: Wall specimen parameters

Wall ID	PG085-48	PG120-48	PG169-48	PG085-32	PG085-24	FG085-00	
A_n	356 (229,677)	356 (229,677)	356 (229,677)	388 (250,322)	421 (271,612)	680 (438,709)	in ² (mm ²)
shear stirrup	(1) #5	(1) #6	(2) #5	(1) #5	(1) #5	(1) #5	
ρ_h	0.00085	0.00120	0.00169	0.00085	0.00085	0.00085	
A_v	0.31 (200)	0.44 (284)	0.62 (400)	0.31 (200)	0.31 (200)	0.31 (200)	in ² (mm ²)
vertical reinforcement	2 #7 x 3 cells	2 #7 x 3 cells	2 #7 x 3 cells	2 #6 x 4 cells	2 #6 x 2 cells 2 #5 x 3 cells	2 #7 x 3 cells	
ρ_v	0.00456	0.00456	0.00456	0.00446	0.00458	0.00456	
$A_{flexural}$	3.60 (2323)	3.60 (2323)	3.60 (2323)	3.52 (2271)	3.62 (2335)	3.60 (2323)	in ² (mm ²)

Constant parameters for all specimens: $h_w = 92$ in (2337 mm); $t = 7.625$ in (194 mm); $d_v = 103.6$ in (2631 mm); $P_u = 11080$ lb (49286 N); $s = 48$ in (1219 mm); $f_y = 63600$ psi (438.5 MPa); $f_m = 1640$ psi (11.3 MPa), except FG085-00 where $f_m = 2860$ psi (19.7 MPa).

Specimen identifiers were assigned using the following pattern: XXSSS-GG. XX is PG for a partially grouted specimen and FG for a fully grouted specimen, SSS is the horizontal reinforcement ratio expressed as a percentage and GG is the grout horizontal spacing in inches.

Table 2-2 lists the specimen identifiers with the corresponding horizontal reinforcement ratios and grout horizontal spacing.

Table 2-2: Wall specimen identifiers, flexural reinforcement and grout horizontal spacing

Specimen Identifier	Partially / Fully Grouted	Horizontal reinforcement ratio (%)	Vertical reinforcement spacing	Grouted cell spacing
PG085-48	Partially	0.085	48 in (1219 mm)	48 in (1219 mm)
PG120-48	Partially	0.120	48 in (1219 mm)	48 in (1219 mm)
PG169-48	Partially	0.169	48 in (1219 mm)	48 in (1219 mm)
PG085-32	Partially	0.085	32 in (813 mm)	32 in (813 mm)
PG085-24	Partially	0.085	24 in (610 mm)	24 in (610 mm)
FG085-00	Fully	0.085	48 in (1219 mm)	fully grouted

All specimens were constructed using hollow concrete masonry units (CMU) having a measured net area compressive strength of 2630 psi (18.1 MPa). All blocks were provided by the same manufacturer and received in the same shipment. CMUs having nominal dimensions of 8 in. x 8 in. x 16 in. (203 mm x 203 mm x 406 mm) for full blocks and 8 in. x 8 in. x 8 in. (203 mm x 203 mm x 203 mm) for half blocks were used in the construction of the test specimens.

Each specimen was grouted using fine aggregate provided by a local ready-mix supplier. Each specimen was grouted in three lifts of 48 in. (1219 mm), 48 in. (1219 mm) and 16 in. (406 mm). The grout had a measured compressive strength $f_g' = 4240$ psi (29.2 MPa) (ASTM C1019-07). Masonry prisms were constructed during wall specimen construction and were tested at 170 to 175 days according to ASTM C1314-07. The masonry compressive strength f_m' was 1640 psi

(11.3 MPa) for ungrouted prisms and 2860 psi (19.7 MPa) for grouted prisms. All the rebar used in the construction was Gr. 60 with measured yield strength of 63.6 ksi (439 MPa). The yield strengths measured on coupons of the rebar are shown in Appendix B. The walls were built in three days. Courses 1 through 6 for each specimen were constructed on the first day. On the second day of construction, courses 1 through 5 and the 6th course bond beam were grouted in each wall and courses 7 through 12 were laid. To connect the lateral load actuator to the wall (as explained later), $\frac{3}{4}$ in. (19 mm) diameter threaded rods were installed in every cell at the 12th masonry course prior to grouting. On the third day of construction, courses 7 through 11 and the 12th course bond beam in each specimen were grouted and courses 13 and 14 were laid and fully grouted.

2.3 Wall Testing

2.3.1 Test Setup

Specimens were tested using an H-frame composed of steel I-beam (W-shapes). The frame had two one-piece columns, a two-piece cross-beam and either a single or dual knee-brace. The dual knee-brace configuration was not initially available, therefore the first four specimens including specimens PG085-48, PG120-48, PG085-32 and PG085-24 were tested using the single knee-brace configuration. Due to concerns that the strength of the single knee-brace configuration was marginal for the remaining two specimens, which were expected to have the highest strength, a dual knee-brace setup was used.

A constant vertical force (P_u) of approximately 11.1 kips (49.4 kN) was applied to the top of all specimens using two hydraulic jacks. The force from the jacks was distributed across the

top surface of the specimens using an HSS4x8x $\frac{1}{4}$ (102 mm x 203 mm x 6 mm) load spreader to achieve an axial stress of 14 psi (0.097 MPa). The jacks were attached to a trolley with a minimal coefficient of friction that was free to move laterally under the cross-beam. The load remained constant during testing

A 200 kips (890 kN) capacity single-ended hydraulic actuator was used to apply the required displacement at the top of the test specimens. The actuator was attached to a column of the H-frame at one end and to a pair of C-channels that were bolted to the masonry specimens using thirteen $\frac{3}{4}$ in. (19 mm) threaded rods that were grouted in place in the 12th CMU course during construction (Figures 2-3 through 2-5).

The test specimens were designed to act as cantilever shear walls, i.e. fixed at the base to the laboratory strong floor and free to deflect and rotate at the wall top. Specimen foundations were post-tensioned to the reaction floor with six threaded rods, three at each end. Foundations were braced laterally with steel fixtures to prevent sliding of the foundation on the reaction floor.

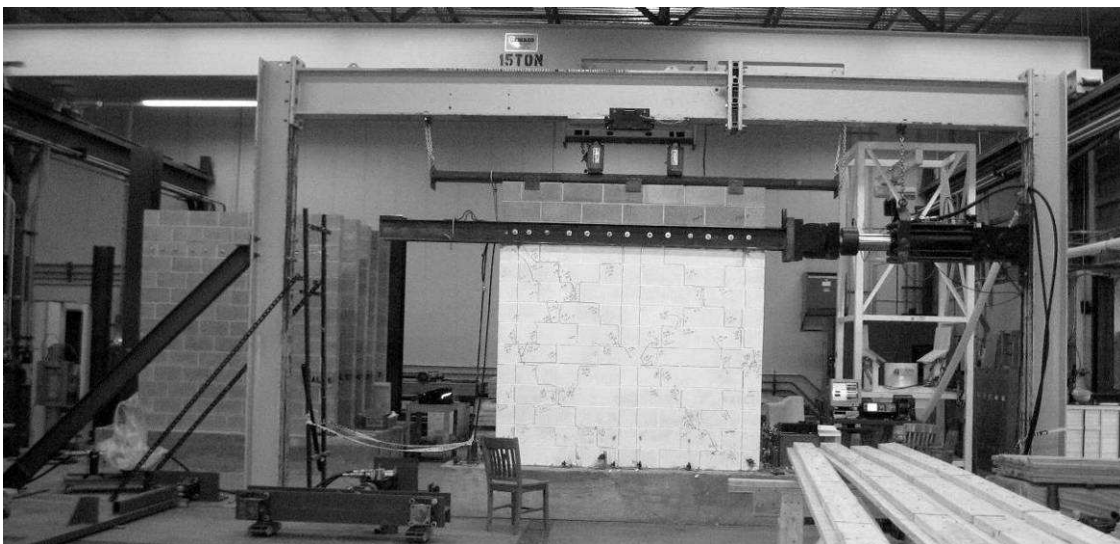


Figure 2-3: PG085-48 after testing in the H-frame using the single knee-brace.

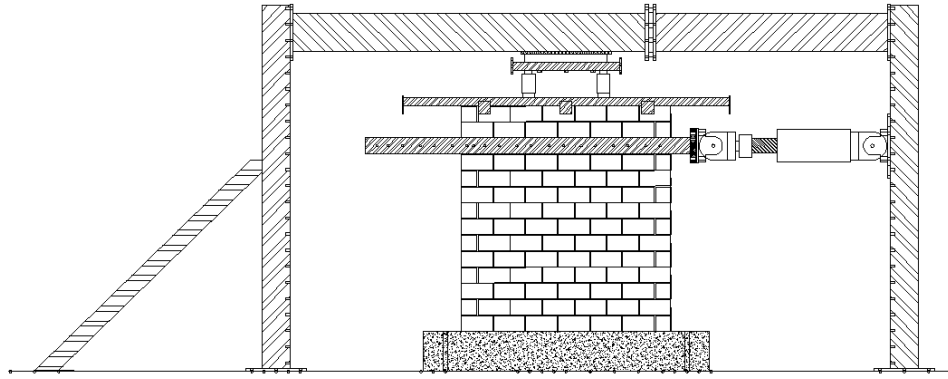


Figure 2-4: H-frame setup using single knee brace

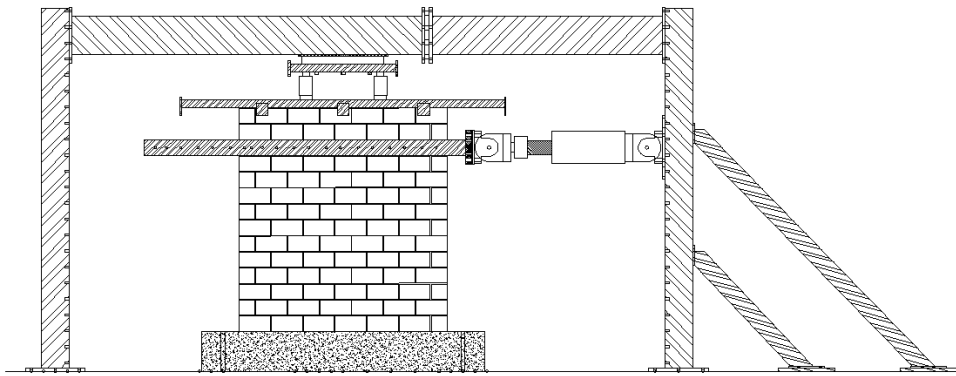


Figure 2-5: H-frame setup using dual knee brace

2.3.2 Test Protocol

Specimens were tested using a displacement based protocol consisting of three cycles at each peak displacement value. An estimate of Δ_y was obtained using Equations 2-1 and 2-2 (Priestley et al. 2007). Using the equations with the values listed after Equations 2-1 and 2-2, Δ_y was estimated to be 0.10 in. (2.5 mm), corresponding to a lateral drift of 0.11%. Displacement peaks started at $0.5 \Delta_y$ and increased in $0.5 \Delta_y$ steps to $4 \Delta_y$. Displacement peaks were then $5 \Delta_y$ and $6 \Delta_y$. Peaks were then increased in $2 \Delta_y$ steps until failure was achieved. The displacement protocol is shown in Figure 2-6. The displacement rate was kept constant at 0.1875 in./min. (4.76 mm/min.) for the entire test duration.

$$\theta_{y_mw} = 0.6 \varepsilon_y \cdot \frac{H_n}{l_w} \quad (2-1)$$

$$\Delta_y = \theta_{y_mw} \cdot H_e \quad (2-2)$$

where:

- H_n = height of wall; $H_n = 92$ in. (2337 mm)
- l_w = wall length; $l_w = 103.6$ in. (2631 mm)
- H_e = effective height at yield; $H_e = 92$ in. (2337 mm)
- ε_y = yield strain of the masonry; $\varepsilon_y = 0.00207$
- θ_{y_mw} = yield drift of masonry wall
- Δ_y = yield displacement

Specimen testing continued until a 20% drop from the peak force was observed or until an unacceptably hazardous situation was created due to the threat of falling masonry debris.

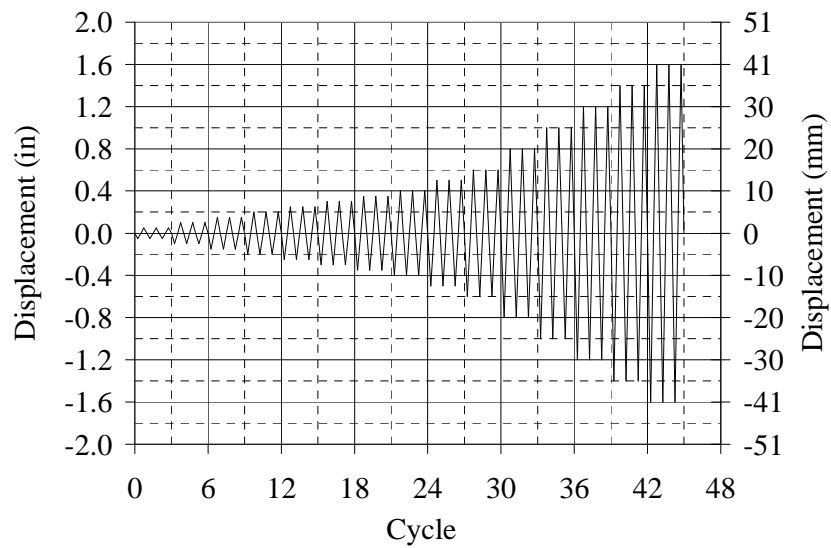


Figure 2-6: Testing protocol showing displacement at each cycle

2.4 Instrumentation

Specimens were typically instrumented with 13 strain gages having a gauge length of 0.250 in. (6.3 mm) bonded to the flexural and shear reinforcing steel prior to construction and 16 string potentiometers (string pots) mounted on the walls and foundations immediately before testing. Vishay Micro-Measurements CEA-06-250UW-120/P2 strain gages were used on all specimens. Two types of string pots were used, Micro-Epsilon WPS-500-MK30-P(01) and UniMeasure LX-PA-10. The applied lateral load was measured using the load cell on the actuator.

Figure 2-7 shows the typical location of strain gages for specimens PG085-48, PG120-48, PG169-48 and FG085-00. The flexural (vertical) reinforcement strain gages were located at or just above the top of the foundation. The middle and top shear reinforcement had four strain gages each. Also shown in Figure 2-7 is the placement and identification number for string pots mounted on specimens PG085-48, PG120-48, PG169-48 and FG085-00. Appendix D contains further information for these specimens and for specimens PG085-32 and PG085-24.

String pot 9 measured the global displacement at the level of force application. String pot 8 measured sliding of the wall on the foundation. String pot 7 measured sliding of the foundation on the reaction floor. String pots 1, 2, 3, 4, 5, 6, 12 and 13 measured vertical displacement at the wall ends. String pots 11 and 12 measured the diagonal displacements. String pots 14, 15, 16 and 17 measured vertical displacements along the west face of the wall.

Data from the strain gages, string pots and actuator were collected using LabView software. Data for the strain gages and string pots was recorded only on the computer running the LabView software. Data from the actuator was collected by the controlling computer for the actuator, written to a file, and passed to the computer running the LabView software.

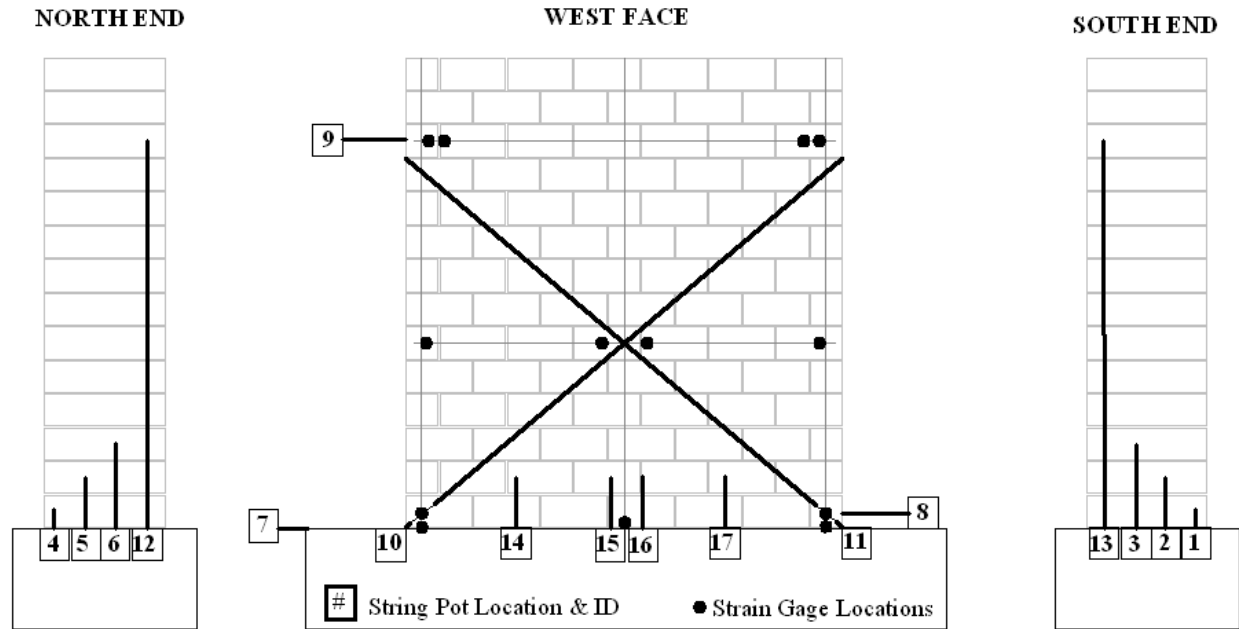


Figure 2-7: Typical location of strain gages and typical location and identifier for string pots on specimens PG085-48, PG120-48, PG169-48 and FG085-00

CHAPTER 3: RESULTS

3.1 Introduction

In this chapter the experimental results of the six specimens designed to fail in shear are presented. The chapter presents the general performance of the test specimens including the first crack loads and displacements, development of cracks in each specimen, and mode of failure. Also, the performance is presented through the hysteretic and the backbone curves of the test specimens.

The following sign conventions are used for all specimens. The actuator was attached to the south end of the specimen. A force pulled toward the south and corresponding drifts, or displacement, are given as positive values and the word “pull”. A force pushed toward the north and corresponding drift, or displacement, are given as negative values and the word “push”. Forces referenced for a particular lateral drift are the average of the peak north and south forces for that drift unless stated otherwise. The lateral drift was calculated by dividing the lateral displacement recorded from the actuator feedback by the height of the wall to the point where the actuator was attached, i.e. 92 in. (2337 mm).

3.2 Wall Tests

3.2.1 General Behavior Of Partially Grouted Specimens

The horizontal distance between the grouted cells had insignificant effects on the cracking pattern of the partially grouted test specimens. In addition, having higher horizontal reinforcement ratios did not change the crack pattern at the beginning of the test. However, it significantly changed the mode of failure as explained later. For a typical partially grouted

specimen, the first crack was a stair-step crack forming in the bottom masonry panels and occurring at a lateral drift of approximately 0.11%. By testing to a lateral drift of 0.22%, the stair-step cracks in the exterior masonry lower panels developed through the full length of the diagonal (Figure 3-1a/b).

As testing continued, a second stair step crack in the mortar joints typically formed in the lower panels above the first crack and a stair step crack typically formed in the upper panels (Figure 3-1(c/d)). Cracking in PG085-32 and PG085-24 occurred in a similar pattern in the outer lower masonry panels of each specimen, but also exhibited cracking in the lower interior masonry panels. As testing continued, 45° cracks formed in the masonry units.

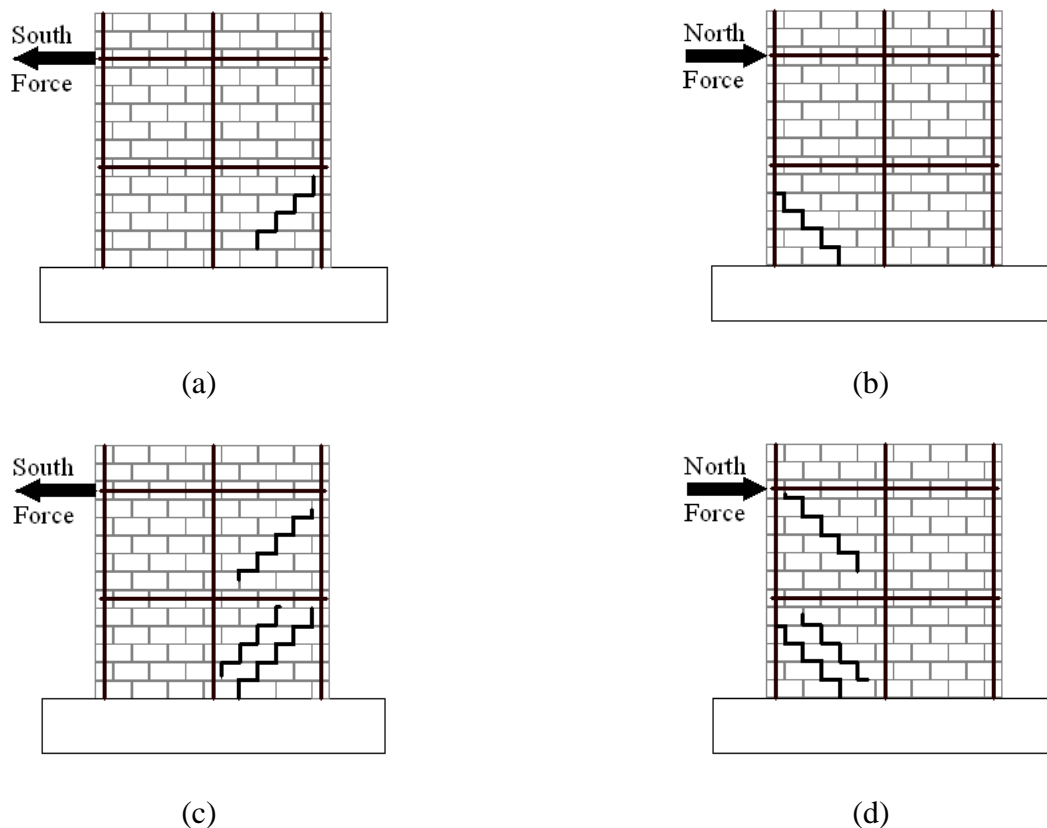


Figure 3-1: Typical location for (a/b) first stair-step crack and (c/d) second stair-step crack in lower panel and first crack in upper panel, for the indicated direction of force application

3.2.2 Specimen PG085-48

Specimen PG085-48 was a partially grouted masonry shear wall constructed with 48 in. (1219 mm) grout horizontal spacing and a single #5 rebar in each bond beam ($\rho_h = 0.085\%$). Figure 3-2 shows the extent of cracking of specimen PG085-48 after testing to a drift of 0.11% (9.0 kips (40.0 kN)). Figure 3-3 shows the extent of cracking of specimen PG085-48 after testing to a drift of 0.65% (34.8 kips (155 kN)) and 1.5% (42.7 kips (190 kN)). The first cracks were stair step cracks passing through the mortar bed and head-joints in the bottom panels in the south and north directions when pushing and pulling the specimen, respectively, to a drift of 0.11% (9.0 kips (40.0 kN)). While pushing toward the north to a drift of 0.27% (19.3 kips (85.9 kN)), a horizontal crack developed in the mortar joint between courses 5 and 6 in the south end grouted cell. In addition, more diagonal stair-steps cracks developed in the lower panels. At a drift of 0.33% (22.1 kips (98.3 kN)), stair-step cracks in the mortar bed and head-joints developed in the upper masonry panels. As testing continued, additional 45° cracks developed through the CMU units in all panels and middle bond beam. At a drift of 0.87% (41.6 kips (185 kN)), a 45° crack at the south end started in the southern most CMU of the 6th course and progressed up and to the north. At a drift of 1.3% (49.9 kips (207 kN)), some cracks opened significantly and the peak strength of the wall was achieved. At this drift, several loud "pops" and bulging of the face shells of several units were noted. At a drift of 1.5% (42.7 kips (190 kN)), an approximate 24% drop in the average lateral strength happened. By the end of the test, all masonry panels had stair-step and/or 45° cracks indicative of the formation of compression struts within the panel (Figure 3-3c/d). In addition, spalling of the south end shells of the 3rd, 4th and 5th CMU courses was observed (Figure 3-4).

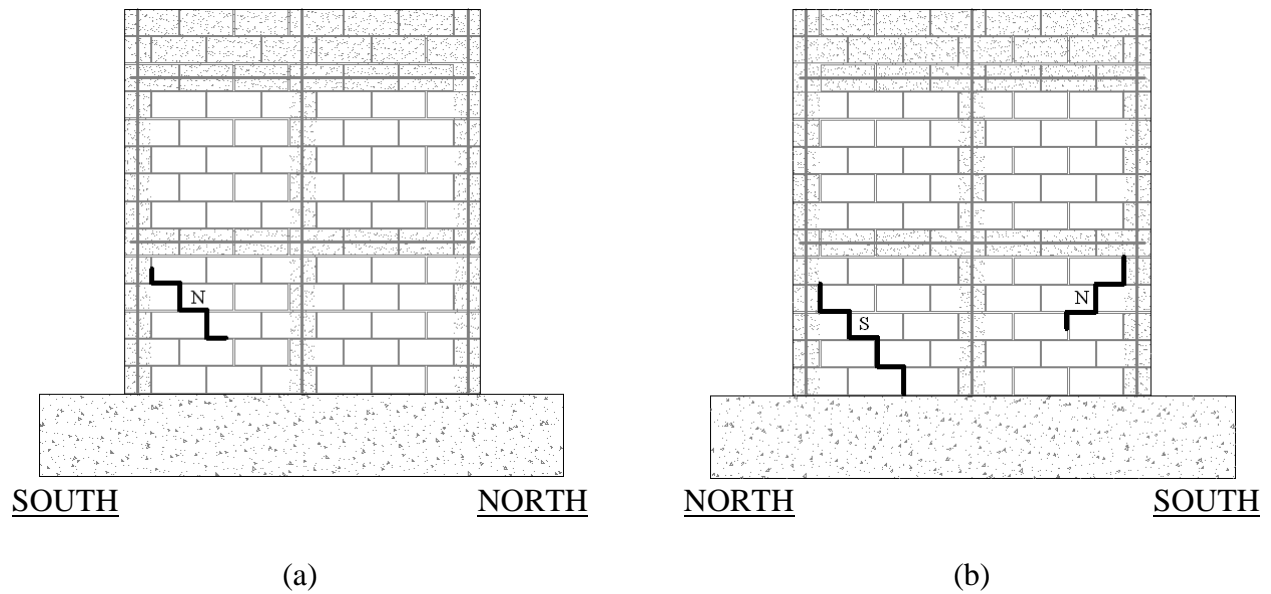
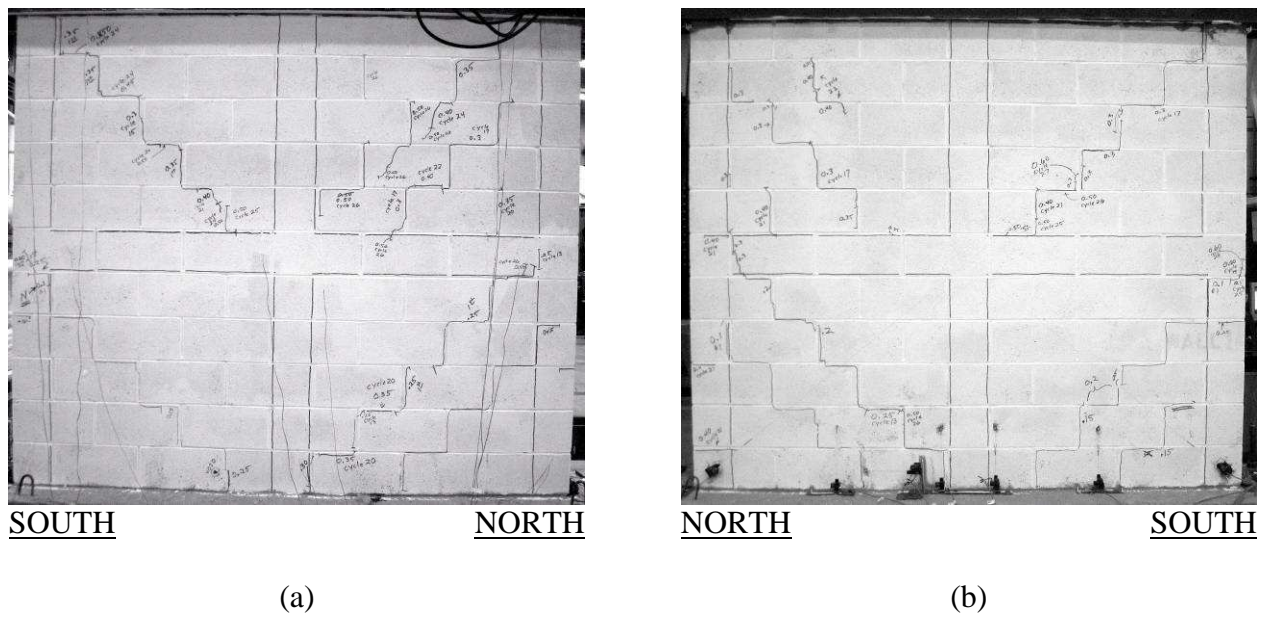
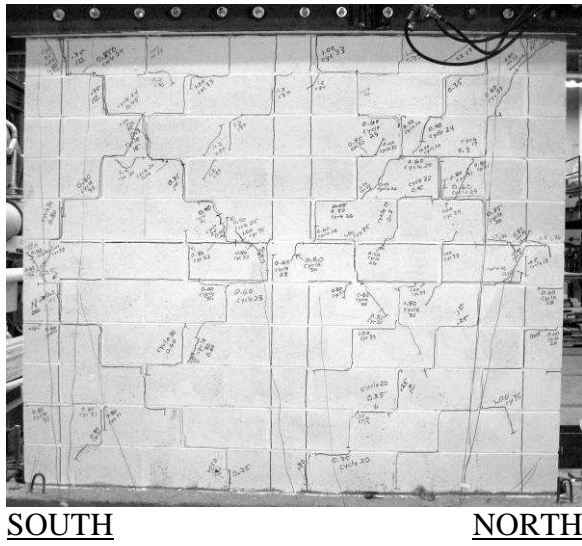
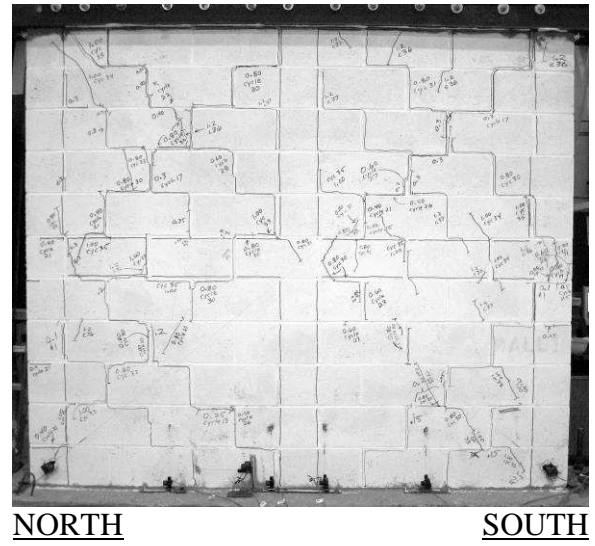


Figure 3-2: Specimen PG085-48, location of first crack at a drift of 0.11% (9.0 kips (40.0 kN)),
 (a) east face, (b) west face. Crack opened with a N = north push, S = south pull.



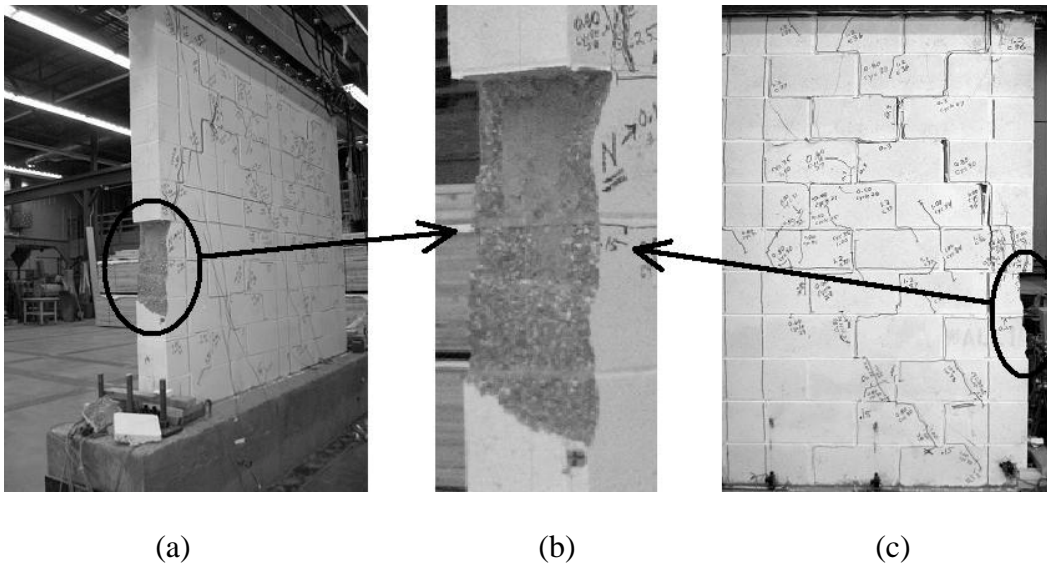


(c)



(d)

Figure 3-3: Specimen PG085-48, left/right are east/west faces, respectively, after testing to a drift of: (a/b) 0.65% (34.8 kips (155 kN)), and (c/d) 1.5% (42.7 kips (190 kN))



(a)

(b)

(c)

Figure 3-4: Specimen PG085-48, south end cracking and damage to CMU courses 3, 4 and 5 during testing, (a) east face and south end, (b) south end close-up, and (c) west face

3.2.3 Specimen PG120-48

Specimen PG120-48 was a partially grouted wall constructed with 48 in. (1219 mm) grout horizontal spacing and a single #6 rebar in each bond beam ($\rho_h = 0.120\%$). Figure 3-5 shows the extent of cracking of specimen PG120-48 after testing to a drift of 0.11% (8.7 kips (38.7 kN)). Figure 3-6 shows the extent of cracking of specimen PG120-48 after testing to a drift of: (a/b) 0.65% (32.1 kips (143 kN)), (c/d) end of test at 1.5% (44.8 kips (199 kN)). The first cracks were stair-step cracks passing through the mortar bed and head-joints in the bottom panels in the south and north directions, respectively, when pushing and pulling the specimen to a drift of 0.11% (8.7 kips (38.7 kN)). During pushing the specimen to a drift of 0.16% (11.6 kips (51.6 kN)), a horizontal crack on the south end, between courses 5 and 6, developed. During testing to a drift of 0.27% (18.6 kips (82.7 kN)), stair-step cracks in the mortar bed and head-joints developed in the upper panels and a 45° crack developed through the last cell of the southern-most CMU in the middle bond beam. Additional 45° cracks developed in the bond beam and the top masonry panels as testing continued. During pulling to a drift of 0.87% (39.1 kips (174 kN)), a vertical crack appeared in the face shell of the southern-most CMU of the middle bond beam. More 45° cracks developed in the mortar joints and masonry units until a drift of 1.5% (44.8 kips (199 kN)) at which point the wall reached its peak strength. A significant vertical splitting crack in the south end shell formed while pulling to a drift of 1.5%. By the end of the 3rd cycle at a drift of 1.5%, significant cracks developed in the wall (Figure 3-6c/d) and the lateral strength dropped by an average of approximately 19%. The test was ended at this point. At the termination of the test, the east side face-shells and end-shells of masonry units in courses 3 through 6 were found to be detached from the wall but still resting in place. Figure 3-7 shows the south end and a close-up of the damage after the detached masonry was removed. Note that all panels have 45°

cracks developed for north and south forces, indicative of the formation of compression struts within the panel.

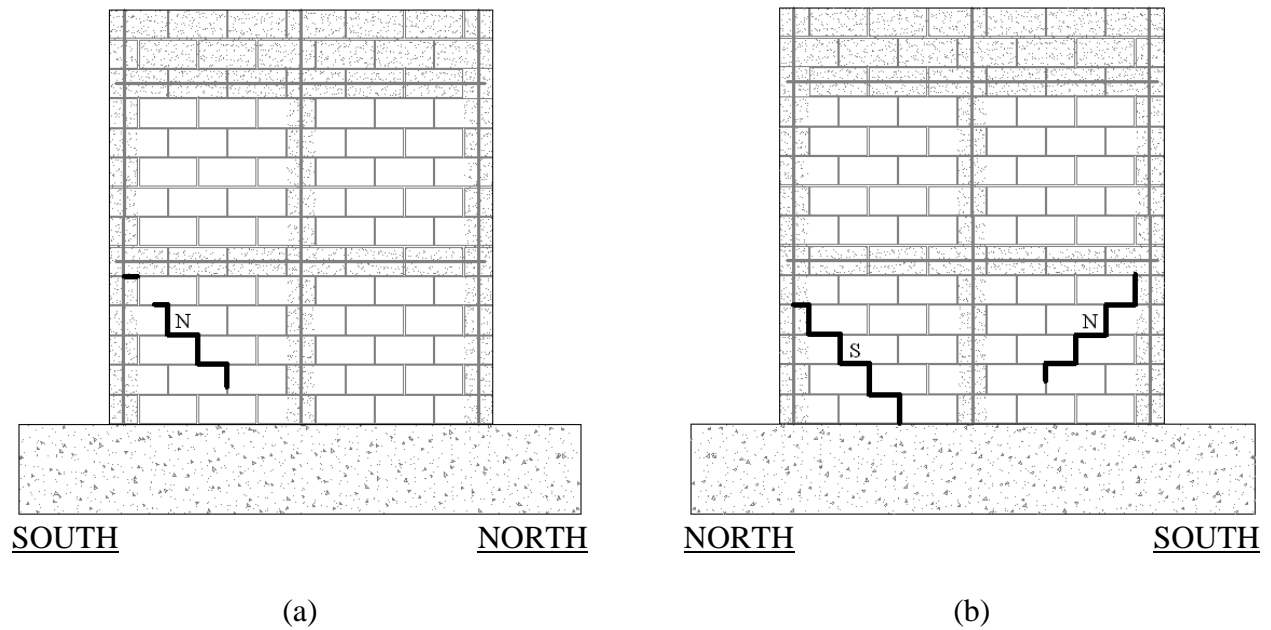
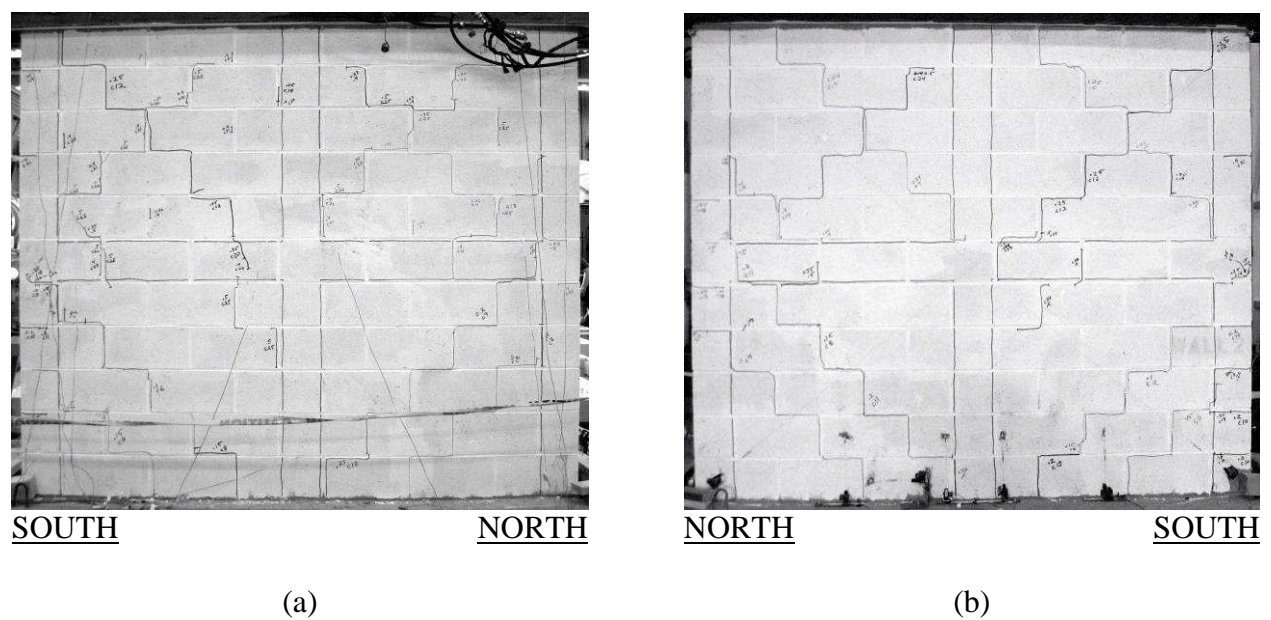
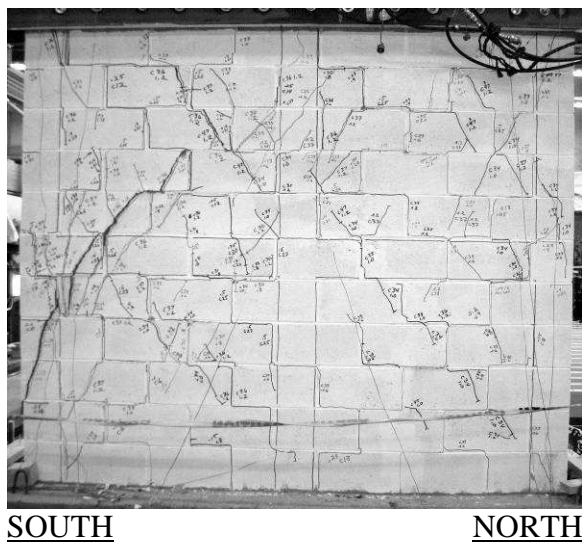
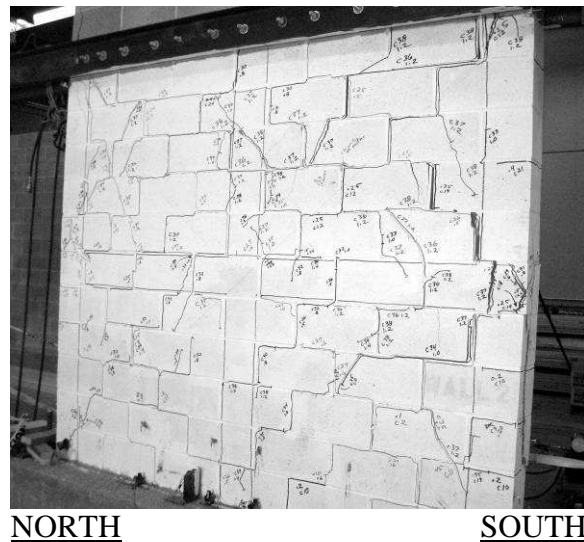


Figure 3-5: Specimen PG120-48, location of first crack at a drift of 0.11% (8.7 kips (38.7 kN)), (a) east face, and (b) west face. Crack opened with a N = north push, S = south pull.



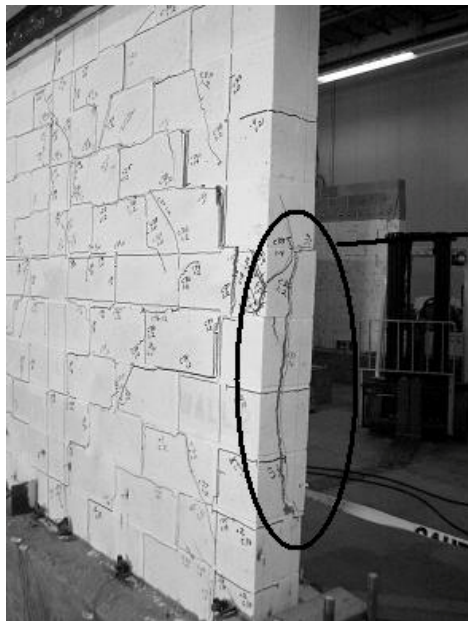


(c)

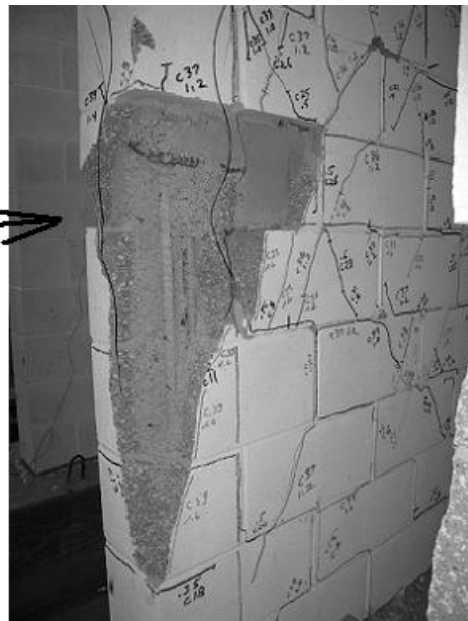


(d)

Figure 3-6: Specimen PG120-48, left/right are east/west faces, respectively, after testing to a drift of: (a/b) 0.65% (32.1 kips (143 kN)), and (c/d) 1.5% (44.8 kips (199 kN))



(a)



(b)

Figure 3-7: Specimen PG120-48, state of damage to south end at end of test, (a) south end and west face, and (b) south end and east face with detached masonry removed

3.2.4 Specimen PG169-48

Specimen PG169-48 was a partially grouted wall constructed with 48 in. (1219 mm) grout horizontal spacing and two #5 rebar in each bond beam ($\rho_h = 0.169\%$). Figure 3-8 shows the extent of cracking of specimen PG169-48 after testing to a drift of 0.05% (7.5 kips (33.4 kN)). Figure 3-9 shows the extent of cracking of specimen PG169-48 after testing to a drift of: (a/b) 0.65% (45.7 kips (203 kN)), and (c/d) 0.87% (35.7 kips (159 kN)).

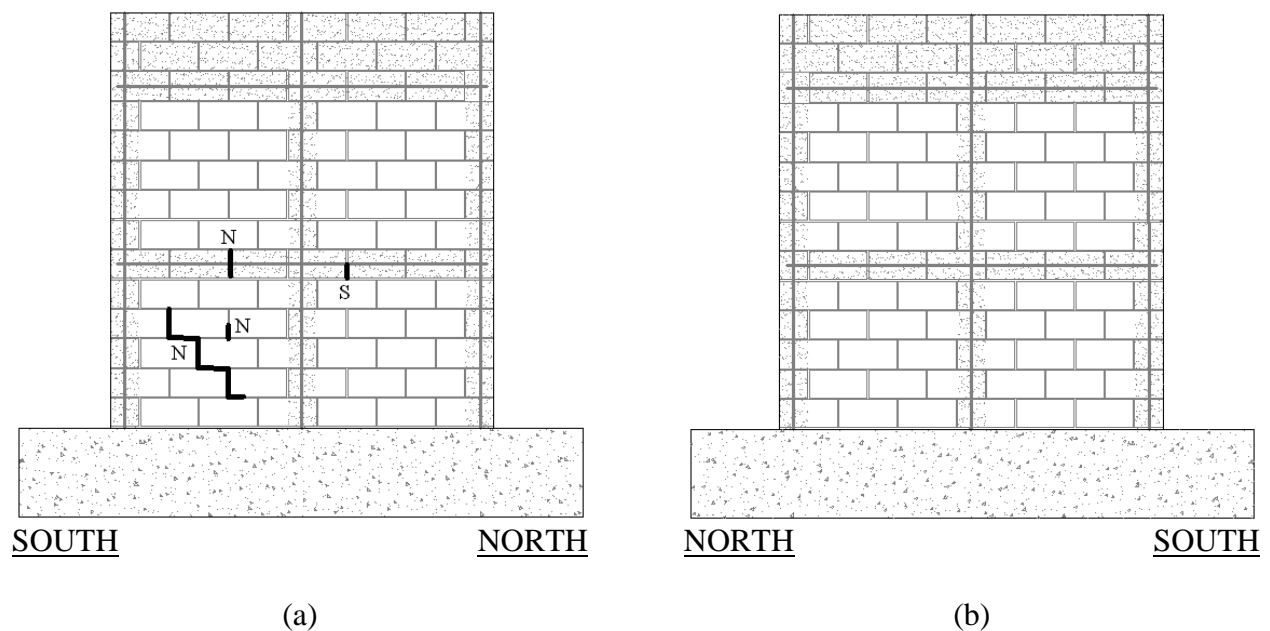
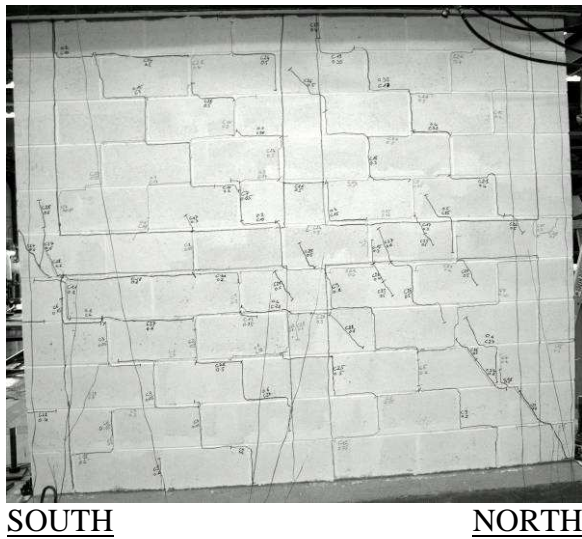


Figure 3-8: Specimen PG169-48, location of first crack at a drift of 0.05% (7.5 kips (33.4 kN)),

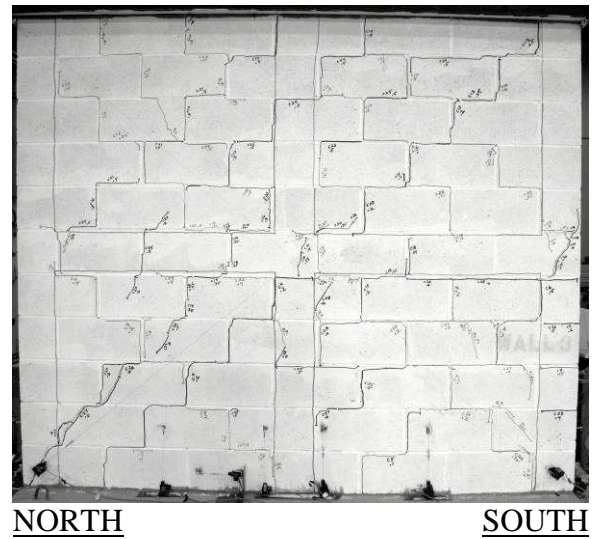
(a) east face, and (b) west face. Crack opened with a N = north push, S = south pull.

The first main crack was a stair-step crack and it appeared in the lower south masonry panel during pushing to a drift of 0.05% (7.5 kips (33.4 kN)). Stair-step cracks had formed in all lower panels on or before testing to a drift of 0.22% (21.3 kips (94.7 kN)). During testing to a drift of 0.22%, stair-step cracks from north and south forces formed in the upper panels. During

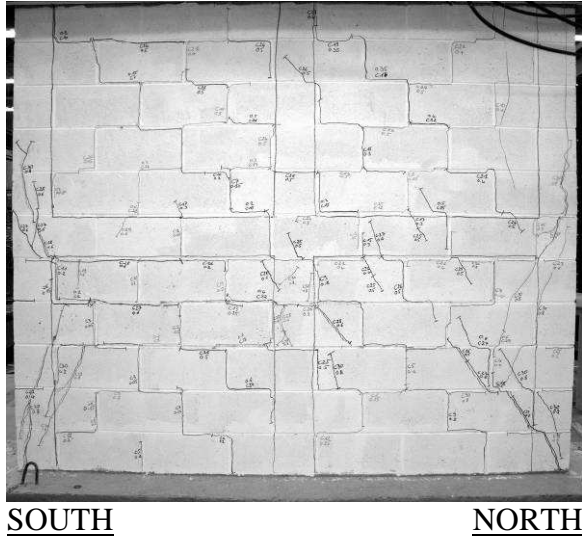
testing to a drift of 0.54% (41.6 kips (185 kN)), a vertical crack in the face shell of a masonry unit developed in the last unit at the south end of the 7th course (Figure 3-10). The initial cracking was similar to the south-end failures of PG085-48 and PG120-48 that led to the detachment of masonry. By a drift of 0.65% (45.7 kips (203 kN)), the specimen reached its peak lateral strength. In addition, cracks passing through the masonry units at the sound end formed a pattern similar to previous south-end splitting failures (Figure 3-10). During testing to a drift of 0.87% (35.7 kips (159 kN)), an approximate 22% drop occurred in the lateral strength of the specimen and the test was stopped (Figure 3-9c/d).



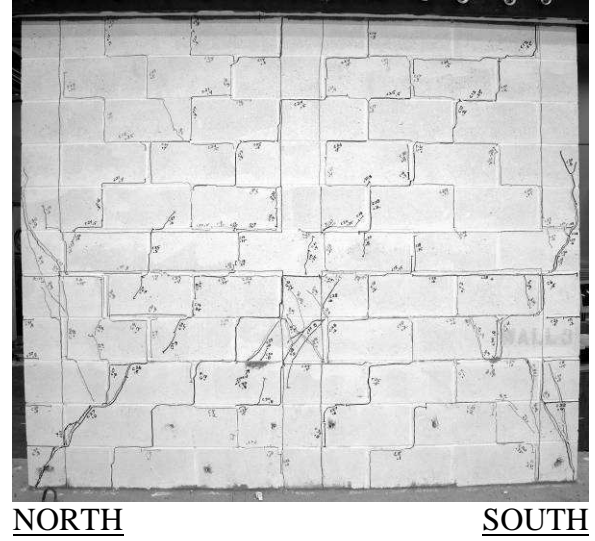
(a)



(b)

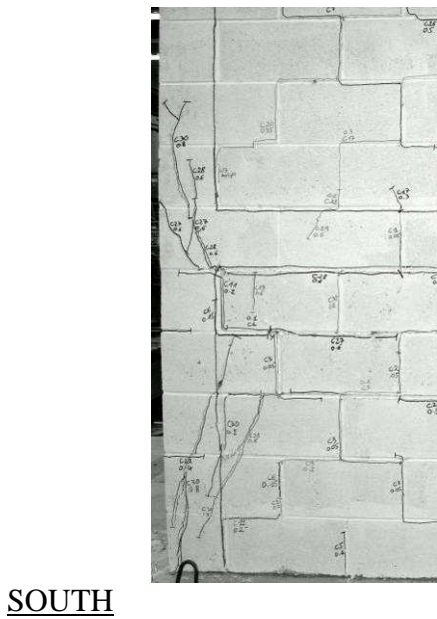


(c)

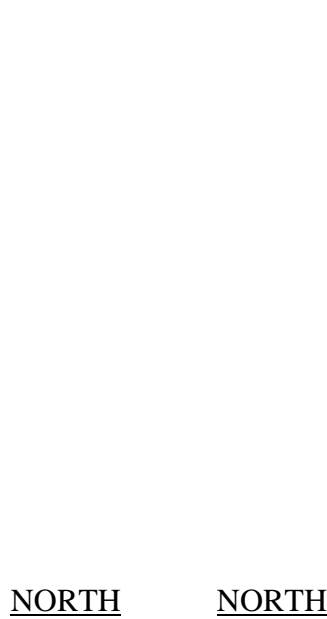


(d)

Figure 3-9: Specimen PG169-48, left/right are east/west faces, respectively, after testing to a drift of: (a/b) 0.65% (45.7 kips (203 kN)), and (c/d) 0.87% (35.7 kips (159 kN))



(a)



(b)

Figure 3-10: Specimen PG169-48, cracking at south end mid-height,

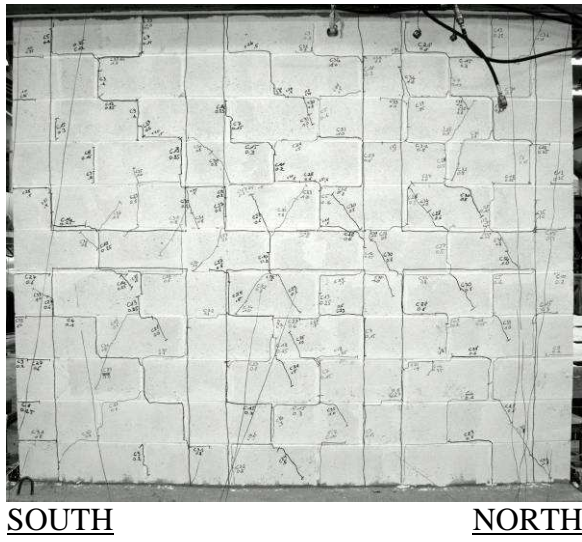
(a) east side, and (b) west side

3.2.5 Specimen PG085-32

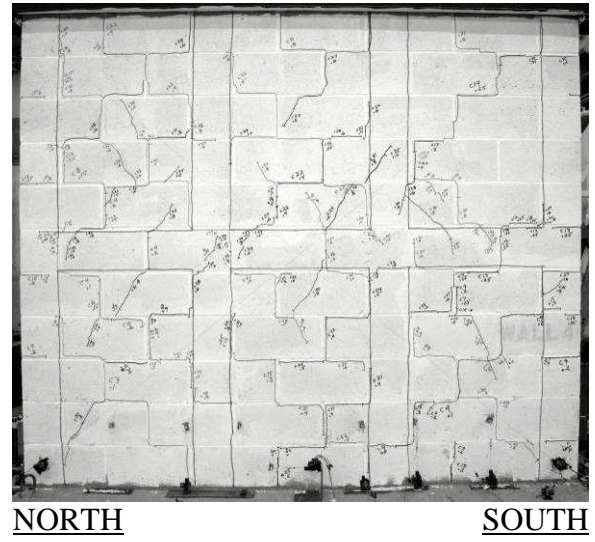
Specimen PG085-32 was a partially grouted wall constructed with 32 in. (813 mm) grout horizontal spacing and a single #5 rebar in each bond beam ($\rho_h = 0.085\%$). Figure 3-11 shows the extent of cracking of specimen PG085-32 after testing to a drift of 0.11% (8.8 kips (39.1 kN)). Figure 3-12 shows the extent of cracking on the east and west faces, respectively, of specimen PG085-32 after testing to a drift of: (a/b) 0.65% (39.7 kips (177 kN)), (c/d) 1.3% (58.5 kips (260 kN)), and (e/f) 1.5% (53.3 kips (237 kN)). The first cracks were stair-step cracks passing through the mortar bed and head-joints and appeared at a drift of 0.11% (8.8 kips (39.1 kN)) in the outermost bottom panels in the south and north directions when pushing and pulling the specimen, respectively (Figure 3-11). In addition, several vertical cracks in the mortar head-joints formed in the upper south and middle panels. As testing continued, additional 45° stair-step cracks developed in the lower masonry panels. While testing to a drift of 0.87% (47.8 kips (213 kN)), 45° cracks developed in the upper north panel. As testing continued, 45° cracks developed through the masonry units and bed and head-joints in all panels. The specimen reached its peak lateral load at a drift of 1.3% (58.5 kips (260 kN)) and a significant diagonal crack passing through masonry units and mortar joints developed along the full diagonal length of the upper south masonry panel. As the applied lateral drift increased to 1.5% (53.3 kips (237 kN)), this crack extended and became a vertical splitting crack passing through the middle bond beam all way through the 3rd brick course. Also, significant 45° cracks passing through the bond beam and face shells in the north-end masonry panels developed (Figure 3-13). These significant cracks led to an approximate reduction of the lateral strength of the specimen by 23%. Figure 3-12(e/f) shows the state of cracking at the end of the test. Note that all panels have 45° cracks developed for north and south forces, indicative of the formation of compression struts within the

(a)

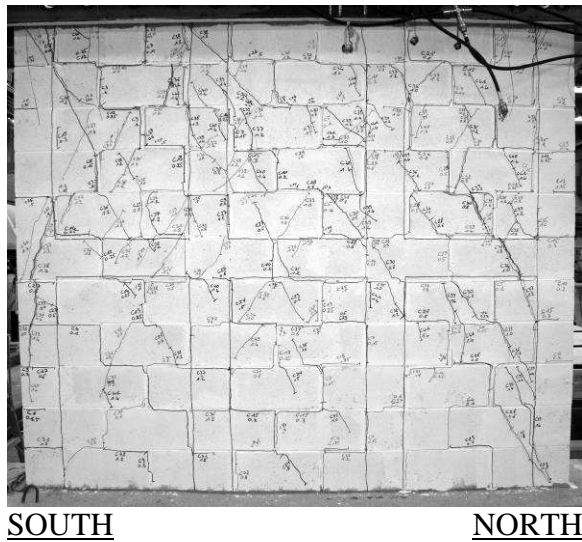
(b)



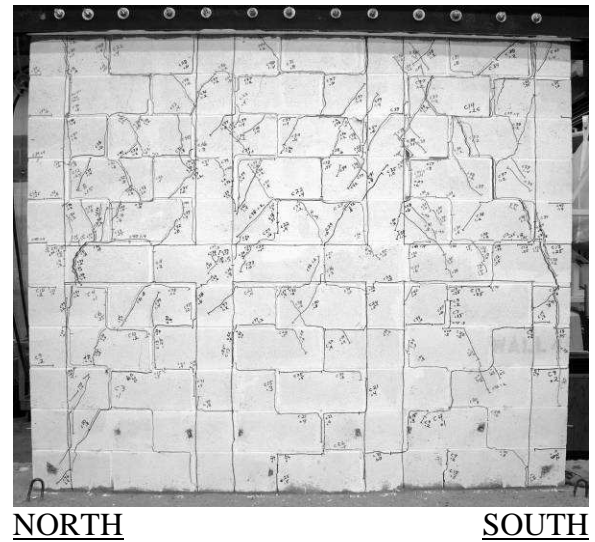
(c)



(d)



(e)



(f)

Figure 3-12: Specimen PG085-32, left/right are east/west faces, respectively, after testing to a drift of: (a/b) 0.65% (39.7 kips (177 kN)), (c/d) 1.3% (58.5 kips (260 kN)), and (e/f) 1.5% (53.3 kips (237 kN))

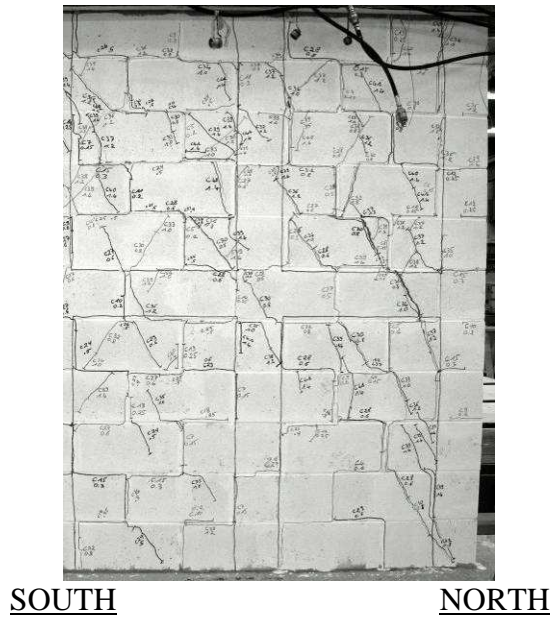


Figure 3-13: Specimen PG085-32, east face, north end cracking at a drift of 1.5%

3.2.6 Specimen PG085-24

Specimen PG085-24 was a partially grouted wall constructed with 24 in. (610 mm) grout horizontal spacing and a single #5 rebar in each bond beam ($\rho_h = 0.085\%$). Figure 3-16 shows the extent of cracking on the east and west faces, respectively, of specimen PG085-24 after testing to a drift of: (a/b) 0.65% (38.2 kips (170 kN)), (c/d) 1.3% (60.5 kips (269 kN)), and (e/f) 1.7% (54.2 kips (241 kN)).

Unique to specimen PG085-24 were minor stair-step cracks that developed while moving the specimen into the testing frame. Cracks developed in the lower northern and southern most panels (Figure 3-14). Once testing commenced, the first new crack was a vertical crack in the middle bond beam that formed while pushing the specimen to a drift of 0.05% (4.3 kips (19.1 kN)) (Figure 3-15).

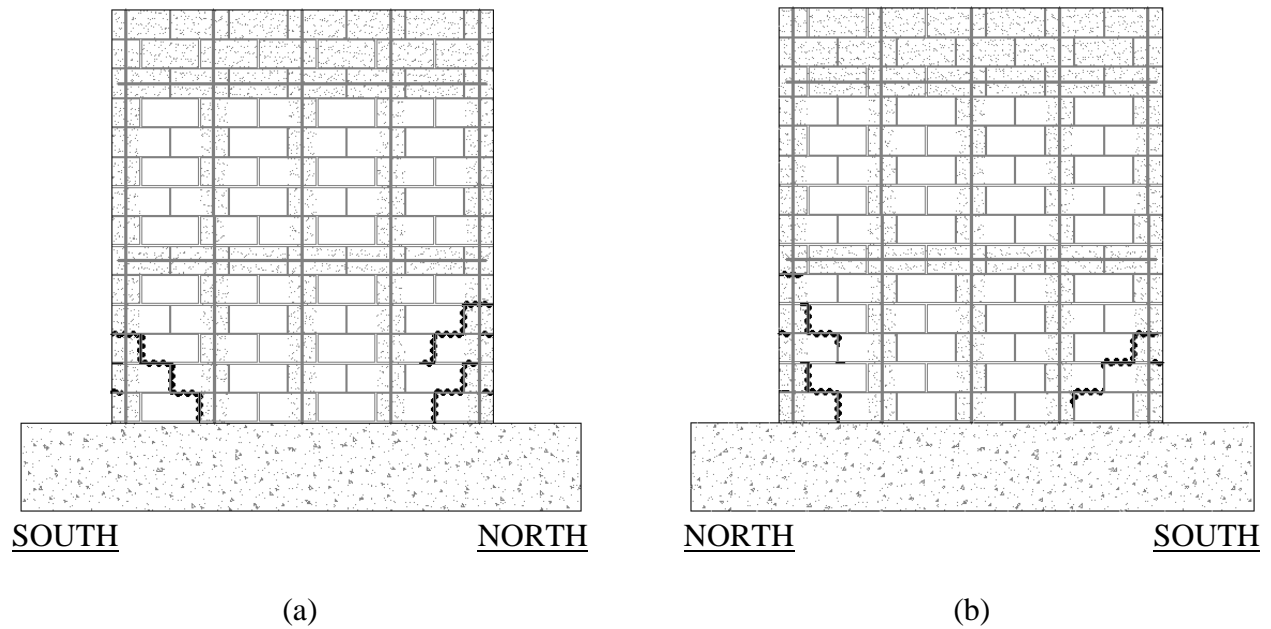


Figure 3-14: Specimen PG085-24 cracking prior to testing, (a) east face, and (b) west face

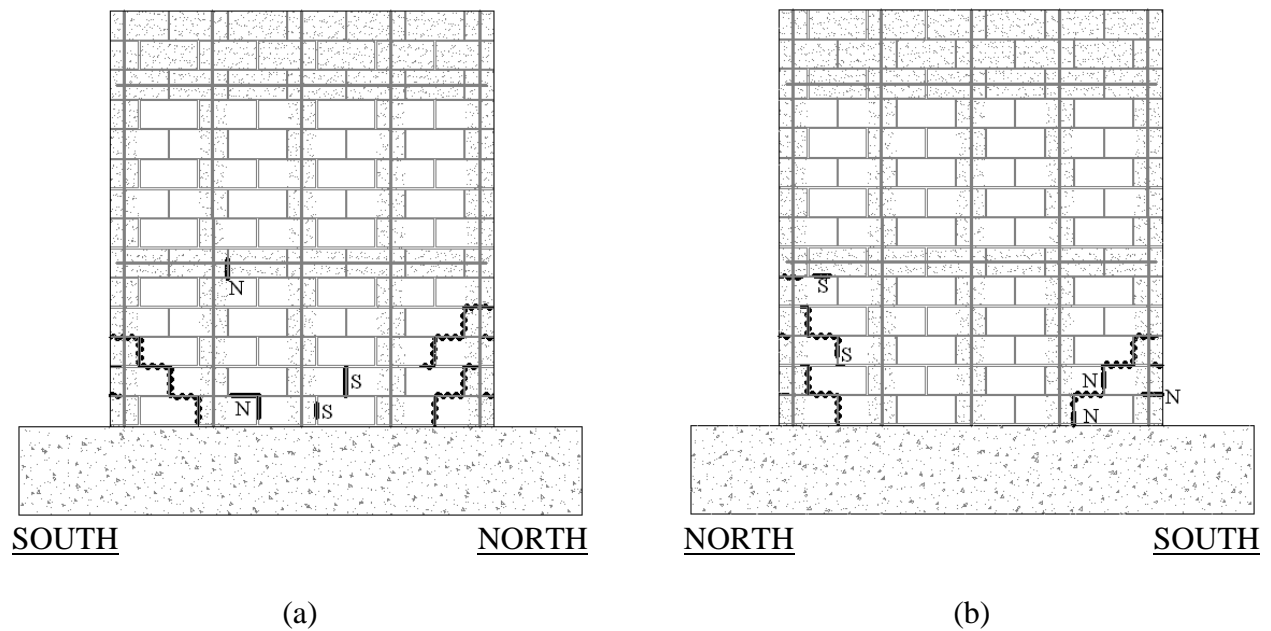
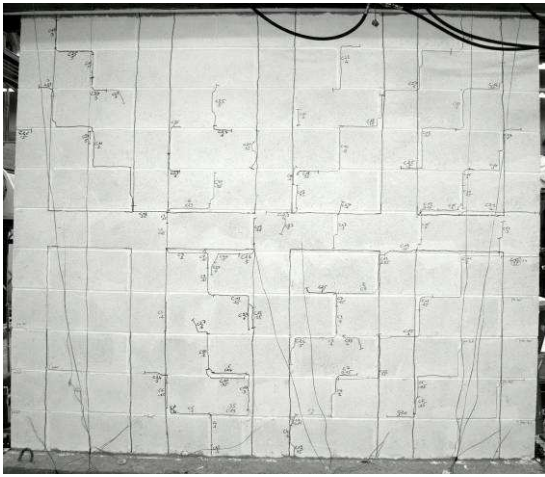


Figure 3-15: Specimen PG085-24, location of first crack at a drift of 0.05% (4.3 kips (19.1 kN)),

(a) east face, and (b) west face. Jagged lines represent pre-test cracks.

Crack opened with a N = north push, S = south pull.

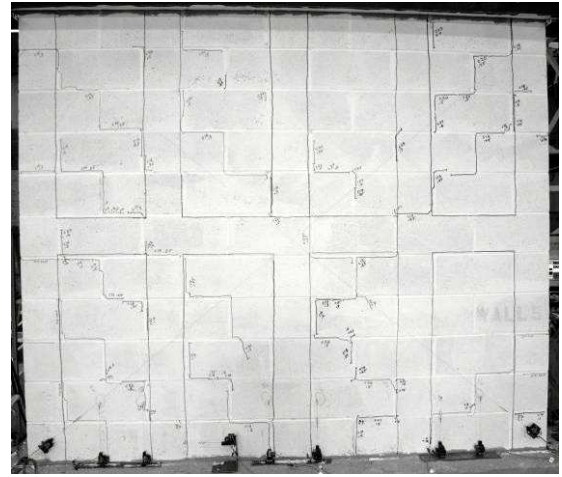
While pulling the specimen to a drift of 0.11% (8.5 kips (37.8 kN)), vertical and horizontal cracks in a few mortar head and bed-joints appeared in the lower northern panel. While testing to a drift of 0.22% (16.2 kips (72.1 kN)), stair-step cracks developed in the upper panels. While testing to a drift of 0.27% (19.1 kips (85.0 kN)), horizontal cracks in the bed-joints between the 5th and 6th courses appeared. As testing continued, 45° cracks developed through the masonry units in all panels. While testing to a drift of 1.1% (54.0 kips (240 kN)), diagonal cracks formed in the east and west face shells in the bond beam and in the upper southern outside panel. While testing to a drift of 1.3% (60.5 kips (269 kN)), a vertical splitting crack on the south end formed in the end shell at the 6th course. While testing to a drift of 1.5% (66.4 kips (295 kN)), the specimen reached its peak strength and the diagonal cracks, that started at a drift of 1.1%, extended down into the lower southern panel. These cracks opened significantly while testing to a drift of 1.7% (54.2 kips (241 kN)) leading to reduction in the lateral strength of the specimen by an average of 19%. In addition, the splitting crack in the south end shells extended along the height of four masonry units. Figure 3-17(a/b) shows the cracking on the south end of the wall and the east and west faces, respectively. Figure 3-16(e/f) shows the state of cracking at the end of the test. Note that all panels have 45° cracks developed for north and south forces, indicative of the formation of compression struts within the panel.



SOUTH

NORTH

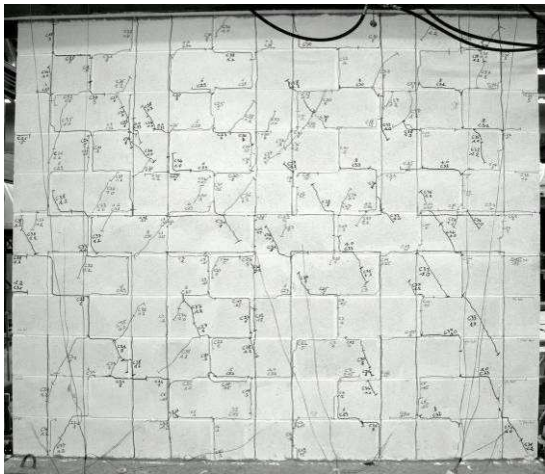
(a)



NORTH

SOUTH

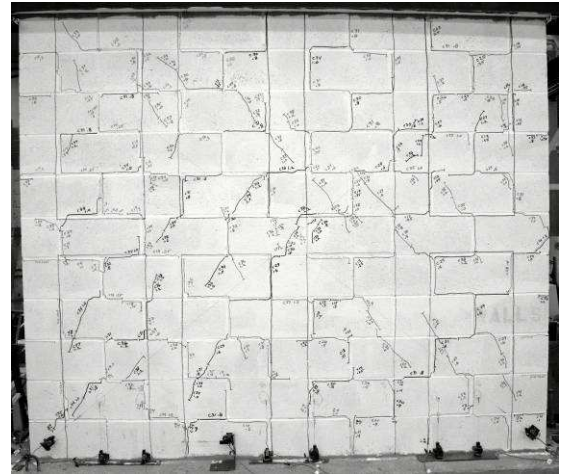
(b)



SOUTH

NORTH

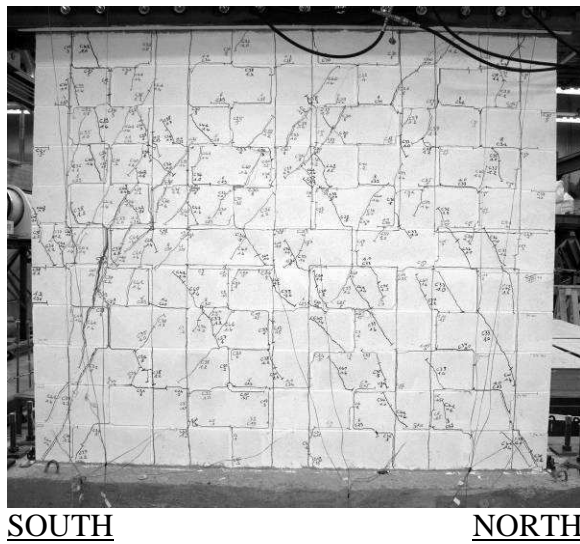
(c)



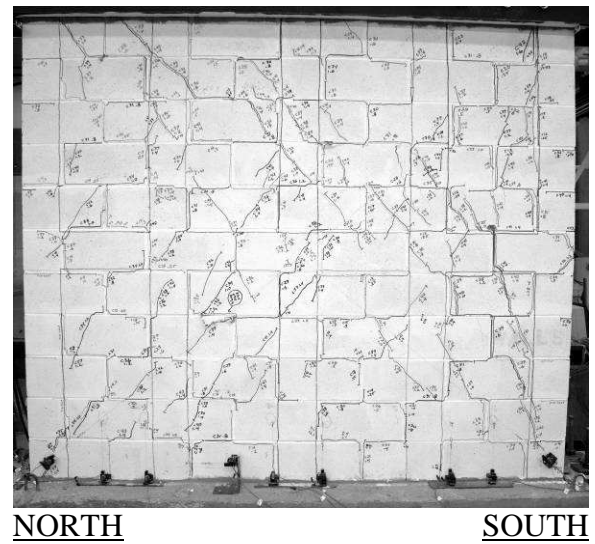
NORTH

SOUTH

(d)

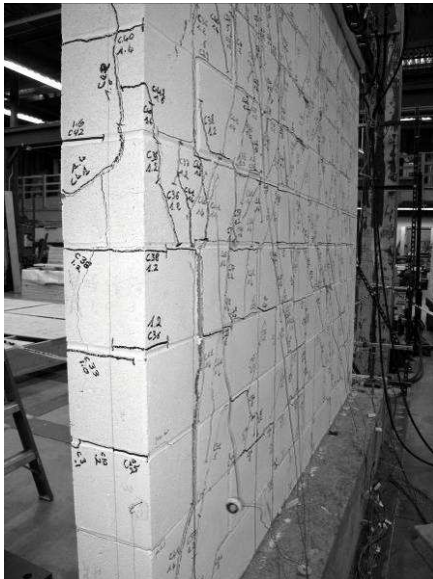


(e)

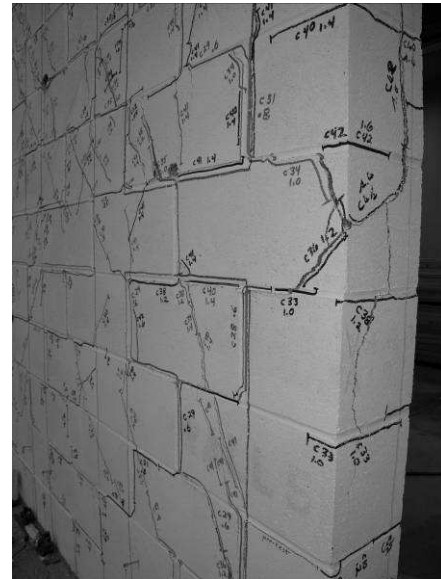


(f)

Figure 3-16: Specimen PG085-24, left/right are east/west faces, respectively, after testing to a drift of: (a/b) 0.65% (38.2 kips (170 kN)), (c/d) 1.3% (60.5 kips (269 kN)), and (e/f) 1.7% (54.2 kips (241 kN))



(a)



(b)

Figure 3-17: Specimen PG085-24 south end damage after testing, (a) south end with east face, and (b) south end with west face

3.2.7 Specimen FG085-00

Specimen FG085-00 was a *fully* grouted wall constructed with 48 in. (1219 mm) spacing between the flexural reinforcement and a single #5 rebar in each bond beam ($\rho_h = 0.085\%$). Figure 3-18 shows the extent of cracking of specimen FG085-00 after testing to a drift of 0.11% (9.0 kips (40.4 kN)). Figure 3-19 shows the extent of cracking on the east and west faces, respectively, of specimen FG085-00 after testing to a drift of: (a/b) 0.65% (60.4 kips (269 kN)), (c/d) 1.3% (69.6 kips (310 kN)). The cracking pattern of specimen FG085-00 did not follow the typical pattern seen for the partially grouted specimens. The first crack was a vertical crack in a head-joint in the middle bond beam and it appeared while pushing the specimen to a drift of 0.11% (13.4 kips (59.6 kN)) (Figure 3-18). While pushing the wall to a drift of 0.22% (25.8 kips (115 kN)), a horizontal crack between the 6th and 7th courses starting from the south end and extended to the mid-point of the wall cross section. The crack location corresponds to the interface between the 1st and 2nd grout lifts during construction.

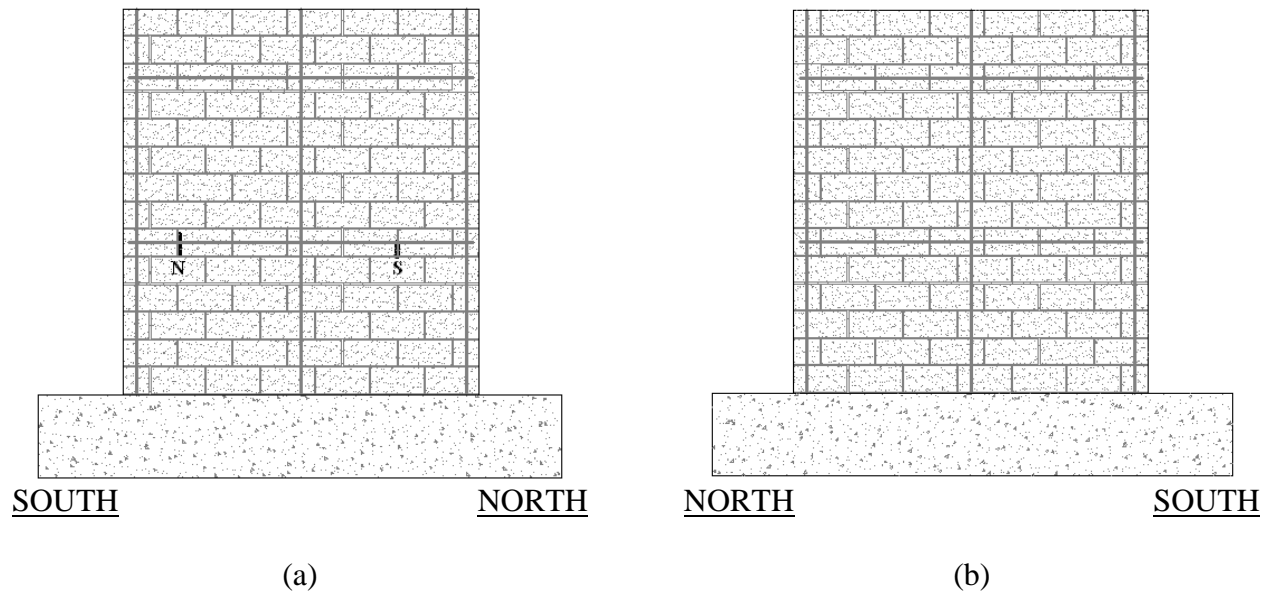
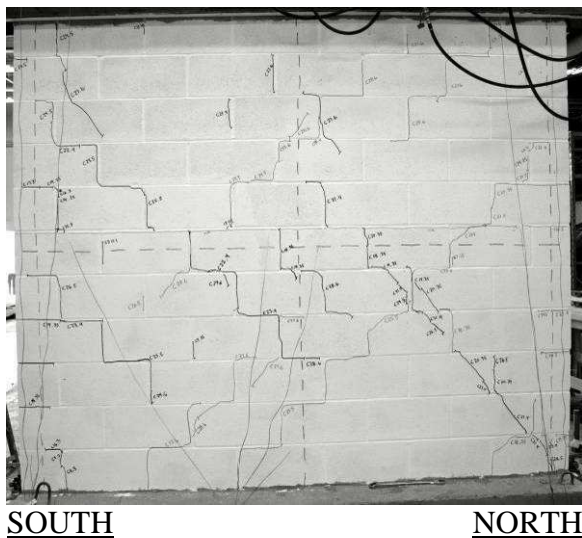
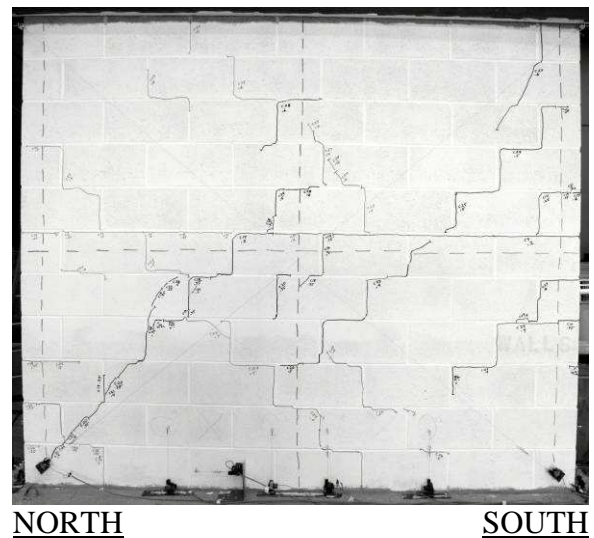


Figure 3-18: Specimen FG085-00, location of first crack at a drift of 0.11% (9.0 kips (40.0 kN)), (a) east face, and (b) west face. Crack opened with a N = north push, S = south pull.

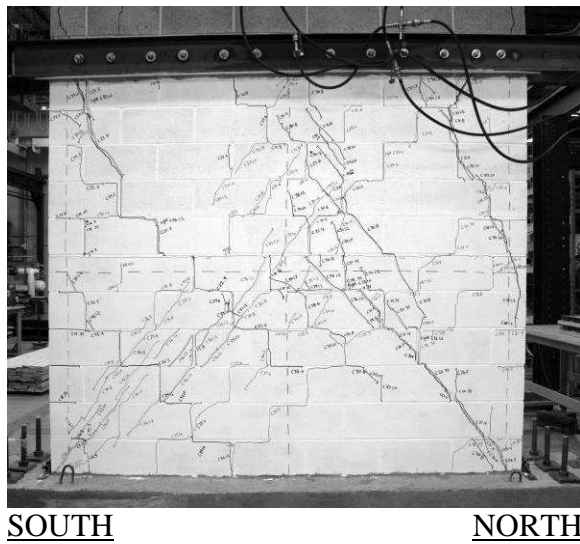
While testing to a drift of 0.38% (42.5 kips (189 kN)), a major crack formed along a line from the center of the 7th course to the north toe. The crack consisted of multiple 45° cracks passing through bed and head-joints as well as the masonry units. A similar crack extended through the center of the wall to the south toe at a drift of 0.65% (60.4 kips (269 kN)). A 45° crack extended from the top north to the center of the wall at a drift of 0.87% (67.5 kips (300 kN)). Also, an inclined steep crack extended from the top north through the end of the bond beam at the north end (Figure 3-20). At a drift of 1.1% (74.7 kips (332 kN)), the peak force was achieved. At a drift of 1.3% (69.6 kips (310 kN)), approximately 22% drop in the lateral strength of the test specimen occurred. Figure 3-19(c/d) shows the state of cracking at the end of the test. Figure 3-20 shows an enlarged view of the cracking at the north end of the test specimen.



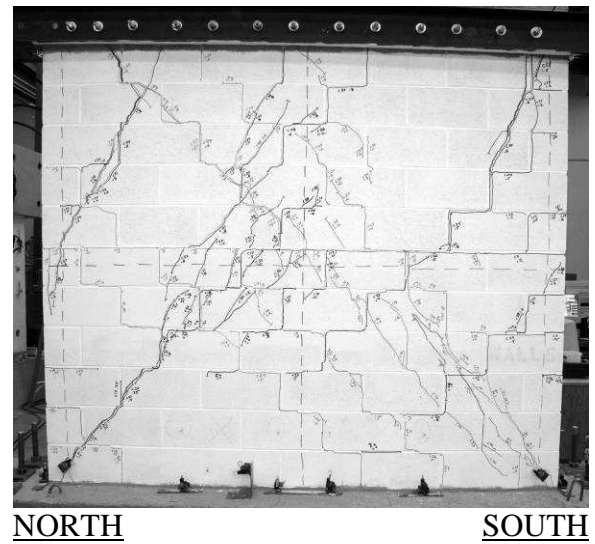
(a)



(b)

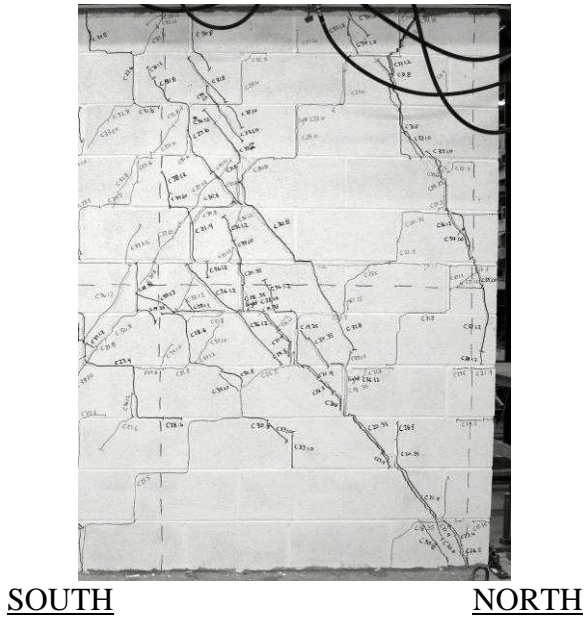


(c)

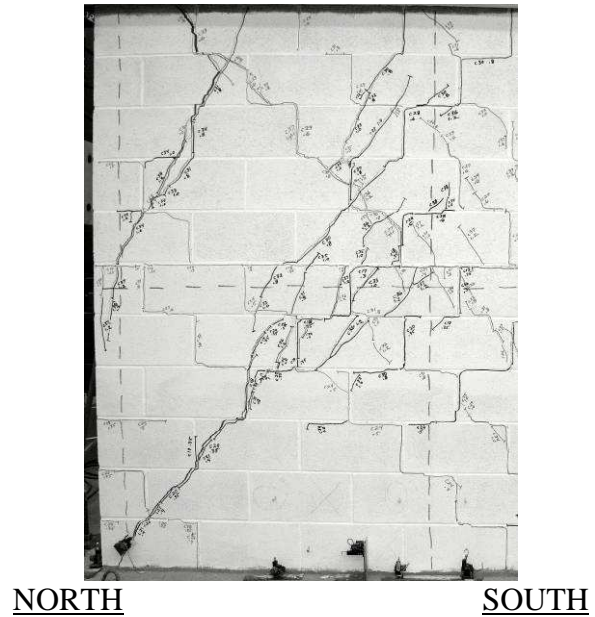


(d)

Figure 3-19: Specimen FG085-00, left/right are east/west faces, respectively, after testing to a drift of: (a/b) 0.65% (60.4 kips (269 kN)), and (c/d) 1.3% (69.6 kips (310 kN))



(a)



(b)

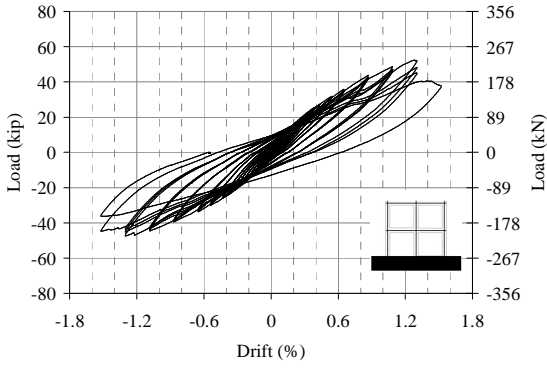
Figure 3-20: Specimen FG085-00 cracking in north half of wall after testing, (a) east face, and (b) west face

3.2.8 Hysteretic Performance Of The Test Specimens

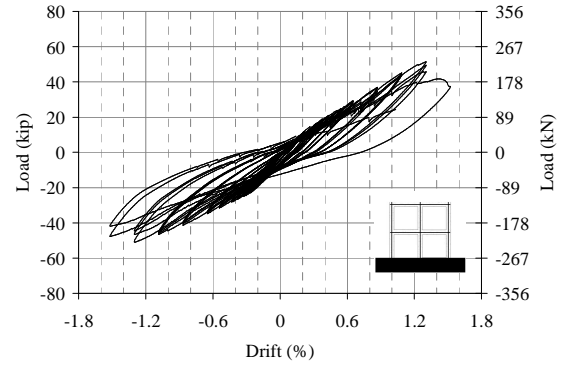
The load-drift hysteretics are shown in Figure 3-21 and the experimental backbone curves and idealized backbone curves are shown in Figure 3-22. The hysteretic response was obtained by plotting the measured lateral forces from the load cell of the actuator versus the measured displacement at 12th masonry course. A backbone curve was obtained using the procedure from Chapter 2 of FEMA 356: "A smooth backbone curve shall be drawn through the intersection of the first cycle curve for the (i)th deformation step with the second cycle curve of the (i-1)th deformation step, for all i steps". In addition, an elastic-perfectly plastic bilinear approximation of each backbone curve is presented. The idealized backbone curve was used to investigate the effects of the different test parameters on the displacement ductility, initial stiffness, and yield stiffness of each specimen. The elastic segment of the bilinear approximation was determined by a line connecting the origin point to the point of V_{max} through the point of $0.75 V_{max}$ on the backbone curve where V_{max} is the strength of the wall under consideration (Figure 3-23). The plastic segment of the bilinear idealization was selected as perfectly plastic i.e. with zero post-elastic stiffness with peak strength of V_{max} . Similar idealization was used by several researchers in the literature (e.g. Wight et al. 2007). The exact absorbed energy and the approximate absorbed energy, i.e. respective areas under the wall response backbone curve and the bilinear approximation, were compared for all specimens and the differences were found to be less than 5%.

As shown in Figure 3-21, the hysteretic behavior of all specimens was similar. All specimens displayed stable symmetrical hysteresis loops with relatively narrow loops before reaching its ultimate lateral strength at lateral drifts of approximately 1.1 to 1.5% except for specimen PG169-48. Specimen PG169-48 reached its ultimate lateral strength at a lateral drift of

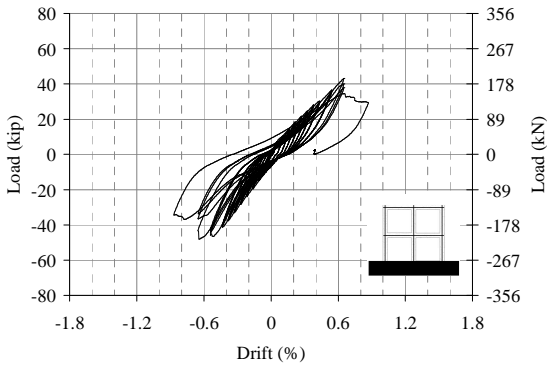
approximately 0.54%. The specimens behaved approximately linear elastic until lateral drifts of 0.05 to 0.11% where the first shear crack occurred. Beyond that the stiffness of the specimen degraded with the specimen still able to carry the applied lateral and vertical forces. Once the specimen started the nonlinear inelastic behavior the residual drift values increased. At the end of the tests the average residual drift value was approximately 35% of the applied peak lateral drift. Once the specimens reached their peak strengths, the strengths degraded very quickly and testing was terminated when the lateral resistance of the specimens dropped by approximately 20% of the peak strength. The specimen was considered to have reached failure at the 20% drop from peak lateral strength. The specimens failed at lateral drifts of approximately 1.3 to 1.7% except for specimen PG169-48 which failed at a lateral drift of 0.87%.



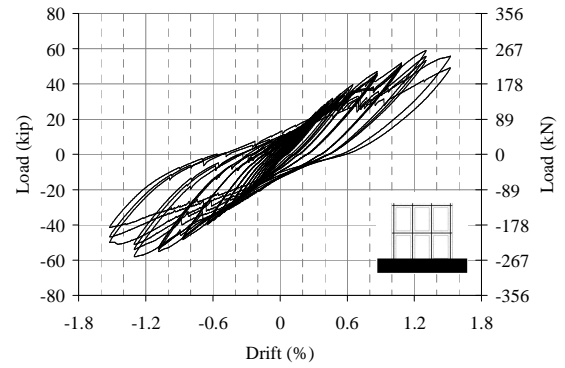
(a)



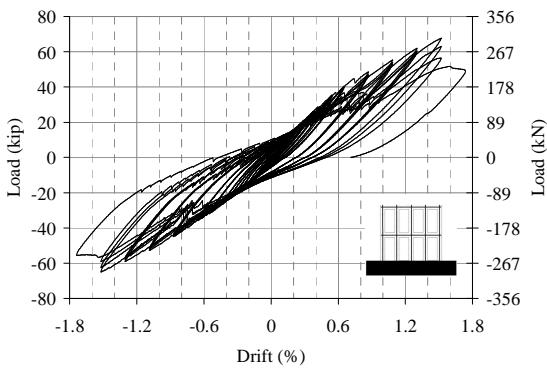
(b)



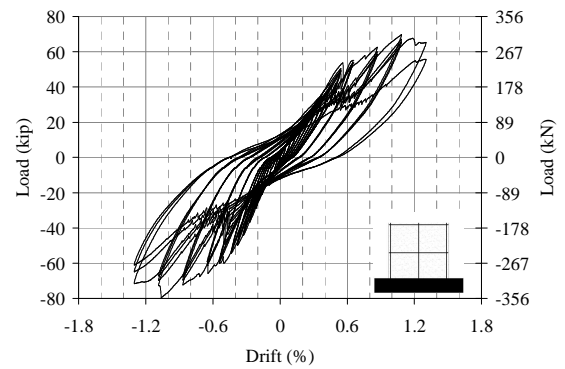
(c)



(d)

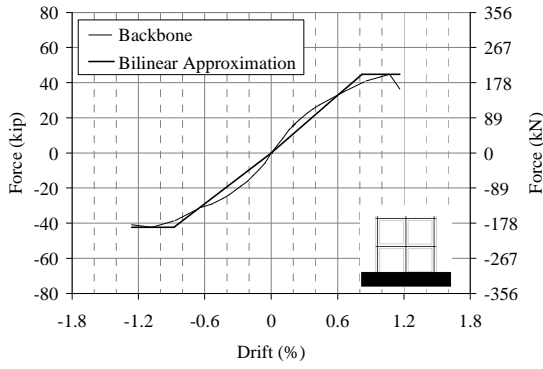


(e)

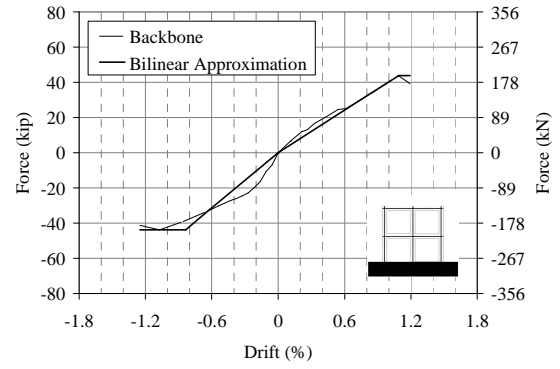


(f)

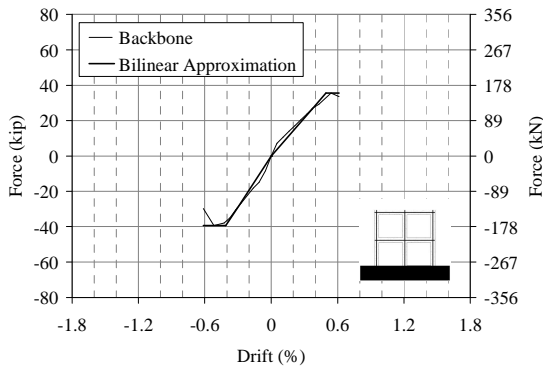
Figure 3-21: Lateral force vs. lateral drift for specimens (a) PG085-48, (b) PG120-48, (c) PG169-48, (d) PG085-32, (e) PG085-24, and (f) FG085-00



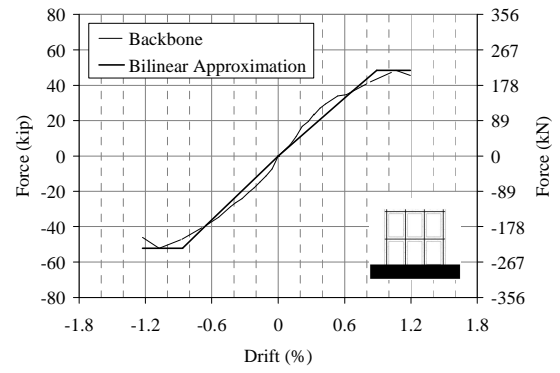
(a)



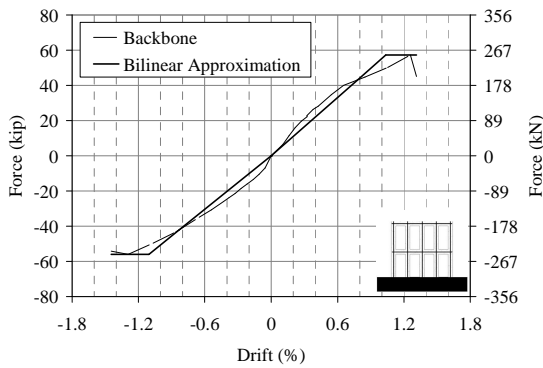
(b)



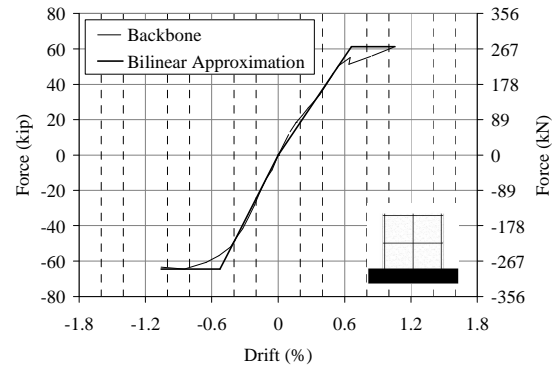
(c)



(d)



(e)



(f)

Figure 3-22: Backbone curve and bilinear idealization for specimens (a) PG085-48, (b) PG120-48, (c) PG169-48, (d) PG085-32, (e) PG085-24, and (f) FG085-00

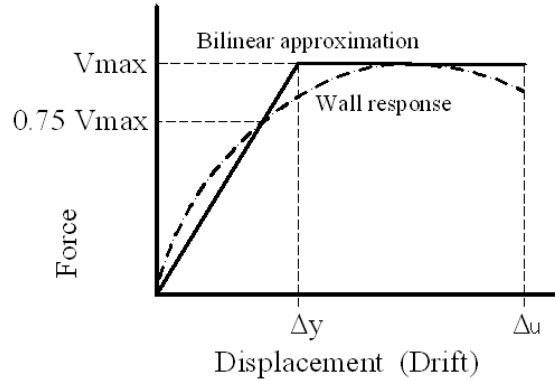


Figure 3-23: Bilinear approximation of backbone curve

3.2.9 Lateral Load vs. Steel Strains

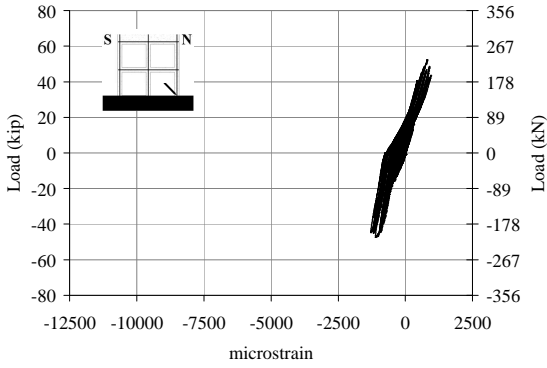
As explained in Chapter 2, strain gages were used to measure the strains on the flexural rebar just above the foundation level. For every specimen, the data of one strain gage that measured the maximum axial strain on the flexural rebar is presented in Figure 3-24 to indicate whether the flexural rebar yielded or not. The remaining measurements of strain gages on the flexural rebar are presented in Appendix E. Strain gage readings are positive for tension and negative for compression. As shown in the figure, the response of the flexural rebar in three specimens, namely PG085-48, PG085-32, and PG120-48, remained in the elastic range with measured ultimate strains of 1300, 2100, and 1500 which is approximately 59%, 96%, and 68% of the yield strains, respectively. For specimens PG169-48, PG085-24, FG085-00 the rebar remained elastic until the specimens reached their peak strength. Beyond that, the strains started to increase significantly and by the end of the test the ultimate strains in the flexural rebar for specimens PG-169-48, PG085-24, and FG085-00 were 3500, 4600, and 10300 micro-strains which is approximately 160%, 210%, and 470% of the yield strain, respectively.

The axial strains in the horizontal rebar in the top and middle bond beams were also measured using eight strain gages (see Chapter 2 for more details). For every specimen, the data

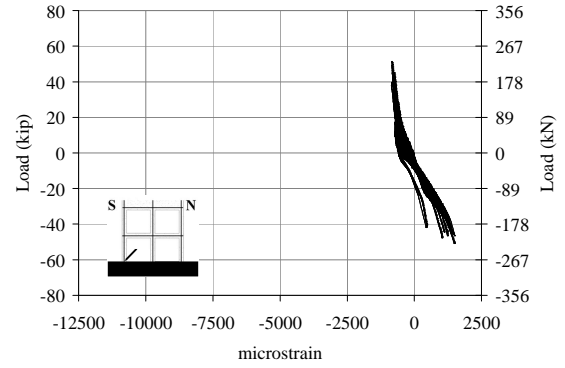
of one strain gage that measured the maximum axial strain in the shear rebar is presented to indicate whether the shear rebar yielded or not. The remaining measurements of strain gages on the shear rebar are presented in Appendix E. The lateral force vs. axial strain in the shear reinforcement is shown in Figure 3-25. As shown in the figure the response was stable and symmetric. For small applied lateral forces, the permanent dilation in the rebar (measured at zero lateral force) is small indicating minimal opening of shear cracks. Once the applied lateral force increased, the rate of increase in the axial strains in the rebar increased and the residual strains at zero lateral force increased indicating increase in the shear crack widths. For specimens having high shear reinforcement ratio, i.e. specimens PG169-48 and PG120-48, the rebar did not reach the yield strains with ultimate strains of 1100 and 1800 micro-strains which are approximately 50% and 82% of the yield strain of the rebar, respectively. By the end of the test, the residual strains in the shear rebar were approximately 200 and 500 micro-strains for specimens PG169-48 and PG120-48, respectively. For specimen PG085-48, the shear rebar reached a peak axial strain of 2600 micro-strain which is approximately 119% of the yield strain of the rebar. By the end of the test, the residual strain in the shear rebar was approximately 700 micro-strains.

The behavior of the shear rebar in specimens PG085-32, PG085-24, and PG085-00 was similar to the other three specimens. However, the ultimate strains were significantly higher than the yield strains with high residual strains. The ultimate strains were 7400, 7000, and 9900 micro-strain which are approximately 338%, 320%, and 452% of the yield strain of the rebar, respectively. By the end of the test, the residual strains in the shear rebar were approximately 4700, 5000, and 2100 micro-strains, respectively. Interestingly, using smaller horizontal spacing between the vertical grouted cells resulted in higher strains in the shear rebar in all specimens. In addition, for the two partially grouted specimens, the shear strengths started to degrade at a strain

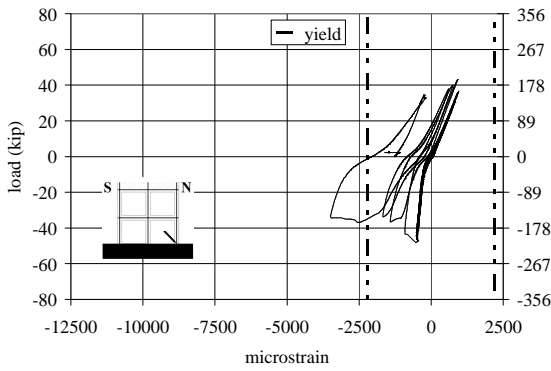
in the rebar of approximately 5000 micro-strains. It is worth noting that for reinforced concrete elements Priestley recommended a value of 0.004 strain beyond which the shear strength of the concrete starts to degrade (Priestley 1996).



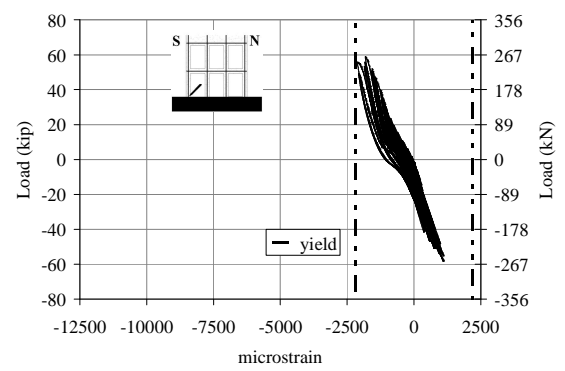
(a)



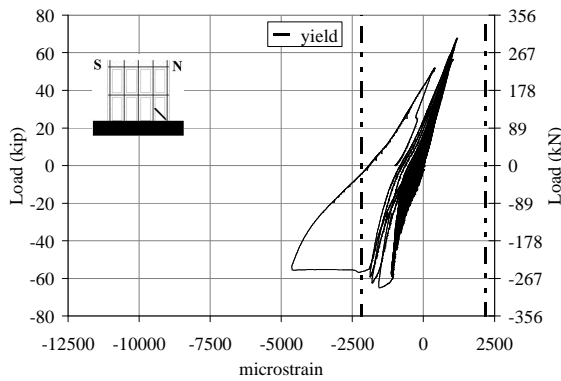
(b)



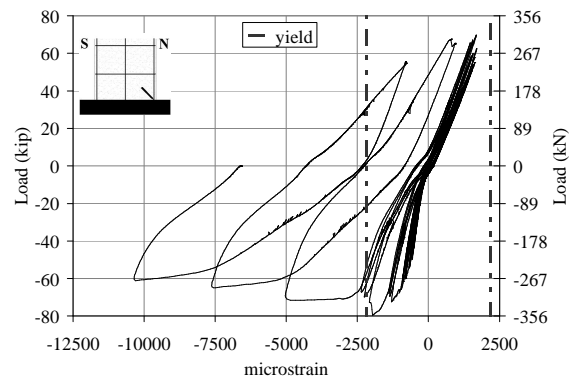
(c)



(d)

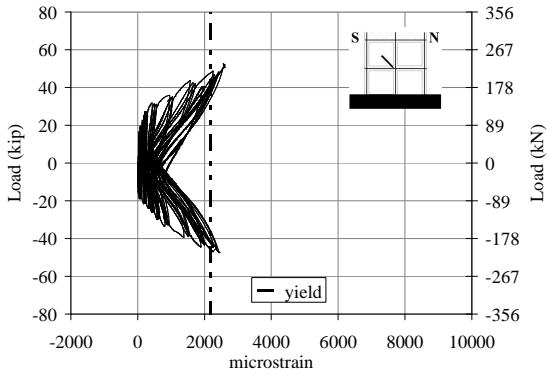


(e)

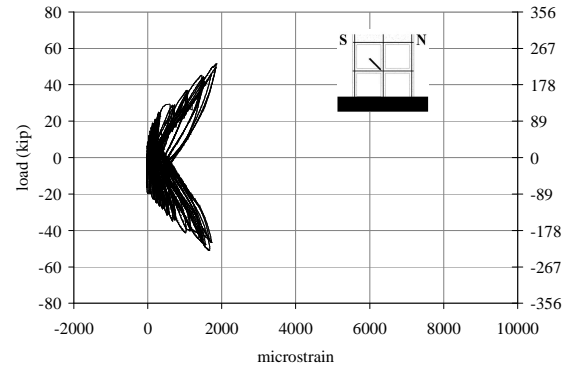


(f)

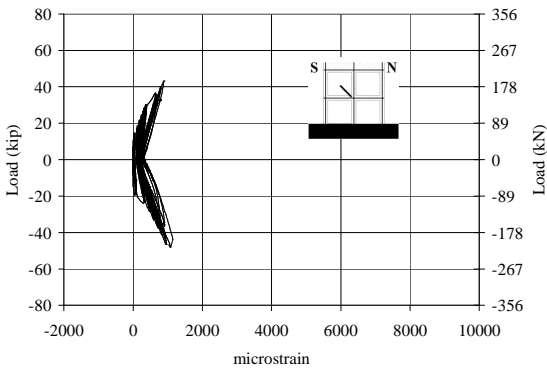
Figure 3-24: Lateral load vs. maximum strain in the flexural steel for specimens (a) PG085-48, (b) PG120-48, (c) PG169-48, (d) PG085-32, (e) PG085-24, and (f) FG085-00



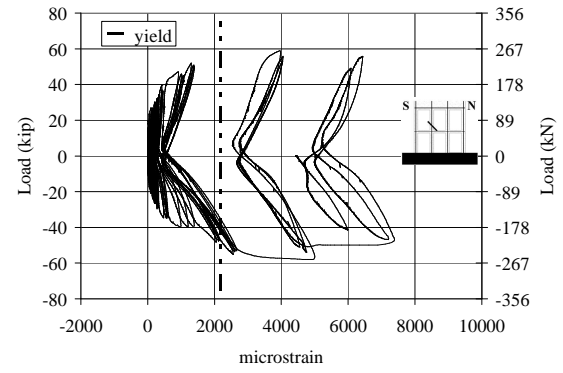
(a)



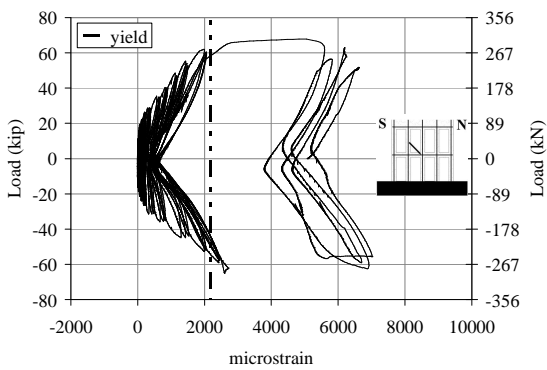
(b)



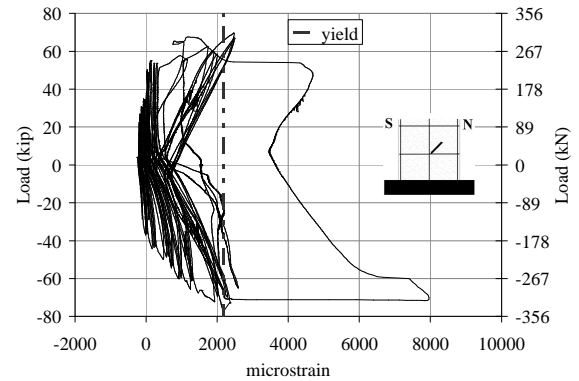
(c)



(d)



(e)



(f)

Figure 3-25: Lateral load vs. maximum strain in the shear steel for specimens (a) PG085-48, (b) PG120-48, (c) PG169-48, (d) PG085-32, (e) PG085-24, and (f) FG085-00

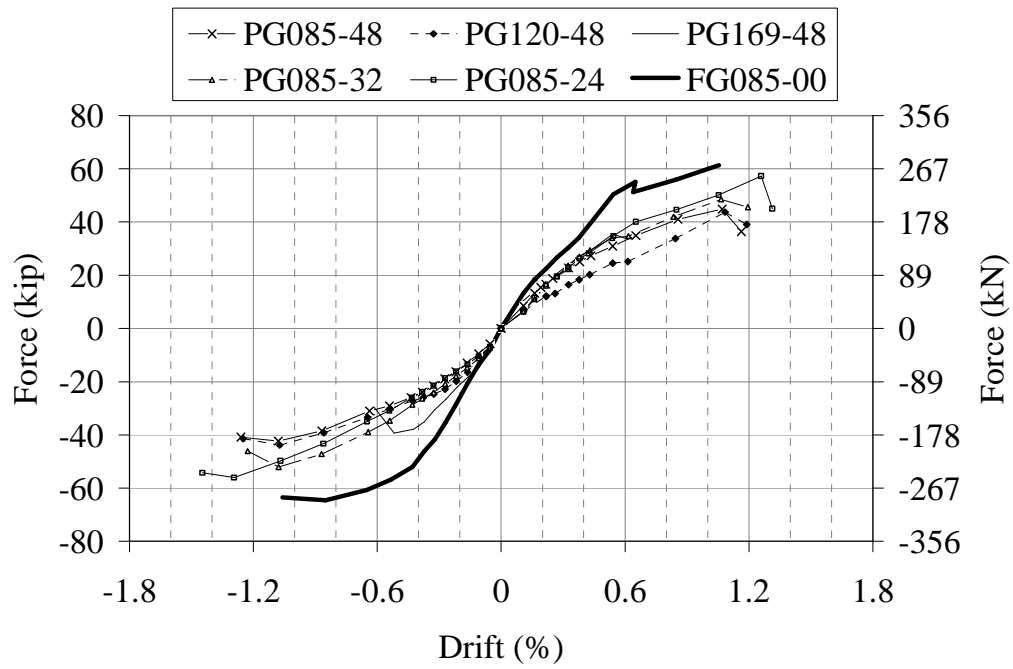
CHAPTER 4: ANALYSIS AND DISCUSSION OF TEST RESULTS

4.1 Introduction

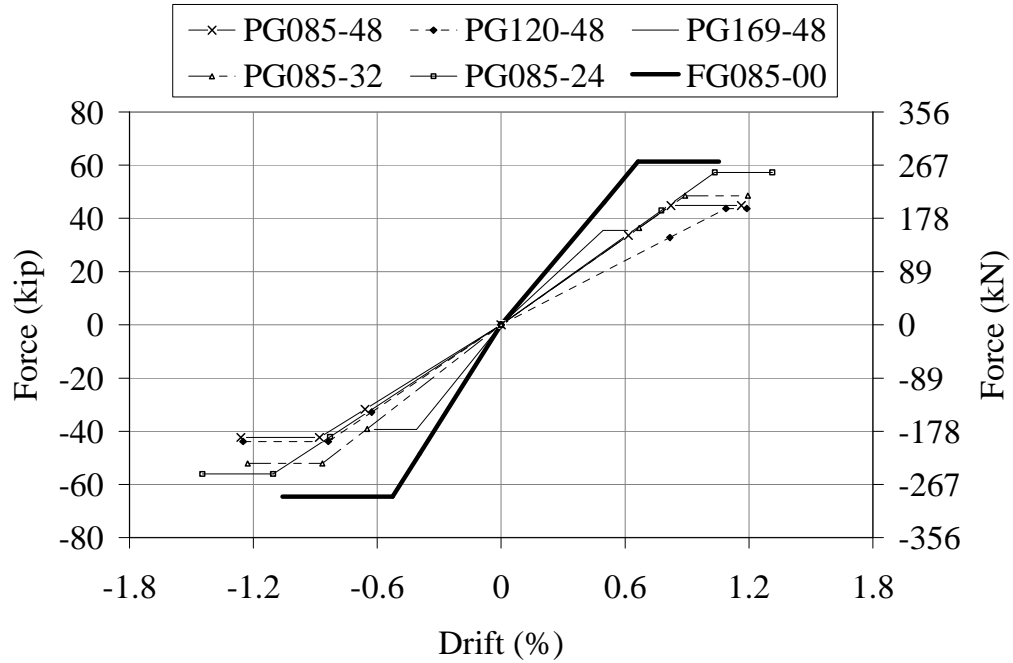
In this chapter the experimental results of the six specimens designed to fail in shear are analyzed and discussed. The chapter presents analysis of the parameter groups, examines whether plane sections remained plane during testing, suggests a modification to the current MSJC shear equation and presents strut and tie models for the specimens. Table 4-1 presents a summary of the test results from chapter 3. Figure 4-1 presents the backbone curves and bilinear approximations for all test specimens.

Table 4-1: Summary of test results and MSJC predictions.

Specimen	V_{max}			MSJC V_n	% Error $(V_{max}-V_n)/V_n$	Displacement ductility (μ_Δ)			d_u	d_{Vmax}
	North	South	Average			North	South	Average		
PG085-48	47.5 kips (211 kN)	52.5 kips (234 kN)	50.0 kips (222 kN)	59.4 kips (264 kN)	-16%	1.23	1.26	1.25	1.5%	1.5% (N) 1.3% (S)
PG120-48	51.0 kips (227 kN)	51.6 kips (230 kN)	51.3 kips (228 kN)	68.2 kips (303 kN)	-25%	1.28	1.00	1.14	1.5%	1.3%
PG169-48	48.3 kips (215 kN)	43.3 kips (193 kN)	45.8 kips (204 kN)	80.5 kips (358 kN)	-43%	1.27	1.10	1.19	0.7% (N) 0.9% (S)	0.7%
PG085-32	58.1 kips (258 kN)	59.0 kips (262 kN)	58.6 kips (260 kN)	62.6 kips (278 kN)	-6%	1.25	1.20	1.23	1.5%	1.3%
PG085-24	65.1 kips (290 kN)	67.8 kips (302 kN)	66.5 kips (296 kN)	65.8 kips (293 kN)	1%	1.17	1.22	1.20	1.7%	1.5%
FG085-00	79.8 kips (355 kN)	69.9 kips (311 kN)	74.9 kips (333 kN)	113.1 kips (503 kN)	-34%	1.61	1.59	1.60	1.3%	1.1%



(a)



(b)

Figure 4-1: For all test specimens, (a) backbone curves, and (b) bilinear approximation.

4.2 Test Parameter Evaluation

4.2.1 Effects Of Grout Horizontal Spacing

The effects of grout horizontal spacing on lateral strength, stiffness, and displacement ductility is investigated in this section. Grout horizontal spacings were 48 in. (1219 mm) (specimen PG085-48), 32 in. (813 mm) (specimen PG085-32), 24 in. (610 mm) (specimen PG085-24) and 8 in. (203 mm), i.e. fully grouted, (specimen FG085-00). These four specimens had a horizontal reinforcement ratio of 0.085%. Figures 4-2 and 4-3 and Tables 4-2 and 4-3 show the effect of the grout horizontal spacing on the lateral strength, stiffness, and displacement ductility. In Figure 4-2(b), the strength of each specimen is normalized by the peak strength of each specimen. As shown in the figure, specimen FG085-00 has the highest strength followed by specimens PG085-24, PG085-32, and PG085-48. Decreasing the grout horizontal spacing increased the strength of the specimens. Figure 4-4(a) shows the lateral drift versus the net shear stresses on the same set of specimens. The shear stress was calculated as the lateral force divided by the net cross sectional area of the specimen assuming face-shell bedding (no contribution to net area from webs). As shown in the figure, all specimens except FG085-00 were able to carry approximately the same shear stress values up to a drift of 1.1%. It is worth noting that the current New Zealand standard, NZS 4230:2004, uses the cross sectional area corresponding to thickness of the face shells as the net cross sectional area in the case of partially grouted walls. This criterion was selected to satisfy the shear flow continuity requirements and to avoid the potentials of vertical shear failure of continuous ungrouted cells (Voon 2007). Figure 4-4(b) shows the shear stress calculated according to NZS 4230:2004 versus the lateral drift for the same set of specimens. As expected, using the NZ recommendations the shear stresses in the

partially grouted specimens were typically twice the fully grouted specimen. This shows using the net cross sectional area is more appropriate.

Table 4-2: Strength, initial stiffness and displacement ductility for $\rho_h = 0.085\%$.

Specimen	V_{max}			Initial Stiffness (k)			Displacement ductility ($\mu\Delta$)		
	North	South	Average	North	South	Average	North	South	Average
PG085-48	47.5 kips (211 kN)	52.5 kips (234 kN)	50.0 kips (222 kN)	91 kips/in (15.9 kN/mm)	85 kips/in (14.9 kN/mm)	88 kips/in (15.4 kN/mm)	1.23	1.26	1.25
PG085-32	58.1 kips (258 kN)	59.0 kips (262 kN)	58.6 kips (260 kN)	105 kips/in (18.4 kN/mm)	78 kips/in (13.7 kN/mm)	92 kips/in (16.0 kN/mm)	1.25	1.20	1.23
PG085-24	65.1 kips (290 kN)	67.8 kips (302 kN)	66.5 kips (296 kN)	98 kips/in (17.2 kN/mm)	78 kips/in (13.7 kN/mm)	88 kips/in (15.4 kN/mm)	1.17	1.22	1.20
FG085-00	79.8 kips (355 kN)	69.9 kips (311 kN)	74.9 kips (333 kN)	140 kips/in (24.5 kN/mm)	125 kips/in (21.9 kN/mm)	133 kips/in (23.2 kN/mm)	1.61	1.59	1.60

Table 4-3: Yield and ultimate stiffness for $\rho_h = 0.085\%$.

Specimen	Stiffness at Idealized Yield (k_i)			Ultimate Stiffness (k_u)		
	North	South	Average	North	South	Average
PG085-48	52 kips/in (9.2 kN/mm)	59 kips/in (10.4 kN/mm)	56 kips/in (9.8 kN/mm)	39 kips/in (6.9 kN/mm)	42 kips/in (7.3 kN/mm)	41 kips/in (7.1 kN/mm)
PG085-32	66 kips/in (11.5 kN/mm)	59 kips/in (10.4 kN/mm)	62 kips/in (10.9 kN/mm)	48 kips/in (8.5 kN/mm)	46 kips/in (8.0 kN/mm)	47 kips/in (8.2 kN/mm)
PG085-24	55 kips/in (9.7 kN/mm)	60 kips/in (10.5 kN/mm)	58 kips/in (10.1 kN/mm)	43 kips/in (7.6 kN/mm)	45 kips/in (8.0 kN/mm)	44 kips/in (7.8 kN/mm)
FG085-00	133 kips/in (23.3 kN/mm)	100 kips/in (17.6 kN/mm)	117 kips/in (20.5 kN/mm)	76 kips/in (13.3 kN/mm)	58 kips/in (10.2 kN/mm)	67 kips/in (11.7 kN/mm)

For the partially grouted specimens, the grout horizontal spacing did not significantly effect the initial stiffness or the idealized initial stiffness. However, specimen FG085-00 which is the fully grouted specimen has significantly higher initial stiffness (133 kips/in. (23.2 kN/mm)) and idealized initial stiffness (117 kips/in. (20.5 kN/mm)).

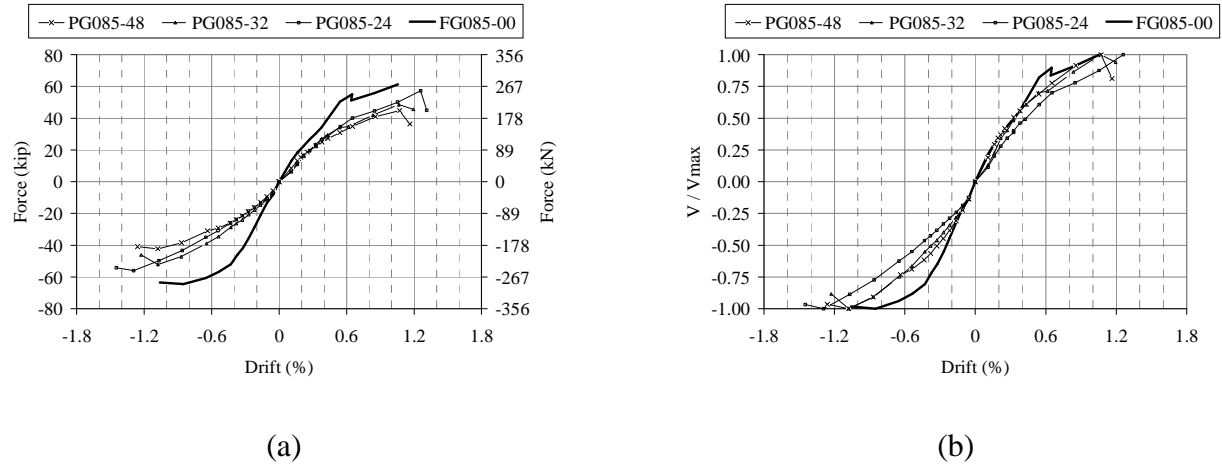


Figure 4-2: (a) Backbone curves for specimens with the same horizontal reinforcement ratio and differing grout horizontal spacing, and (b) backbone curves normalized to peak strength.

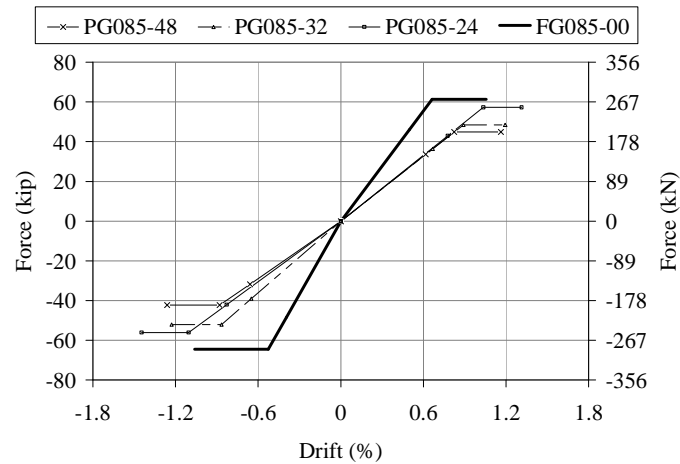


Figure 4-3: Idealized backbone curves for specimens with the same horizontal reinforcement ratio (0.085%) and differing grout horizontal spacing.

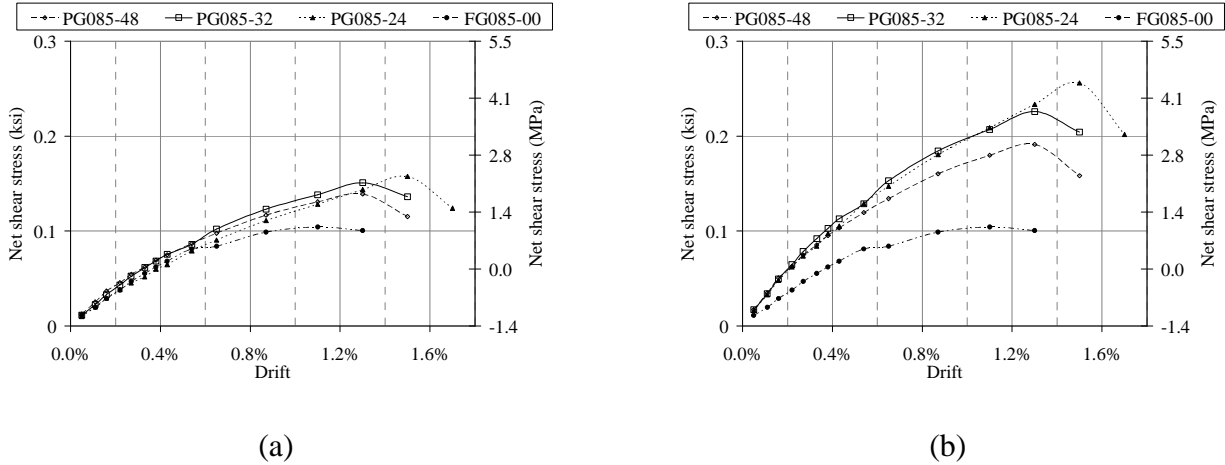


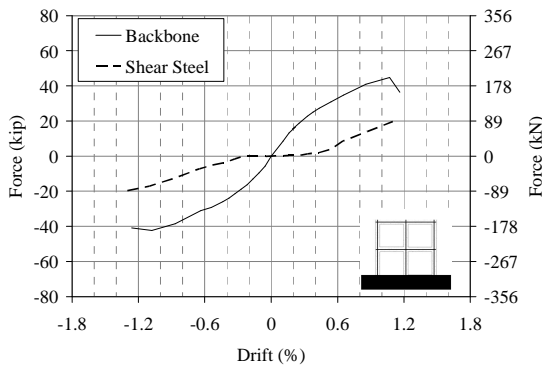
Figure 4-4: Drift vs. net shear stress for $\rho_h = 0.085\%$, (a) using net area from MSJC equations, and (b) using net area from New Zealand standard.

The grout horizontal spacing did not have systematic effects on the deformability of the test specimens. All test specimens reached ultimate drifts ranging from 1.3 to 1.7% with specimen FG085-00 having the lowest ultimate drift and specimen PG085-32 having the highest ultimate drift. Similarly, there were no systematic effects of the grout horizontal spacing on the displacement ductility of the specimens. The three partially grouted specimens reached a displacement ductility factor of approximately 1.25 while the fully grouted specimen reached a displacement ductility factor of 1.6. It is worth noting that FEMA 356 (2.4.4.3) categorized shear failure of masonry shear walls as a force control failure.

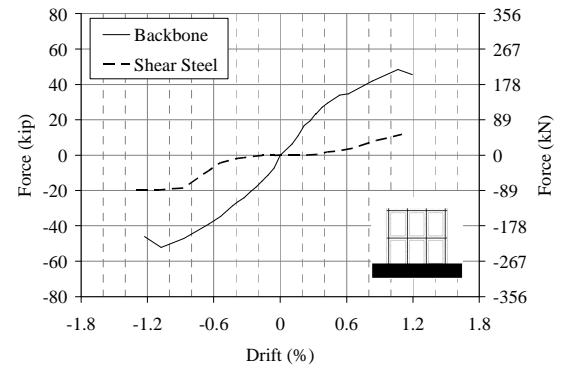
Figure 4-5 shows the lateral drift vs. the total force in the shear reinforcement in the mid-wall bond beam (6th CMU course) and lateral drift vs. the applied shear force (backbone curve). The force in the shear reinforcement is calculated using the measured ϵ with ϵ_y as the upper limit for calculating σ_y which was then multiplied by the area of shear reinforcement, A_v , to obtain the force in the shear reinforcement. The difference between the force in the shear reinforcement and the backbone curve represents the force carried by masonry alone. As shown in the figures, the

partially grouted specimens exhibited similar patterns of force development in the masonry with the engagement of the shear reinforcement started at a lateral drift of approximately 0.4%.

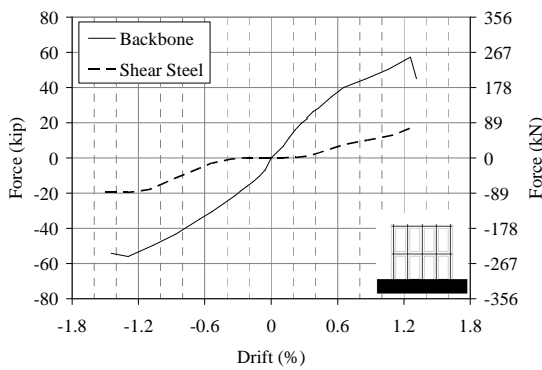
Before that, the masonry alone is resisting the applied shear force. The fully grouted specimen exhibited a faster increase in the force in the masonry and the shear rebar started to be engaged in resisting the applied shear force at a lateral drift of 0.6%. Interestingly, the masonry contribution to the shear strength increased with decreasing grout horizontal spacing.



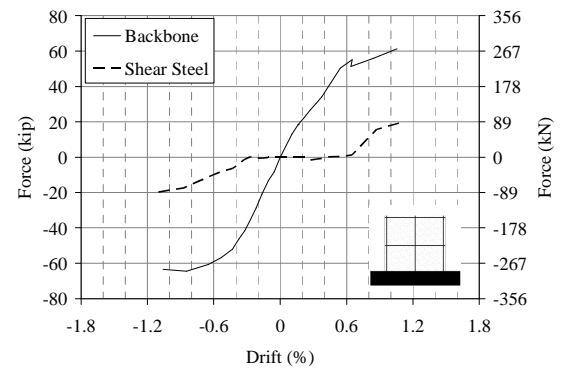
(a)



(b)



(c)



(d)

Figure 4-5: Drift vs. force in shear reinforcement and applied force (backbone curve) for specimens with $\rho_h = 0.085\%$ and varying grout horizontal spacing. Specimen (a) PG085-48, (b) PG085-32, (c) PG085-24, and (d) FG085-00.

4.2.2 Effects Of Horizontal Reinforcement Ratio

Horizontal reinforcement was provided at ratios of 0.085% (specimen PG085-48), 0.120% (specimen PG120-48) and 0.169% (specimen PG169-48). The three specimens had a grout horizontal spacing of 48 in. (1219 mm). For specimens PG085-48, PG120-48, and PG169-48, Figure 4-6 show the backbone curves, Figure 4-7 shows the bilinear idealizations, and Figure 4-8 shows the average peak strength vs. provided horizontal reinforcement ratio.

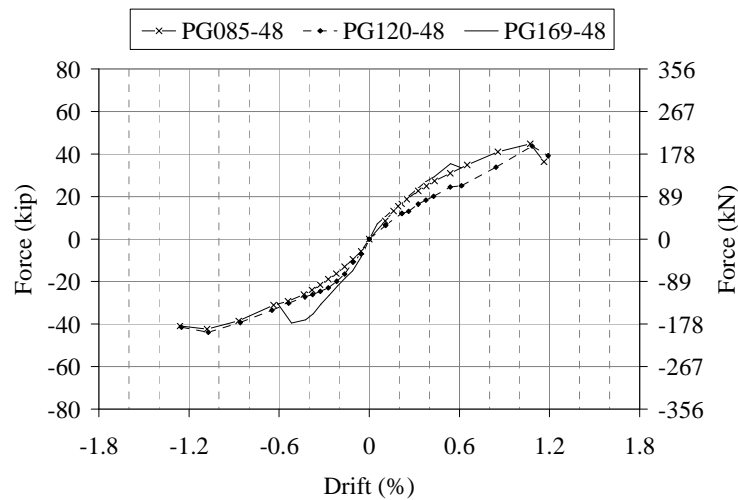


Figure 4-6: Backbone curves for specimens with 48 in. (1219 mm) grout horizontal spacing and varying horizontal reinforcement ratios.

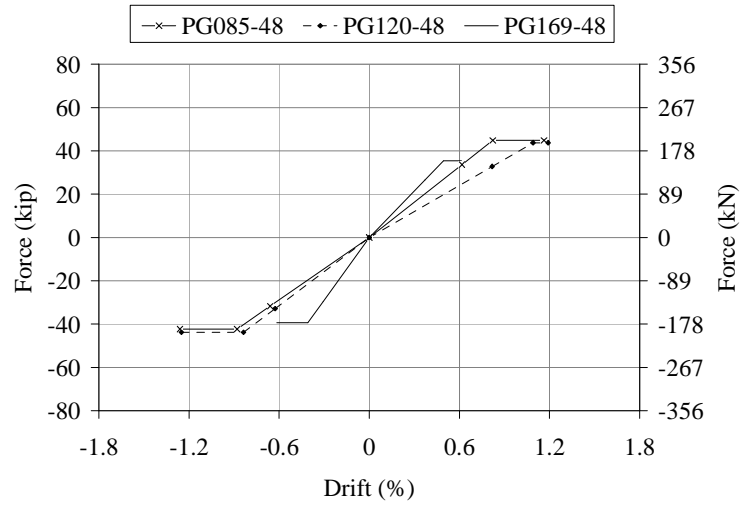


Figure 4-7: Idealized backbone curves for specimens with 48 in. (1219 mm) grout horizontal spacing and varying horizontal reinforcement ratios.

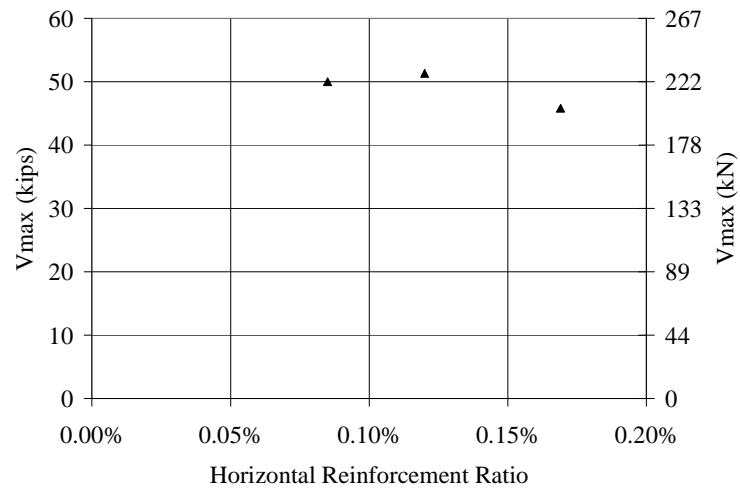


Figure 4-8: Effects of ρ_h on shear strength

As shown in Figure 4-8 and Table 4-6, increasing the shear reinforcement from 1#5 in specimen PG085-48 to 1#6 in specimen PG120-48 slightly increased the lateral strength from 50 kips (222 kN) to 51.5 kips (229 kN). However, such increase in the shear strength with

increasing the shear reinforcement ratio was not observed in specimen PG169-48. The shear reinforcement ratio of specimen PG169-48 was double that of specimen PG085-48 but the shear strength was only approximately 92% of specimen PG085-48. It is worth noting that Voon (2007) observed similar behavior for fully grouted walls. When the shear reinforcement was increased by a factor of 2.5, the shear strength remained constant. Voon (2007) concluded that for a given masonry wall there is a certain threshold of shear reinforcement beyond which there is no effect from any additional shear reinforcement. Figure 4-9 shows the maximum axial strains in the horizontal reinforcement vs. the shear reinforcement ratio. As the figure shows, a linear increase in the shear reinforcement ratio caused a linear decrease in the ultimate strain in the shear reinforcement. Based on the trendline, a horizontal reinforcement ratio of approximately 0.11%, or less, will result in yielding of the horizontal reinforcement. The assumption in the MSJC (2008) is the horizontal reinforcement will yield, which is not met for horizontal reinforcement ratios greater than approximately 0.11%.

Figure 4-10 shows the lateral drift vs. the total force in the shear reinforcement in the mid-wall bond beam (6th CMU course) and lateral drift vs. the applied shear force (backbone curve). For specimens PG085-48 and PG120-48, before a lateral drift of approximately 0.4%, the masonry alone resisted the applied shear force. Beyond that, the shear rebar started to be engaged. For specimen PG169-45, the shear rebar started to be engaged at a lateral drift of approximately 0.2%. Interestingly, the masonry and steel rebar developed approximately the same force contributions in all three specimens.

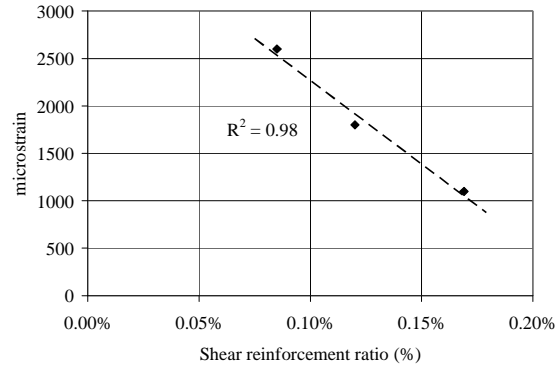


Figure 4-9: Shear reinforcement ratio (%) vs. maximum strain in shear reinforcement

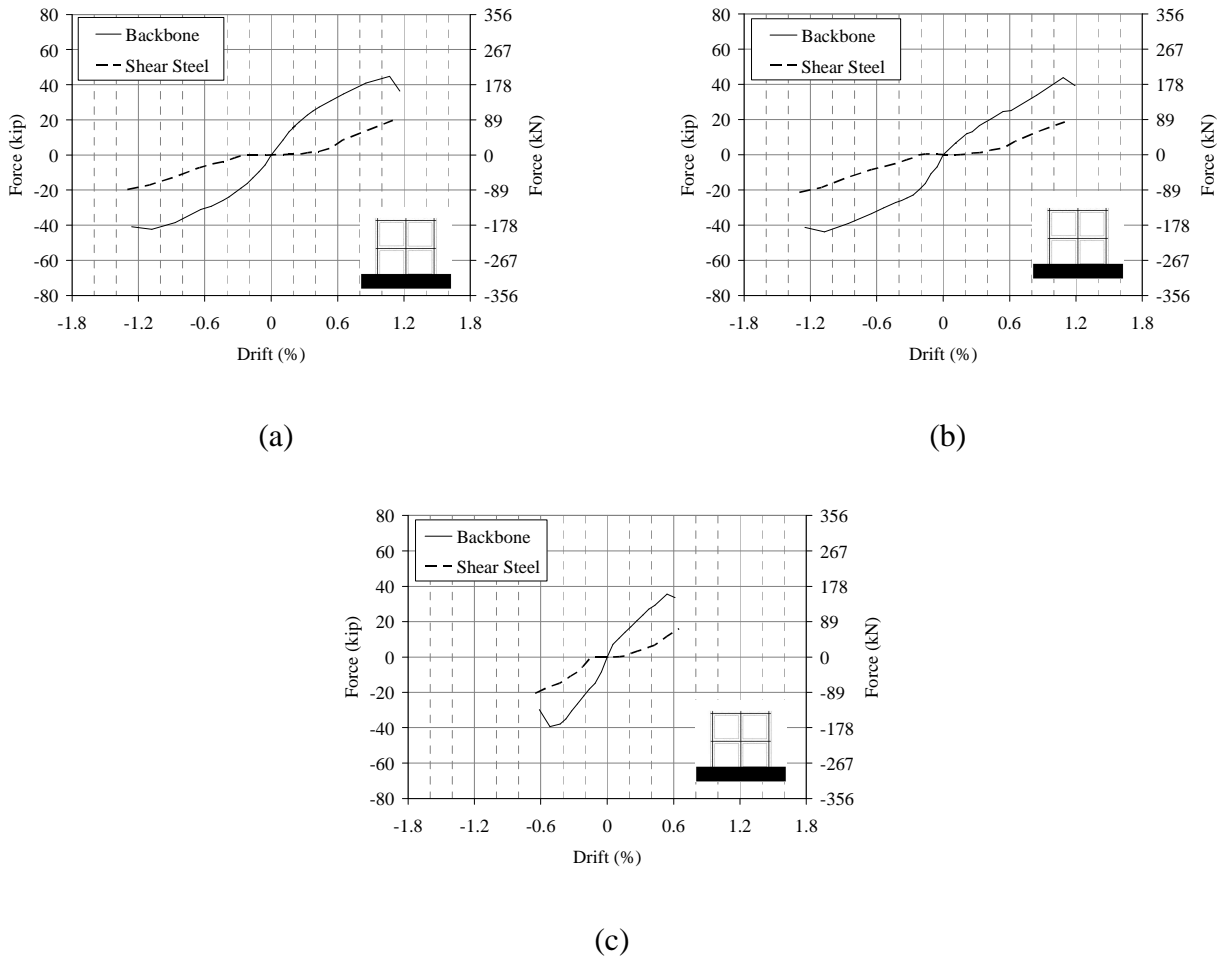


Figure 4-10: Drift vs. force in shear reinforcement and applied force (backbone curve) for specimens with 48 in. (1219 mm) grout spacing and varying horizontal reinforcement ratios.

Specimen (a) PG085-48, (b) PG120-48, and (c) PG169-48.

The effects of shear reinforcement ratio on initial, yield, and ultimate stiffness as well as deformability are shown in Tables 4-4 and 4-5. As shown in the tables, changing the horizontal reinforcement ratio from 0.085% to 0.120% had insignificant effects on the stiffness and deformability. However, the significant increase in the shear reinforcement ratio from 0.085% to 0.169% increased the initial, yield, and ultimate stiffness by factors of 1.3, 1.6 and 1.7, respectively, compared to the corresponding values for specimen PG085-48. Finally, there was no effect of the horizontal reinforcement ratio on the displacement ductility capacity of the test specimens.

Table 4-4: Strength, initial stiffness and displacement ductility for grout horizontal spacing = 48 in. (1219 mm)

Specimen	V_{max}			Initial Stiffness (k)			Displacement ductility ($\mu\Delta$)		
	North	South	Average	North	South	Average	North	South	Average
PG085-48	47.5 kips (211 kN)	52.5 kips (234 kN)	50.0 kips (222 kN)	91 kips/in (15.9 kN/mm)	85 kips/in (14.9 kN/mm)	88 kips/in (15.4 kN/mm)	1.23	1.26	1.25
PG120-48	51.0 kips (227 kN)	51.6 kips (230 kN)	51.3 kips (228 kN)	112 kips/in (19.6 kN/mm)	62 kips/in (10.9 kN/mm)	87 kips/in (15.2 kN/mm)	1.28	1.00	1.14
PG169-48	48.3 kips (215 kN)	43.3 kips (193 kN)	45.8 kips (204 kN)	134 kips/in (23.5 kN/mm)	102 kips/in (17.9 kN/mm)	118 kips/in (20.7 kN/mm)	1.27	1.10	1.19

Table 4-5: Yield and ultimate stiffness for grout horizontal spacing = 48 in. (1219 mm)

Specimen	Stiffness at Idealized Yield (k_i)			Ultimate Stiffness (k_u)		
	North	South	Average	North	South	Average
PG085-48	52 kips/in (9.2 kN/mm)	59 kips/in (10.4 kN/mm)	56 kips/in (9.8 kN/mm)	39 kips/in (6.9 kN/mm)	42 kips/in (7.3 kN/mm)	41 kips/in (7.1 kN/mm)
PG120-48	57 kips/in (10.0 kN/mm)	44 kips/in (7.6 kN/mm)	50 kips/in (8.8 kN/mm)	41 kips/in (7.2 kN/mm)	40 kips/in (7.1 kN/mm)	41 kips/in (7.1 kN/mm)
PG169-48	105 kips/in (18.3 kN/mm)	78 kips/in (13.7 kN/mm)	91 kips/in (16.0 kN/mm)	76 kips/in (13.3 kN/mm)	66 kips/in (11.5 kN/mm)	71 kips/in (12.4 kN/mm)

4.3 Measured vs. Predicted Shear Strength Using MSJC (2008) Shear Equations

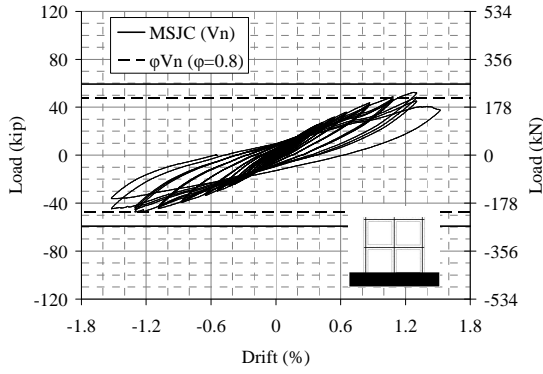
The test strength of each specimen, the predicted strength using the MSJC (2008) shear equation, and the percent difference between the actual strength and predicted strength are listed in Table 4-6. Force-drift hysteretic graphs with the data of Table 4-6 are shown in Figure 4-11. As shown in the table and figure, the equations overestimated the shear strengths for all specimens with a single exception, i.e. specimen PG085-24. For grout horizontal spacing of 24 in. (610 mm) and 32 in. (813 mm), the predictions were quite good with an over-prediction of 7% for specimen PG085-32 and an under-prediction of 1% for specimen PG085-24. For the three specimens with 48 in. (1219 mm) grout horizontal spacing and variable shear reinforcement ratios, the MSJC (2008) shear equations over-predicted the shear strengths with an error ranged from 16% to 43%. The errors in the predictions correlated to the increase in the shear reinforcement ratio (Figure 4-12). The strength of specimen PG085-48 with the lowest reinforcement ratio of 0.085% was over-predicted with an error of 16% while the strength prediction of specimen PG169-48 with the highest reinforcement ratio of 0.169% was over-predicted with an error of 43%. An examination of the horizontal reinforcement ratio versus the percentage of error between actual and predicted shear strengths (Figure 4-12) shows a strong correlation ($R^2 = 0.99$) between increased reinforcement ratio and the error, strongly pointing to a problem with the method of accounting for any increased shear strength from increased reinforcement. The error correlates with increasing reinforcement ratio due to the horizontal rebar not being able to develop its yield strength prior to wall failure. The wall failure was associated with either a splitting crack passing through the end-shells and the grout or through the grout face-shell interface. Based on this analysis, it appears that limiting the horizontal

reinforcement ratio to 0.11% will result in an improved prediction of shear strength using the MSJC (2008) equations.

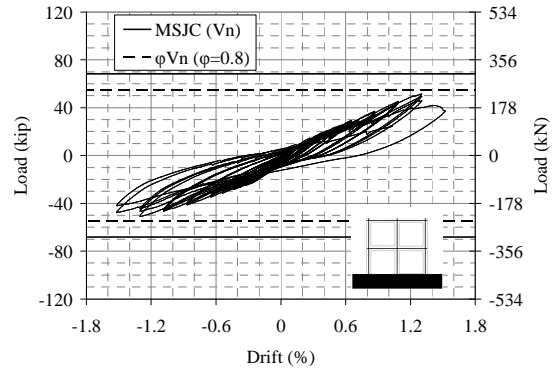
For the fully grouted specimen, the equations significantly over-estimated the strength with an error of 34% ($V_{\max} / V_n = 0.66$). It is worth noting that Davis (2008) calibrated the shear strength of 56 fully grouted specimens against the MSJC (2008) shear equations and found the measured strengths vs. MSJC (2008) Strength Design predictions to vary between 0.77 to 1.55 (ratio is V_{\max} / V_n). The horizontal reinforcement ratio of the specimens in the literature varied from 0 to 0.67% while specimen FG085-00 had a reinforcement ratio of 0.085%. However, based on the analysis by Davis (2008), there is no clear correlation between under and over-predictions using the MSJC (2008) Strength Design equations and the shear reinforcement ratio.

With the shear reinforcement ratio constant, V_{ns} is constant for all four specimens. Therefore, the total nominal shear strength (Equation 1-1) varies due to V_{nm} , the nominal shear strength contributed by the masonry (Equation 1-2). The contribution to V_{nm} from the axial load is constant for all four specimens. The only variable between the four specimens is the net cross sectional area of masonry. If the net cross sectional area is linearly correlated to the nominal shear strength, then a graph of the net cross sectional area, A_n , vs. shear strength, V_{\max} , should yield a linear relationship. Figure 4-13(a) shows the relationship between net area and V_{\max} is nonlinear. Figure 4-13(b) shows the relationship between the grout horizontal spacing and V_{\max} . As shown in the figure, there is a strong correlation ($R^2 = 0.99$) between grout horizontal spacing and V_{\max} . However, Equation 1-2 predicts a nonlinear relationship. It appears the MSJC (2008) equations do not account for the net area properly. An examination of grout horizontal spacing versus the percent error between actual and predicted shear strength (Figure 4-14(a)) shows a lack of correlation ($R^2 = 0.19$) between grout horizontal spacing and error for the group. Since

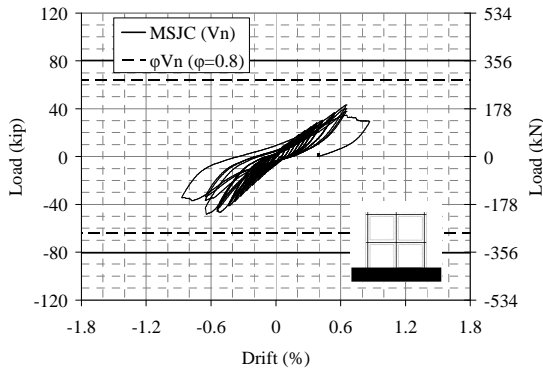
the shear rebar yielded in these specimens, the error is due to an error in calculating V_{nm} . If only the partially grouted specimens are examined, there is a strong correlation ($R^2 = 0.99$) between increased grout horizontal spacing and increased error (Figure 4-14(b)). This suggests that a reduction factor of some type should be applied to the nominal shear strength contributed by the masonry, V_{nm} , for partially grouted shear walls. Based on this limited data set, a reduction factor based on the net area, A_n , will be proposed in section 4.4.



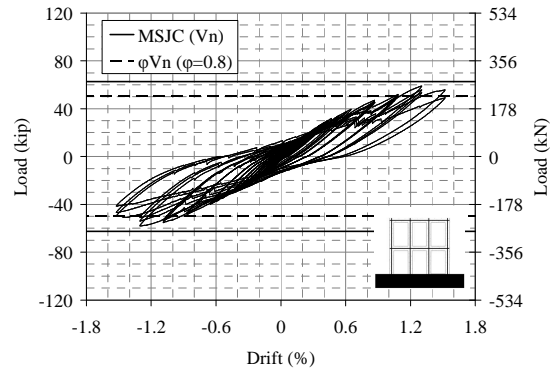
(a)



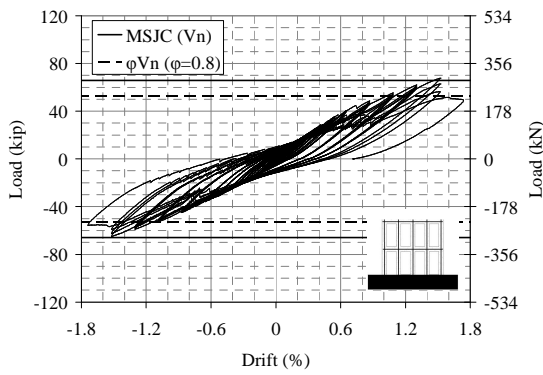
(b)



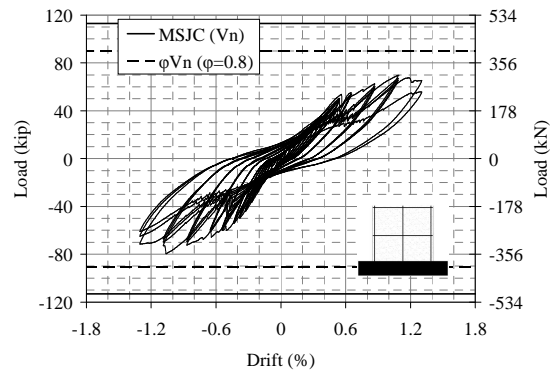
(c)



(d)



(e)



(f)

Figure 4-11: Load-drift hysteretics for (a) PG085-48, (b) PG120-48, (c) PG169-48, (d) PG085-32, (e) PG085-24, and (f) FG085-00

Table 4-6: MSJC predicted shear strength, V_n , experimental shear strength, V_{max} , and % Error

	PG085-48	PG120-48	PG169-48	PG085-32	PG085-24	FG085-00
MSJC (V_n)	59.4 kips (264 kN)	68.2 kips (303 kN)	80.5 kips (358 kN)	62.6 kips (278 kN)	65.8 kips (293 kN)	113.1 kips (503 kN)
test strength (V_{max})	50.0 kips (222 kN)	51.3 kips (228 kN)	45.8 kips (204 kN)	58.6 kips (261 kN)	66.4 kips (295 kN)	74.9 kips (333 kN)
% Error [$V_{max} - V_n$]/[V_n]	-16%	-25%	-43%	-6%	1%	-34%

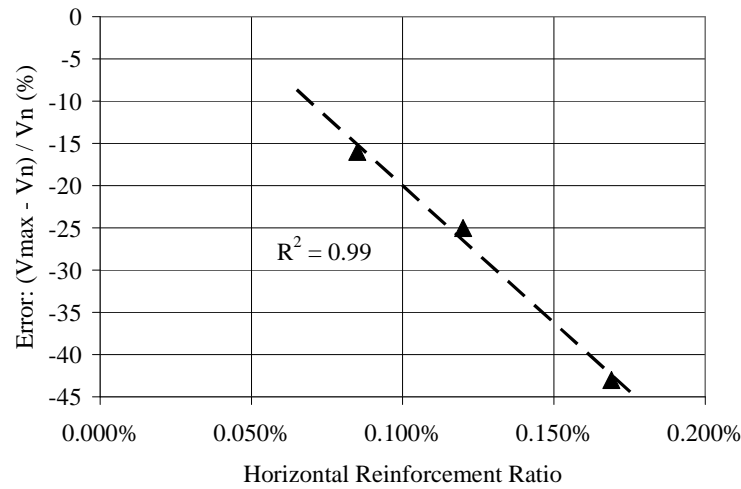


Figure 4-12: Effects of ρ_h on the predictions using MSJC (2008) shear design equations

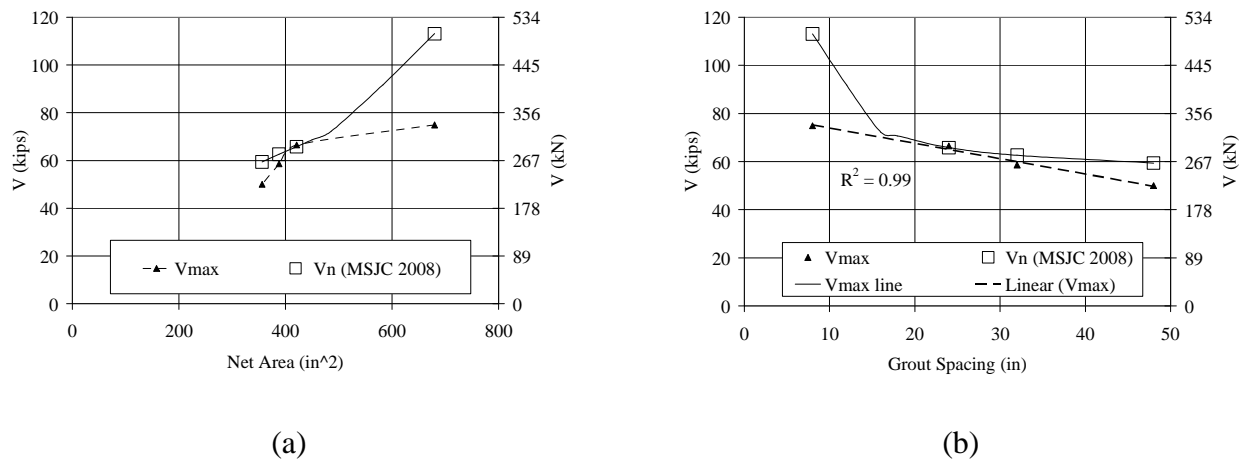
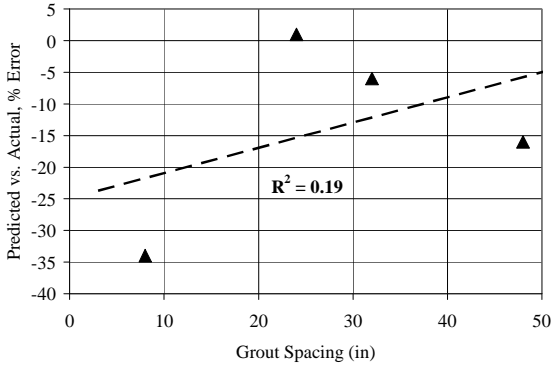
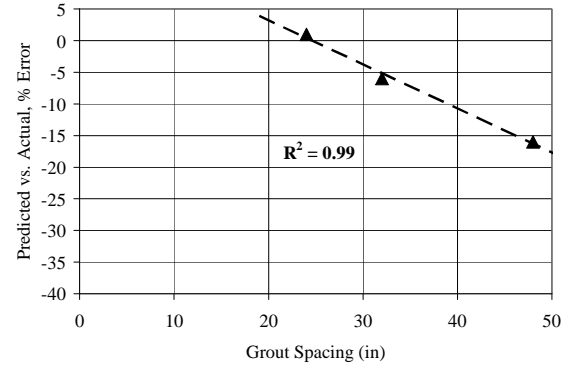


Figure 4-13: Specimens with $\rho_h = 0.085\%$, (a) net area vs. V_{max} and V_n , and (b) grout horizontal spacing vs. V_{max} and V_n , with linear trendline for V_{max}



(a)



(b)

Figure 4-14: Effects of grout horizontal spacing on the % error between predicted and actual shear strength (a) all group specimens, and (b) partially grouted only

4.4 Modification To The MSJC (2008) Shear Equation

As described in section 1.4, the current MSJC shear equations are as follows. The total nominal shear strength provided by the masonry and reinforcement steel, V_n , is given by Equation 4-1. The nominal shear strength contributed by the masonry, V_{nm} , is given by Equation 4-2. The nominal shear strength contributed by the reinforcing steel, V_{ns} , is given by Equation 4-3. The values for each specimen that were used in Equations 4-2 and 4-3 are given in Table 4-7.

$$V_n = V_{nm} + V_{ns} \quad (4-1)$$

$$V_{nm} = \left[4.0 - 1.75 \left(\frac{M_u}{V_u \cdot d_v} \right) \right] \cdot A_n \cdot \sqrt{f'_m} + 0.25 P_u \quad (4-2)$$

$$V_{ns} = 0.5 \cdot \left(\frac{A_v}{s} \right) \cdot f_y \cdot d_v \quad (4-3)$$

Table 4-7: Inputs to Equations 4-2 and 4-3, V_{nm} , V_{nm} and V_n

Wall ID	PG085-48	PG120-48	PG169-48	PG085-32	PG085-24	FG085-00	
A_n	356 (229,677)	356 (229,677)	356 (229,677)	388 (250,322)	421 (271,612)	680 (438,709)	in ² (mm ²)
A_v	0.31 (200)	0.44 (284)	0.62 (400)	0.31 (200)	0.31 (200)	0.31 (200)	in ² (mm ²)
V_{nm}	38.0 (169)	38.0 (169)	38.0 (169)	41.2 (183)	44.5 (198)	91.7 (408)	kips (kN)
V_{ns}	21.4 (95.0)	30.1 (134)	42.5 (189)	21.4 (95.0)	21.4 (95.0)	21.4 (95.0)	kips (kN)
V_n	59.4 (264)	68.2 (303)	80.5 (358)	62.6 (278)	65.8 (293)	113 (503)	kips (kN)

Constant parameters for all specimens: $h_w = 92$ in (2337 mm); $d_v = 103.6$ in (2631 mm); $P_u = 11080$ lb (49286 N); $s = 48$ in (1219 mm); $f_y = 63600$ psi (438.5 MPa); $f_m = 1640$ psi (11.3 MPa), except FG085-00 where $f_m = 2860$ psi (19.7 MPa).

The current MSJC method of calculating the nominal shear strength provided by the shear reinforcement, V_{ns} , does not adequately consider the path of a 45° shear crack and the number of stirrups available to resist shear. A simple rearrangement of Equation 4-3 into Equation 4-4 helps clarify what the situation:

$$V_{ns} = \left(\frac{1}{2}\right) \cdot (A_v \cdot f_y) \cdot \left(\frac{d_v}{s}\right) \quad (4-4)$$

The $(1/2)$ is an empirical reduction factor addressing the expectation that some steel rebar will not reach yield. The $(A_v \cdot f_y)$ component is the yield strength of one stirrup. The (d_v / s) component addresses how many stirrups are involved in resisting shear. This component has a problem. In the case of the specimens tested, $d_v / s = 103.6$ in. / 48 in. = 2.16. Therefore, Equation 4-3 calculates V_{ns} based on 2.16 stirrups resisting shear. Examination of Figure 4-15 reveals that, at most, two stirrups are available to resist shear.

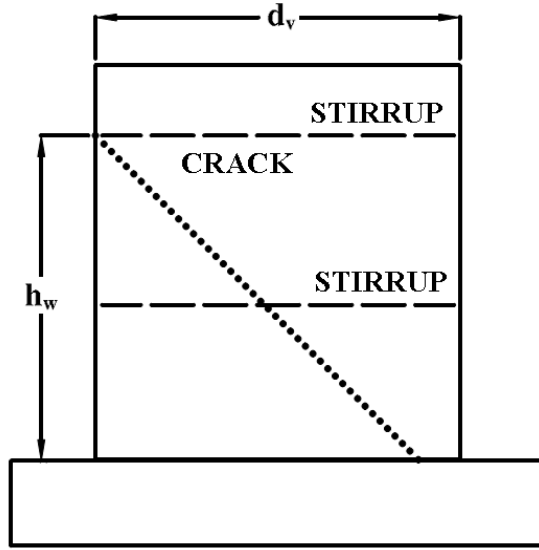


Figure 4-15: 45° shear crack

The first modification (m1-MSJC) is that d_v should reflect the horizontal projection of the 45° shear crack, i.e. d_v should be the smaller of the wall length, l_w , or wall height, h_w . If (h_w / s) is used, then the equation includes $92 \text{ in.} / 48 \text{ in.} = 1.92$ stirrups (Equation 4-5). With this modification, the equation no longer includes stirrups that aren't actually present. Implementing this modification will result in a slight reduction in the error. Table 4-8 presents a comparison of the MSJC (2008) and m1-MSJC to the experimental results.

$$V_{ns} = \left(\frac{1}{2} \right) \cdot (A_v \cdot f_y) \cdot \left(\frac{d_{45}}{s} \right) \quad (4-5)$$

where d_{45} = the lesser of $\{d_v, h_w\}$

Table 4-8: MSJC (2008) and m1-MSJC vs. the experimental results

	PG085-48	PG120-48	PG169-48	PG085-32	PG085-24	FG085-00
MSJC (2008) (MSJC)/(test)	1.19	1.33	1.76	1.07	0.99	1.51
m1-MSJC (m1-MSJC)/(test)	1.14	1.27	1.66	1.03	0.95	1.48
Test (test)/(test)	1.00	1.00	1.00	1.00	1.00	1.00

The second modification (m2-MSJC) applies an α factor within Equation 4-2 as shown in Equation 4-6. The α factor corrects for errors associated with accounting for how the net area, A_n , effects V_{nm} . With this modification, the error ranges from -5% to +48%. Table 4-9 presents a comparison of the MSJC (2008) and m3-MSJC to the experimental results.

$$V_{nm} = \alpha \cdot \left[4.0 - 1.75 \left(\frac{M_u}{V_u \cdot d_v} \right) \right] \cdot A_n \cdot \sqrt{f_m} + 0.25 P_u \quad (4-6)$$

where: $\alpha = 1.0$ for $A_n / A_g \geq 0.5$, else

$$\alpha = 3.44 \left(\frac{A_n}{A_g} \right) - 0.8 \geq 0 \quad (4-7)$$

Table 4-9: MSJC (2008) and m2-MSJC vs. the experimental results

	PG085-48	PG120-48	PG169-48	PG085-32	PG085-24	FG085-00
MSJC (2008) (MSJC)/(test)	1.19	1.33	1.76	1.07	0.99	1.51
m2-MSJC (m2-MSJC)/(test)	0.96	1.09	1.46	0.95	0.95	1.48
Test (test)/(test)	1.00	1.00	1.00	1.00	1.00	1.00

The third modification (m3-MSJC) addresses placing a limit on the amount of shear reinforcement that may be considered to contribute to shear strength. A β factor is introduced into Equation 4-5, giving Equation 4-8, to place a penalty on high horizontal reinforcement ratios.

$$V_{ns} = \beta \cdot \left(\frac{1}{2} \right) \cdot (A_v \cdot f_y) \cdot \left(\frac{d_{45}}{s} \right) \quad (4-8)$$

where d_{45} = the lesser of $\{d_v, h_w\}$

where: $\beta = 1.0$ for $\rho_h < 0.001$, else

$$\beta = 1 - 2 \cdot \rho_h \geq 0 \quad (4-9)$$

where ρ_h is calculated as:

$$\rho_h = \frac{A_v}{s \cdot t} \quad (4-10)$$

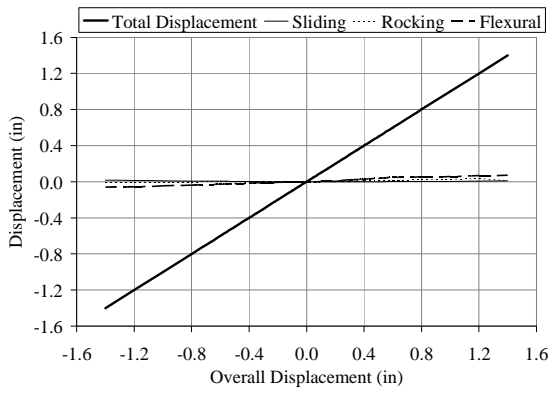
Table 4-10 presents a comparison of the MSJC (2008) and m4-MSJC to the experimental results. As Table 4-10 shows, the modified method is more conservative than the MSJC (2008) for all specimens. The modified method is conservative for all specimens except PG169-48 and FG085-00.

Table 4-10: MSJC (2008) and m3-MSJC vs. the experimental results.

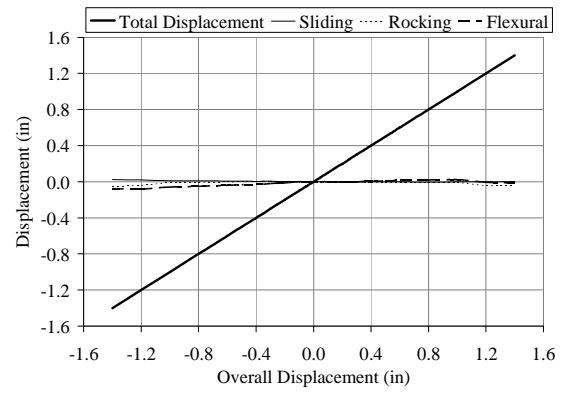
	PG085-48	PG120-48	PG169-48	PG085-32	PG085-24	FG085-00
MSJC (2008) (MSJC)/(test)	1.19	1.33	1.76	1.07	0.99	1.51
m3-MSJC (m3-MSJC)/(test)	0.96	0.97	1.18	0.95	0.95	1.48
Test (test)/(test)	1.00	1.00	1.00	1.00	1.00	1.00

4.5 Shear Displacement vs. Sliding, Rocking And Flexural Displacement

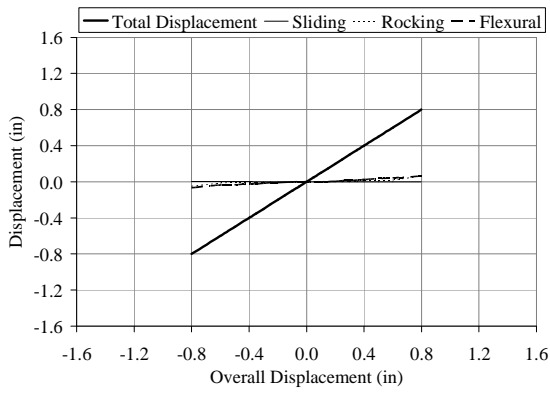
Figure 4-16 shows the displacement due to sliding of the wall on the foundation, rocking, flexural deformation, and shear deformation for all specimens. Sliding of the wall on the foundation was measured directly with a string pot fixed to the foundation and to a CMU near the middle of the 1st CMU course. This is the first line plotted in Figure 4-16. Rocking was determined using the string pots attached to the north and south end shells at the 1st CMU course. Using the string pot data, corrected for rod length, θ_R (rocking angle) was determined. Multiplying θ_R by the wall height gave Δ_R , the rocking displacement. The rocking displacement was added to the sliding displacement and plotted as the second line in Figure 4-16. Flexural displacement used the string pots attached to the north and south end shells at the 1st, 2nd, 3rd, and 12th CMU courses. Using the string pot data, corrected for rod length, the rotation between the 1st and 2nd, 2nd and 3rd, and 3rd and 12th CMU courses was determined. Multiplying by the heights over which the rotations acted and summing the results provided the flexural displacement. The flexural displacement was added to the sliding and rocking displacements and plotted as the third line in Figure 4-16. The remaining displacement between the total displacement line and the flexural displacement line is due to shear displacement. In all cases, shear deformation overwhelmingly dominated the displacement. The dominance of shear deformation provides an assurance that the results reflect a shear failure.



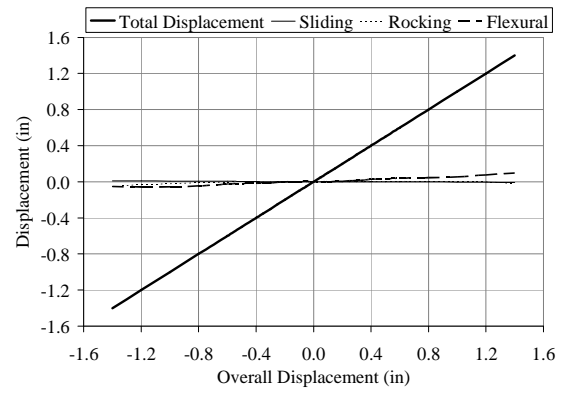
(a)



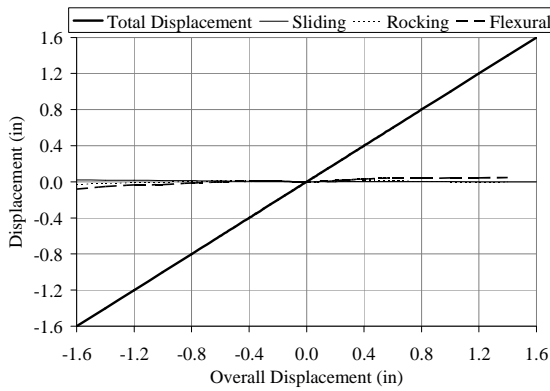
(b)



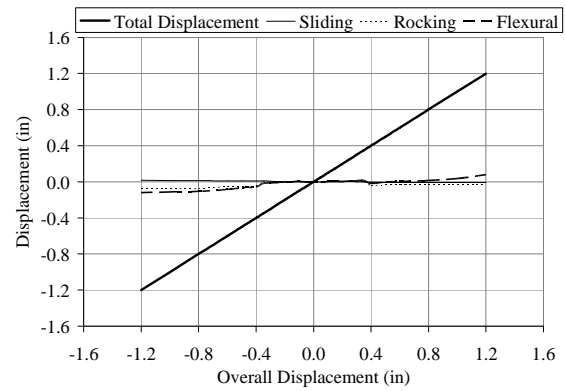
(c)



(d)



(e)



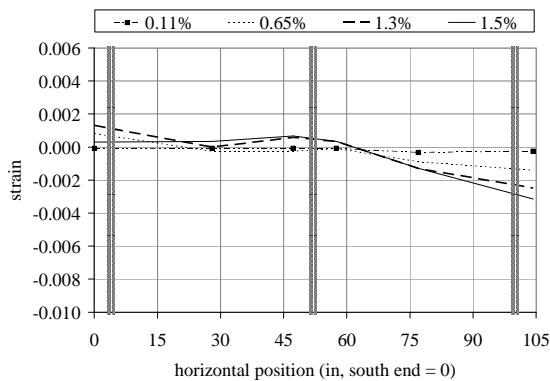
(f)

Figure 4-16: Sliding, Rocking, Flexural and Shear Displacement components for specimens

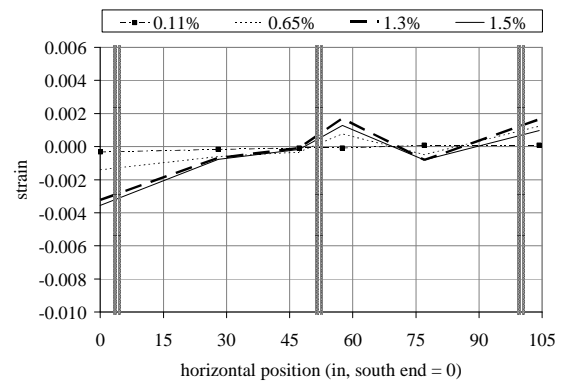
(a) PG085-48, (b) PG120-48, (c) PG169-48, (d) PG085-32, (e) PG085-24, and (f) FG085-00

4.6 Deformations Of Plane Sections

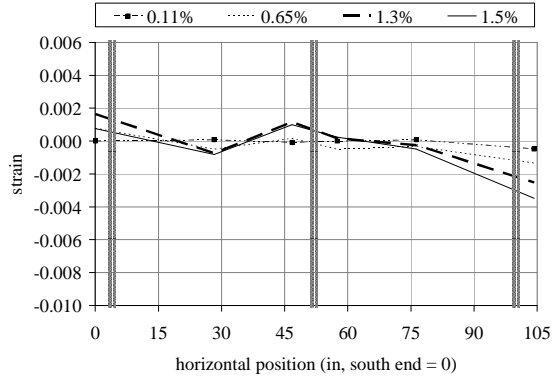
Plane sections did not remain plane for all specimens, as shown in Figure 4-17. The strains plotted in Figure 4-17 were calculated from the string pots on the 2nd CMU course of each specimen. The measured displacement of each pot was divided by its gauge length to calculate a strain value. String pots located on the north and south end shells were corrected for rod length prior to calculating the strain. For specimens PG085-48, PG120-48 and PG169-48, all with a 48 in. (1219 mm) grout horizontal spacing, the deformations are suggestive of an infill frame (Figure 4-17(a/b), (c/d), (e/f), respectively). For specimens PG085-32, PG085-24 and FG085-00, the results are less suggestive. There is insufficient data to make a definitive statement concerning the exact nature of how plane sections deform for all grout horizontal spacings and horizontal reinforcement ratios examined. Additional experimental data is needed in order to characterize this behavior.



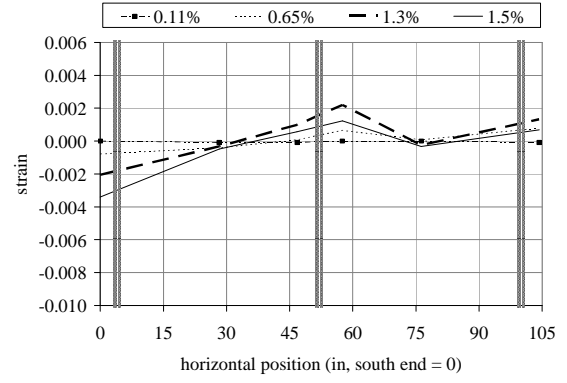
(a)



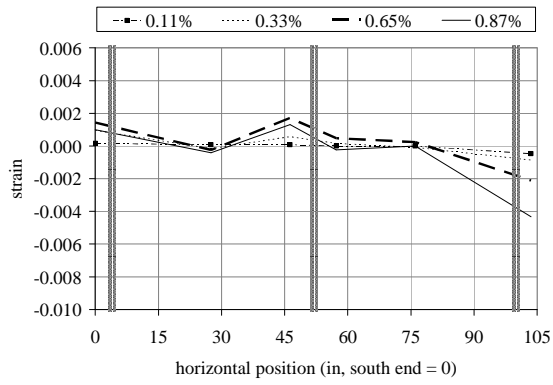
(b)



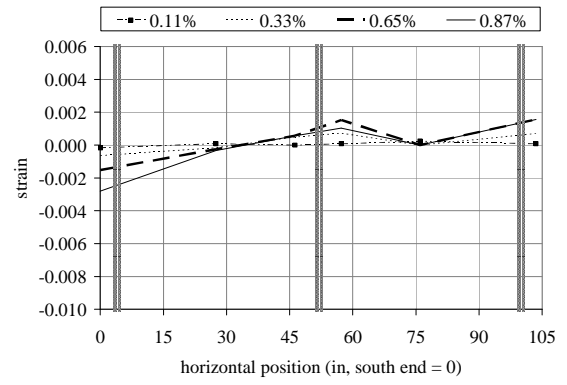
(c)



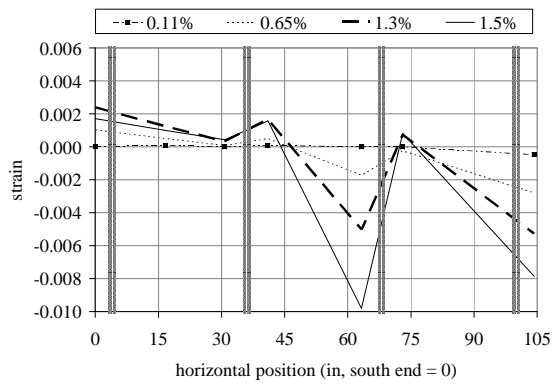
(d)



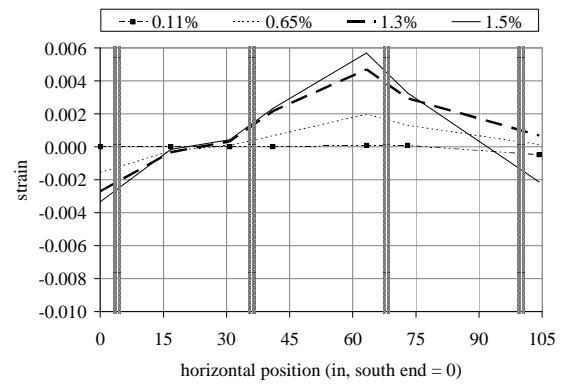
(e)



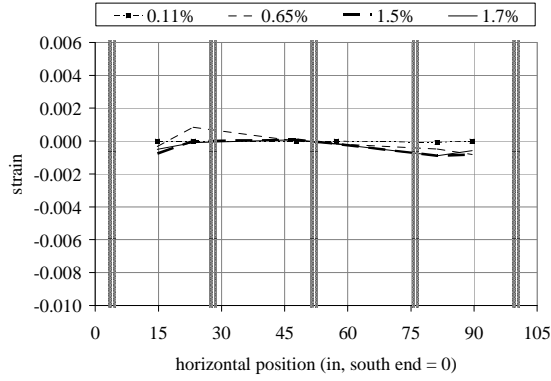
(f)



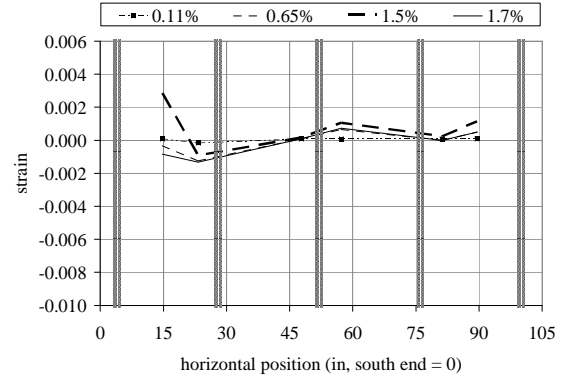
(g)



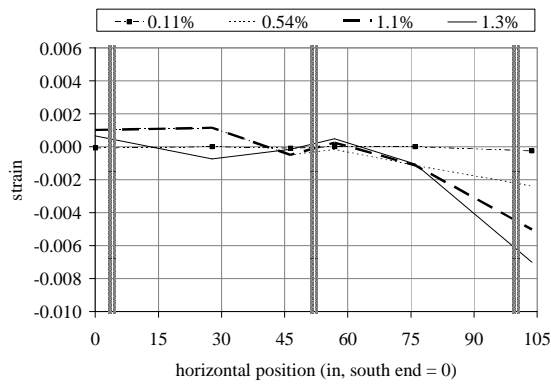
(h)



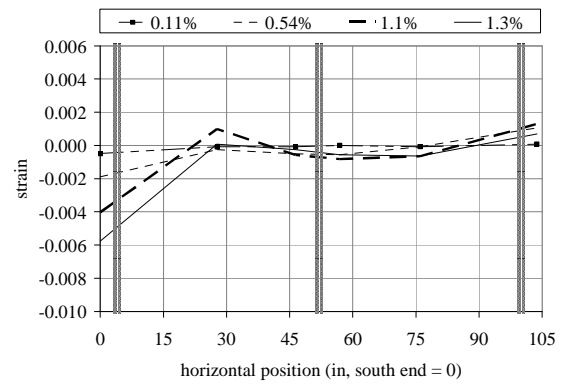
(i)



(j)



(k)



(l)

Figure 4-17: Strains at the 2nd CMU course under a north push and south pull, left and right respectively, for specimens (a/b) PG085-48, (c/d) PG120-48, (e/f) PG169-48, (g/h) PG085-32, (i/j) PG085-24, and (k/l) FG085-00

4.7 Strut And Tie Model

4.7.1 General Model Outline

The normal and shear forces were distributed across the top nodes of the model based on tributary area. The actual yield stress of the steel, 63.6 ksi (439 MPa), was used to determine the yield strength of the shear and flexural reinforcement. Compression strut strength was

determined as presented in ACI 318-05 Appendix A using Equations 4-8, 4-9, and 4-10. Table 4-11 lists the values used in the ACI equations and the resulting strut and node strengths. The nominal compressive strength of a strut, F_{ns} , is given by Equation 4-11:

$$F_{ns} = f_{ce} \cdot A_{cs} \quad (4-11)$$

In Equation 4-10, A_{cs} is the net cross sectional area of the strut and f_{ce} is the lesser of the effective compressive strength of the masonry in a strut (Equation 4-12) or the effective compressive stress on a face of a nodal zone (Equation 4-13).

$$f_{ce} = 0.85\beta_s \cdot f_m \quad (4-12)$$

where $\beta_s = 1.0$ for a strut of uniform cross-sectional area over its length

$$f_{ce} = 0.85\beta_n \cdot f_m \quad (4-13)$$

where $\beta_n = 0.6$ for a nodal zone anchoring two or more ties

The strut width was determined as shown in Figure 4-18. Figure 18(a) shows how to determine the strut angle between nodes A and B. A straight line is drawn from node A to node B (line AB). The angle between a horizontal line and line AB is the strut angle. Figure 4-18(b) shows how to determine the strut width. Point D is located at the bottom edge of the bond beam. A line is drawn from point D, as shown, such that angle C is equal to the strut angle. Point E is the intersection of this line with the top edge of the bond beam. Lines are drawn from points D and E extending to node B such that angles F and G are equal to 90° . These lines form the sides of the strut. The strut width is the distance from point D to point E, i.e. the length of line DE.

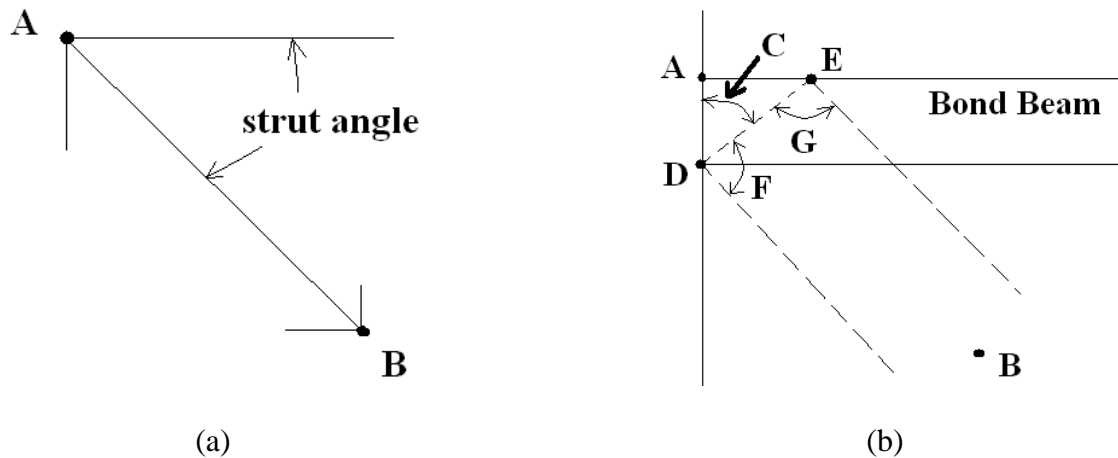


Figure 4-18: Determination of (a) strut angle, and (b) strut width.

Table 4-11: Parameters for ACI equations and resulting strengths

	Partially Grouted			Fully Grouted	
	45 degree strut	56 degree strut	63 degree strut	45 degree strut	
strut f'_m	1640 (11.3)	1640 (11.3)	1640 (11.3)	2860 (19.7)	psi (MPa)
node f'_m	2860 (19.7)	2860 (19.7)	2860 (19.7)	2860 (19.7)	psi (MPa)
β_s	1.0	1.0	1.0	1.0	
β_n	0.6	0.6	0.6	0.6	
strut f_{ce}	1394 (9.6)	1394 (9.6)	1394 (9.6)	2431 (16.8)	psi (MPa)
node f_{ce}	1459 (10.1)	1459 (10.1)	1459 (10.1)	1459 (10.1)	psi (MPa)
strut A_{cs}	28.3 (18258)	36 (23226)	45 (28903)	86.2 (55613)	in ² (mm ²)
node A_{cs}	86.2 (55613)	110 (70968)	136 (87742)	86.2 (55613)	in ² (mm ²)
F_{ns}	39.5 (175)	50.2 (223)	62.5 (278)	126 (559)	kips (kN)

Struts are labeled as degrees below a horizontal line. Struts are found in specimens: 45 deg - PG085-48, PG120-48, PG169-48, FG085-00 and PG085-24; 56 deg PG085-32; 63 deg - PG085-24.

The least angle between a compression strut and nearest tie was 27° and the greatest was 45° . This conforms to the minimum allowable angle between a strut and tie (27°) of ACI 318-05. A model was determined to have failed under the applied loading when the force in any compression strut was approximately at the strength of the compression strut. If a tension tie yielded prior to the failure of a compression strut, the tension tie member was replaced with a force equal to the yield strength of the tie and the model runs continued until a compression strut reached failure.

4.7.2 Model For Specimens PG085-48, PG120-48, And PG169-48

The strut and tie model for a grout horizontal spacing of 48 in. (1219 mm) did not vary between specimens PG085-48, PG120-48 and PG169-48. Compression strut capacity was determined to be 39.5 kips (176 kN). Specimen PG085-48 had the lowest shear stirrup capacity at 19.7 kips (87.6 kN). Failure was reached due to compression failure in member 4 (Figure 4-19) under an applied shear force of 43.2 kips (192 kN) before the shear reinforcement yielded at the lowest ρ_h value. Therefore, increasing the shear reinforcement did not increase the strength and all three specimens have the same shear strength. The experimental results showed that the three specimens reached approximately the same lateral strength of 49.0 kips (218 kN). The calculated strength was approximately 84-94% of the experimental results. Note that member 8, a shear stirrup, is close to yielding in specimen PG085-48 (yield = 19.7 kips (87.6 kN)). The model indicates that the axial strains in the shear reinforcement in specimens PG085-48, PG120-48 and PG169-48 should be 96, 68 and 48% of the yield strains. The experimental results showed that the axial strains in the shear reinforcement in the middle bond beams were

approximately 119, 82 and 50% of the yield strain for specimens PG085-48, PG120-48 and PG169-48. See Table 4-12 for SI values for Figure 4-19(b).

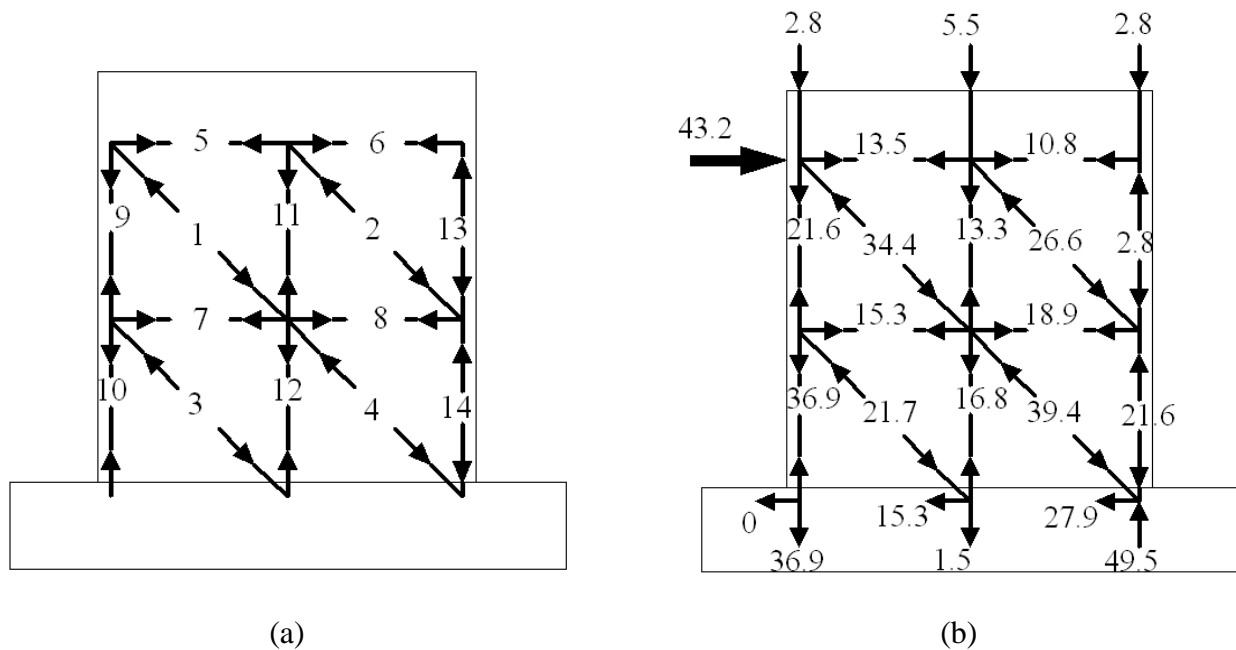


Figure 4-19: Strut and tie model for partially grouted specimens with 48 in. (1219 mm) grout horizontal spacing (a) member labels, and (b) member forces at yield in kips

Table 4-12: SI values for the strut and tie model shown in Figure 4-19(b)

Member	kips	kN
1	-34.4	-153
2	-26.6	-118
3	-21.7	-96.5
4	-39.4	-175
5	13.5	60.1
6	10.8	48.0
7	15.3	68.1

Member	kips	kN
8	18.9	84.1
9	21.6	96.1
10	36.9	164
11	13.3	59.2
12	16.8	74.7
13	-2.8	-12.5
14	-21.6	-96.1

4.7.3 Model For Specimen FG085-00

The model for specimen FG085-00 is the same as discussed in section 4.6.2 except the compression strut strength is 126 kips (560 kN). First yield was reached under an applied shear force of 45.2 kips (201 kN) when member 8, a shear stirrup, reached its yield point of 19.7 kips (87.6 kN) (Figure 4-20). This load is 60% of the experimental result. See Table 4-13 for SI values for Figure 4-20(b).

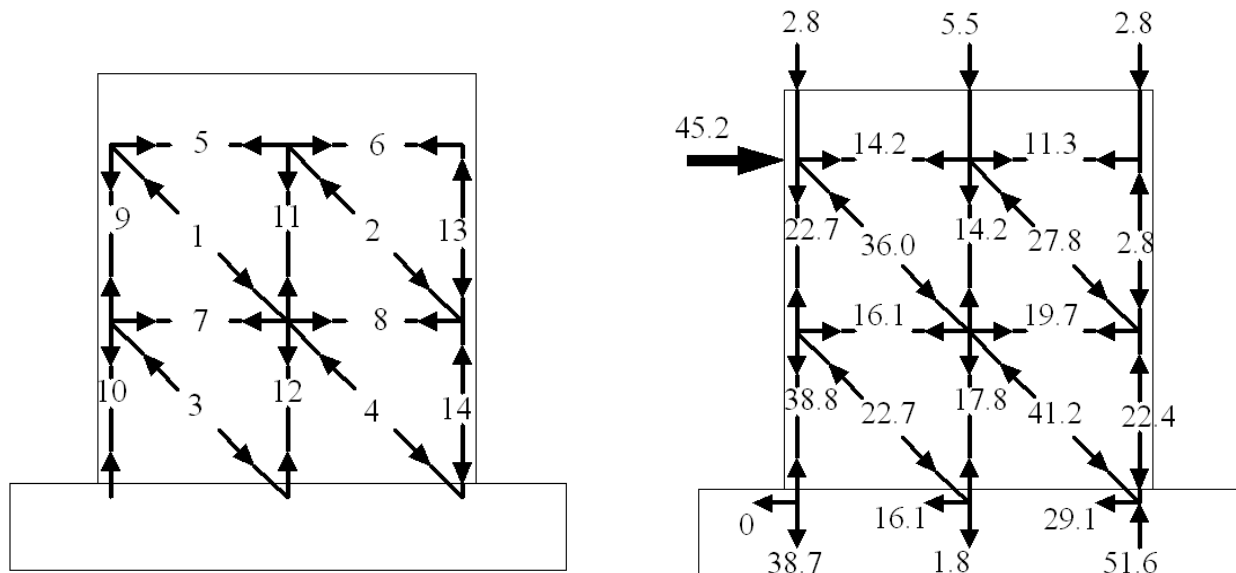


Figure 4-20: Strut and tie model for specimen FG085-00 at first yield, (a) member labels, and (b) member forces at yield in kips

Table 4-13: SI values for the strut and tie model shown in Figure 4-20(b)

Member	kips	kN
1	-36.0	-160
2	-27.8	-124
3	-22.7	-101.0
4	-41.2	-183
5	14.2	63.2
6	11.3	50.3
7	16.1	71.6
8	19.7	87.6
9	22.7	101.0
10	38.8	173
11	14.2	63.2
12	17.8	79.2
13	-2.8	-12.5
14	-22.4	-99.6

Failure was reached at a load of 140 kips (623 kN), when member 2, a compression strut, reached yield at 128 kips (569 kN) (Figure 4-21). This load is 187% of the experimental result.

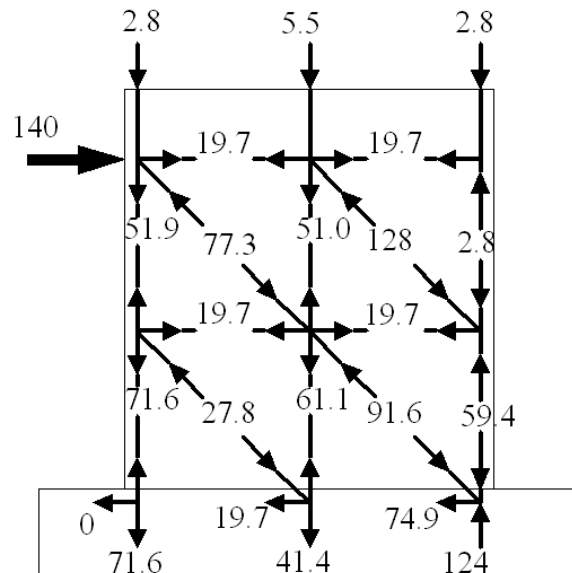


Table 4-14: SI values for the strut and tie model shown in Figure 4-21.

4.7.4 Models For Specimen PG085-32

capacity of 50.2 kips (223 kN) (Figure 4-22). This load is 108% of the experimental result. See Table 4-15 for SI values for Figure 4-22(b).

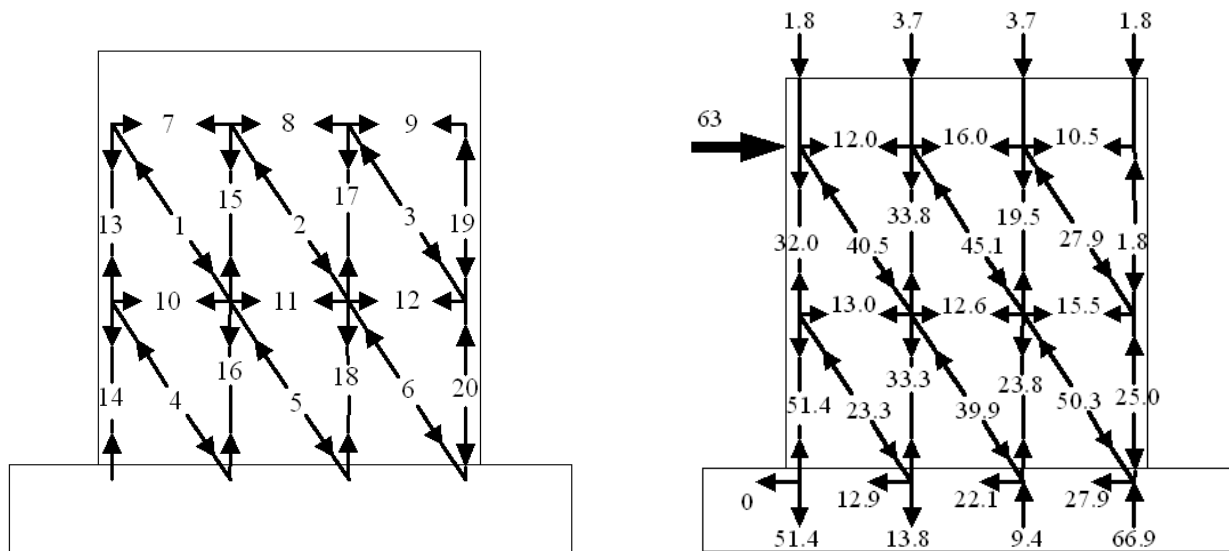


Figure 4-22: Most conservative strut and tie model for specimen PG085-32,
(a) member labels, and (b) member forces at yield in kips.

Table 4-15: SI values for the strut and tie model shown in Figure 4-22(b).

Member	kips	kN
1	-40.5	-180
2	-45.1	-201
3	-27.9	-124
4	-23.3	-104
5	-39.9	-177
6	-50.3	-224
7	12.0	53.4
8	16.0	71.2
9	10.5	46.7
10	13.0	57.8
11	12.6	56.0
12	15.5	68.9
13	32.0	142
14	51.4	229
15	33.8	150
16	33.3	148
17	19.5	86.7
18	23.8	106
19	-1.8	-8.0
20	-25.0	-111

A second model that was examined, and rejected, for PG085-32 is shown in Figure 4-23. This model failed under an applied shear force 69.9 kips (311 kN), which is 111% of the first model. Full results are reported only for the more conservative model.

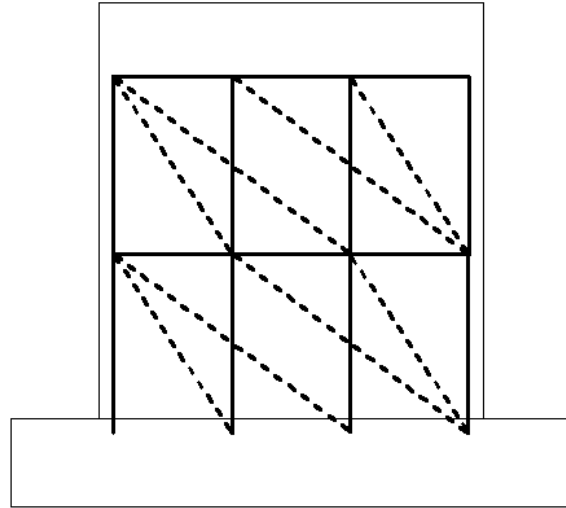


Figure 4-23: Rejected strut and tie model for specimen PG085-32. Dashed lines are compression struts, heavy solid lines are tension ties.

4.7.5 Models For Specimen PG085-24

Three models were examined for specimen PG085-24. The most conservative model failed under a shear force of 63.0 kips (280 kN) when member 10, a compression strut, reached its failure load of 39.2 kips (174 kN) (Figure 4-24). This shear force is 95% of the experimental result. See Table 4-16 for SI values for Figure 4-24(b).

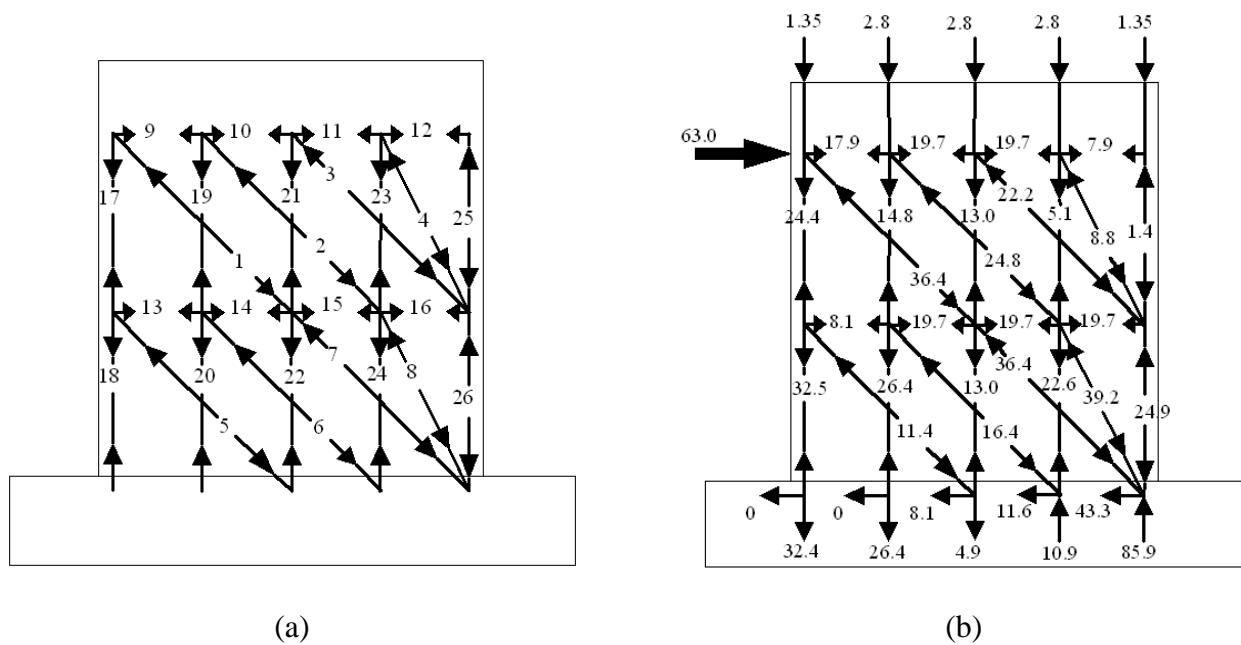


Figure 4-24: Most conservative strut and tie model for specimen PG085-24, (a) member labels, and (b) member forces at failure in kips.

Table 4-16: SI values for the strut and tie model shown in Figure 4-24(b).

Member	kips	kN
1	-36.4	-162
2	-24.8	-110
3	-22.2	-98.8
4	-8.8	-39.1
5	-11.4	-50.7
6	-16.4	-73.0
7	-36.4	-162
8	-39.2	-174
9	17.9	79.6
10	19.7	87.6
11	19.7	87.6
12	7.9	35.1
13	8.1	36.0
14	19.7	87.6
15	19.7	87.6
16	19.7	87.6
17	24.4	109
18	32.5	145
19	14.8	65.8
20	26.4	117
21	13.0	57.8
22	13.0	57.8
23	5.1	22.7
24	22.6	101
25	-1.4	-6.2
26	-24.9	-111

The second and third models (Figure 4-25) reached failure under shear forces of 84.9 kips (378 kN) and 112 kips (498 kN), which is 135% and 178%, respectively, of the most conservative model.. Only the most conservative model is reported in detail.

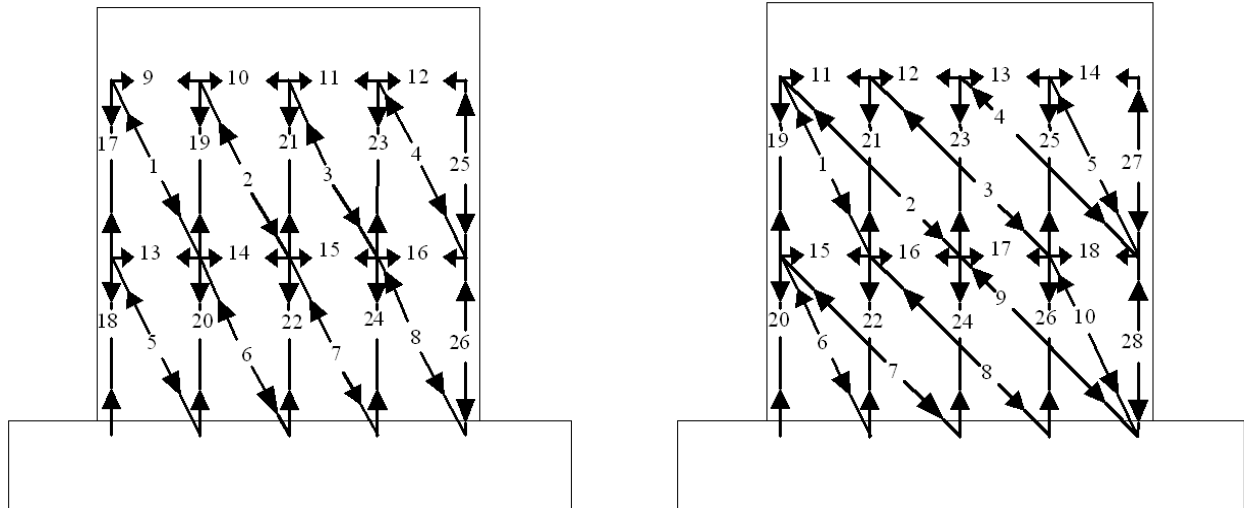


Figure 4-25: Rejected strut and tie models for specimen PG085-24, model reached failure at (a) 84.9 kips (378 kN) and (b) 112 kips (498 kN).

4.7.6 Strut And Tie vs. Experimental Results

Table 4-17 shows a comparison of the predicted shear strengths using the strut and tie models to the experimental results. The MSJC (2008) predictions are included for additional comparison. A value less than one is conservative while a value greater than one is unconservative. As shown in the table, the strut and tie models were good predictors of shear strength for the partially grouted specimens with errors from -14% to +8%. Contrary to expectations, the fully grouted specimen was poorly predicted with an error of +87%.

Table 4-17: Strut & Tie and MSJC (2008) predictions vs. experimental results.

	PG085-48	PG120-48	PG169-48	PG085-32	PG085-24	FG085-00
MSJC (V_n) (V_n)/(V_{max})	1.19	1.33	1.76	1.07	0.99	1.51
Strut & Tie (V_{ST}) (V_{ST})/(V_{max})	0.86	0.84	0.94	1.08	0.95	1.87
Test (V_{max}) (V_{max})/(V_{max})	1.00	1.00	1.00	1.00	1.00	1.00

4.8 Other Codes And Methods

4.8.1 Equations By Fattal

Fattal (1993a and b) proposed the following equations for predicting shear strength of masonry shear walls. The total nominal shear strength, V , is given by Equation 4-14:

$$V = A \cdot v \quad (4-14)$$

The shear stress, v , is given by Equation 4-15:

$$v = v_m + v_s + v_p \quad (4-15)$$

The shear stress from the masonry, v_m , is given by Equation 4-16:

$$v_m = k_o \cdot k_u \cdot \left(\frac{0.5}{r + 0.8} + 0.18 \right) \cdot \rho_v^{0.7} \cdot \sqrt{f_y \cdot f'_m} \quad (4-16)$$

The shear stress from the steel shear reinforcement, v_s , is given by Equation 4-17:

$$v_s = 0.011 \cdot \rho_h^{0.31} \cdot f_{yh} \cdot \gamma \cdot \delta \quad (4-17)$$

The shear stress from an applied normal force, v_p , is given by Equation 4-18:

$$v_p = 0.012 k_o \cdot f'_m + 0.2 \sigma \quad (4-18)$$

Where the following notation and constants apply to the test specimens:

A = Gross area (790 in.² (509676 mm²))

k_o = 0.8 for partially grouted and 1.0 for fully grouted

k_u = 0.64 for partially grouted and 1.0 for fully grouted

r = wall aspect ratio ($r = 0.93$ for all specimens)

ρ_v = ratio of vertical reinforcement in one end cell

ρ_h = horizontal reinforcement ratio

f_y = yield strength of reinforcement ($f_y = 63.6$ ksi (438 MPa))

f_{yh} = yield strength of horizontal reinforcement ($f_y = 63.6$ ksi (438 MPa))

f_m = compressive strength of masonry prisms (1640 psi (11.3 MPa) ungrouted, 2860 psi (19.7 MPa) grouted)

γ = 0.6 for partially grouted, 1.0 for fully grouted

δ = 0.6 for cantilever boundary conditions

Table 4-18 lists the predicted shear stress components and shear strength for the specimens using the Fattal equations. Table 4-19 compares the Fattal and MSJC shear strength predictions to the experimental results. Note that the Fattal equations were more conservative than the MSJC equations for all partially grouted specimens, but not for the fully grouted specimen. They were also significantly better than the MSJC equations for predicting the strengths of the specimens with 48 in. (1219 mm) grout horizontal spacing.

Table 4-18: Fattal equation shear stress components and predicted shear capacity.

	V_m	V_s	V_p	v	V
PG085-48	0.0261 ksi (0.1800 MPa)	0.0281 ksi (0.1940 MPa)	0.0185 ksi (0.1279 MPa)	0.0728 ksi (0.5019 MPa)	57.5 kips (256 kN)
PG120-48	0.0261 ksi (0.1800 MPa)	0.0313 ksi (0.2159 MPa)	0.0185 ksi (0.1279 MPa)	0.0760 ksi (0.5238 MPa)	60.0 kips (267 kN)
PG169-48	0.0261 ksi (0.1800 MPa)	0.0348 ksi (0.2401 MPa)	0.0185 ksi (0.1279 MPa)	0.0795 ksi (0.5479 MPa)	62.8 kips (279 kN)
PG085-32	0.0210 ksi (0.1449 MPa)	0.0281 ksi (0.1940 MPa)	0.0185 ksi (0.1279 MPa)	0.0677 ksi (0.4667 MPa)	53.5 kips (238 kN)
PG085-24	0.0210 ksi (0.1449 MPa)	0.0281 ksi (0.1940 MPa)	0.0185 ksi (0.1279 MPa)	0.0677 ksi (0.4667 MPa)	53.5 kips (238 kN)
FG085-00	0.0673 ksi (0.4642 MPa)	0.0469 ksi (0.3233 MPa)	0.0371 ksi (0.2560 MPa)	0.1513 ksi (1.0435 MPa)	120 kips (532 kN)

Table 4-19: Fattal and MSJC predictions as a percentage of the experimental results.

	PG085-48	PG120-48	PG169-48	PG085-32	PG085-24	FG085-00
Fattal	115%	117%	137%	91%	80%	160%
MSJC	119%	133%	176%	107%	99%	151%
Test	100%	100%	100%	100%	100%	100%

4.8.2 New Zealand Code

The shear provisions of the New Zealand code are found in section 10.3 of NZS 4230:2004. The New Zealand code considers shear stress contributions from the masonry, axial force, and shear reinforcement and multiplies this by the effective, not gross, area. The nominal shear strength of a section, V_n , is given by Equation 4-19. The total shear stress, v_n , is given by Equation 4-20.

$$V_n = v_n \cdot b_w \cdot d \quad (4-19)$$

$$v_n = v_m + v_p + v_s \quad (4-20)$$

The shear stress from masonry, v_m , is given by Equation 4-21. The factors C_1 and C_2 are given by Equations 4-22 and 4-23, respectively.

$$v_m = (C_1 + C_2) \cdot v_{bm} \quad (4-21)$$

$$C_1 = 33 \cdot \rho_w \cdot \frac{f_y}{330} \quad (4-22)$$

$$C_2 = 0.42 \left(4 - 1.75 \frac{h_e}{L_w} \right) \quad (4-23)$$

The shear stress from the axial force, v_p , is given by Equation 4-24. Note that N^* from NZS 4230:2004 is presented as N^x here due to constraints of the software used to present the equation.

$$v_p = 0.9 \cdot \frac{N^x}{b_w \cdot d} \cdot \tan(\alpha) \quad (4-24)$$

where N^x shall not be taken greater than $0.1 \cdot f_m \cdot A_g$, and

v_p shall not be taken greater than $0.1 \cdot f_m$

The shear stress from the shear reinforcement, v_s , is given by Equation 4-25.

$$v_s = C_3 \cdot \frac{A_v \cdot f_y}{b_w \cdot s} \quad (4-25)$$

where $C_3 = 0.8$ for walls

When shear reinforcement is required, the minimum required shear reinforcement is given by Equation 4-26.

$$A_v \geq \frac{0.15 b_w \cdot s}{f_y} \quad (4-26)$$

The notation used in Equations 4-19 through 4-26 is as follows:

A_{ps}	Area of prestressed reinforcement in flexural tension zone, mm^2
A_s	Area of non-prestressed reinforcement, mm^2
A_v	Area of shear reinforcement within a distance, s , mm^2
b_w	Effective web width, mm. <i>For partially grouted walls, b_w = net thickness of the face shells. For fully grouted walls, b_w = thickness of the wall.</i>
C_1	Shear strength coefficient
C_2	Shear strength coefficient
C_3	Shear strength coefficient
d	Distance from extreme compression fibre to centroid of longitudinal tension reinforcement, but needs not be less than $0.8 L_w$ for walls or $0.8 h$ for prestressed components, mm. <i>For all specimens: $d = 0.8 * L_w$</i>
\hat{f}_m	Specified compressive strength of masonry, MPa. <i>Limited to 4 MPa or 12 MPa depending on the observation type of masonry selected (C or B, respectively)</i>
f_y	Lower characteristic yield strength of non-prestressed reinforcement, MPa. <i>For all specimens: $f_y = 63.6 \text{ ksi} (438.5 \text{ MPa})$.</i>
h_e	Effective wall height in the plane of applied loading, mm. <i>For all specimens: 96 in. (2438 mm).</i>
L_w	Horizontal length of wall, in direction of applied shear force, mm. <i>For all specimens: 103.6 in. (2631 mm).</i>
N^x	Design axial load in compression at given eccentricity, N. <i>For all specimens, applied axial load = 11,080 lbf (49286 N).</i>
p_w	$(A_s + A_{ps}) / b_w d$

s	Spacing of shear reinforcement in direction parallel to longitudinal reinforcement, mm. <i>For all specimens: 48 in. (1219 mm).</i>
v_{bm}	Basic type-dependant shear strength of masonry, MPa. <i>For all specimens: $v_{bm} = 0.30$ or 0.70 depending on observation type of masonry selected (C or B, respectively)</i>
v_n	Total shear stress corresponding to V_n , MPa
v_m	Maximum permitted type-dependent shear stress provided by masonry, MPa
v_p	Shear stress provided by axial load, MPa
v_s	Shear stress provided by shear reinforcement, MPa
V_n	Nominal shear strength of section, N
α	Angle formed between lines of axial load action and resulting reaction on a component, degree. <i>For all specimens, $\tan \alpha = 0.46$.</i>

Assuming Type C for the observational type of masonry, the predicted shear strengths and shear stress components of the specimens are presented in Table 4-20. Table 4-21 shows a comparison of the predictions using NZS 4230:2004 and the MSJC versus the experimental results. For specimens PG085-32 and PG085-24, the New Zealand code is more conservative than the MSJC and under-estimates the experimental results by 6 and 17%, respectively. For specimen PG085-48 and PG120-48, the New Zealand code is more conservative than the MSJC but still over-estimates the strength of the other specimens. For specimens PG169-48 and FG085-00, the New Zealand code was less conservative than the MSJC.

Table 4-20: Shear strengths and shear stress components predicted by New Zealand code, observational type of masonry C.

	V_n	v_n	v_m	v_p	v_s
PG085-48	55.1 kips (245 kN)	0.2661 ksi (1.8347 MPa)	0.0766 ksi (0.5283 MPa)	0.0580 ksi (0.4000 MPa)	0.1315 ksi (0.9064 MPa)
PG120-48	66.6 kips (296 kN)	0.3213 ksi (2.2154 MPa)	0.0766 ksi (0.5283 MPa)	0.0580 ksi (0.4000 MPa)	0.1867 ksi (1.2871 MPa)
PG169-48	82.4 kips (366 kN)	0.3976 ksi (2.7411 MPa)	0.0766 ksi (0.5283 MPa)	0.0580 ksi (0.4000 MPa)	0.2629 ksi (1.8128 MPa)
PG085-32	55.0 kips (245 kN)	0.2654 ksi (1.8296 MPa)	0.0759 ksi (0.5232 MPa)	0.0580 ksi (0.4000 MPa)	0.1315 ksi (0.9064 MPa)
PG085-24	55.2 kips (245 kN)	0.2663 ksi (1.8359 MPa)	0.0768 ksi (0.5295 MPa)	0.0580 ksi (0.4000 MPa)	0.1315 ksi (0.9064 MPa)
FG085-00	122 kips (543 kN)	0.1931 ksi (1.3311 MPa)	0.0543 ksi (0.3746 MPa)	0.0073 ksi (0.0500 MPa)	0.1315 ksi (0.9064 MPa)

Table 4-21: NZS 4230:2004 and MSJC predictions as a percentage of the experimental results, observational type of masonry C.

	PG085-48	PG120-48	PG169-48	PG085-32	PG085-24	FG085-00
NZS	110%	130%	180%	94%	83%	163%
MSJC	119%	133%	176%	107%	99%	151%
Test	100%	100%	100%	100%	100%	100%

Tables 4-22 and 4-23 show the same data as Tables 4-20 and 4-21, except with the assumption of Type B for the observational type of masonry. For all specimens, the New Zealand code was significantly less conservative than the MSJC. Assuming an observational type of masonry B for the specimens is not a valid assumption.

Table 4-22: Shear strengths and shear stress components predicted by New Zealand code,
observational type of masonry B

	V_n	v_n	v_m	v_p	v_s
PG085-48	86.2 kips (383 kN)	0.4161 ksi (2.8686 MPa)	0.1788 ksi (1.2327 MPa)	0.1058 ksi (0.7295 MPa)	0.1315 ksi (0.9064 MPa)
PG120-48	97.6 kips (434 kN)	0.4713 ksi (3.2493 MPa)	0.1788 ksi (1.2327 MPa)	0.1058 ksi (0.7295 MPa)	0.1867 ksi (1.2871 MPa)
PG169-48	113 kips (505 kN)	0.5475 ksi (3.7750 MPa)	0.1788 ksi (1.2327 MPa)	0.1058 ksi (0.7295 MPa)	0.2629 ksi (1.8128 MPa)
PG085-32	85.8 kips (382 kN)	0.4143 ksi (2.8567 MPa)	0.1771 ksi (1.2208 MPa)	0.1058 ksi (0.7295 MPa)	0.1315 ksi (0.9064 MPa)
PG085-24	86.3 kips (384 kN)	0.4165 ksi (2.8714 MPa)	0.1792 ksi (1.2355 MPa)	0.1058 ksi (0.7295 MPa)	0.1315 ksi (0.9064 MPa)
FG085-00	168 kips (746 kN)	0.2655 ksi (1.8306 MPa)	0.1268 ksi (0.8741 MPa)	0.0073 ksi (0.0500 MPa)	0.1315 ksi (0.9064 MPa)

Table 4-23: NZS 4230:2004 and MSJC predictions as a percentage of the experimental results,
observational type of masonry B

	PG085-48	PG120-48	PG169-48	PG085-32	PG085-24	FG085-00
NZS	172%	190%	248%	147%	130%	224%
MSJC	119%	133%	176%	107%	99%	151%
Test	100%	100%	100%	100%	100%	100%

4.8.3 MSJC (2008) ASD

The MSJC (2008) ASD provisions have undergone a major revision for the MSJC (2011), which is out for public comment at the time of writing this thesis. Since the MSJC (2008) ASD provisions will shortly be superseded for new design, they will not be examined here.

CHAPTER 5: CONCLUSIONS

5.1 Summary

This research investigated the effectiveness of the current MSJC Strength Design shear strength equations for predicting the shear strength of partially grouted masonry walls. Variables investigated included grout horizontal spacing and horizontal (shear) reinforcement ratio. The effects of grout horizontal spacing and horizontal reinforcement ratio were analyzed. Recommendations were then made for modifications to the current MSJC shear equations.

5.2 Conclusions

The current MSJC shear equations over-estimated the strength of partially grouted walls with 48 in. (1219 mm) grout horizontal spacing. A significant source of this error is from over-estimating the contribution of the shear reinforcement. In addition, the MSJC (2008) equations overestimated the masonry contribution. For partially grouted walls with grout horizontal spacing 32 in. (813 mm), or less, and a horizontal reinforcement ratio of 0.085%, the equations were adequate. Davis (2008) concluded the MSJC (2008) equations were adequate for fully grouted walls, albeit with improvement possible. However, the fully grouted specimen tested for this study was significantly below the MSJC prediction.

There appears to be a maximum shear reinforcement ratio after which no additional shear capacity is achieved. Based on the experimental results, the maximum value appears to be in the range of 0.085% to 0.100% for specimens with a 48 in. (1219 mm) grout horizontal spacing. Increasing the shear reinforcement beyond this level did not increase the shear strength of the specimens. Beyond a horizontal reinforcement ratio of 0.085%, i.e. at 0.120% and 0.169%, failure in the wall specimens occurred without the shear reinforcement reaching yield. A similar

statement cannot be made for the 32 in. (813 mm) and 24 in. (610 mm) grout horizontal spacings due to there being only one shear reinforcement level, 0.085%, tested at these grout horizontal spacings.

A shear reinforcement anchorage problem may exist even when using code-compliant 180° hooks. Two specimens, PG085-48 and PG085-24, showed end shell vertical splitting cracks indicative of an anchorage problem. The other specimens showed face shell cracking patterns similar to the face shell cracking patterns associated with the end shell vertical cracks of specimens PG085-48 and PG085-24, possibly indicating a developing anchorage problem. A possible source for this problem may be the use of too large a rebar in an 8 in. (203 mm) CMU. With a code-compliant hook radius, a #5 rebar is a tight fit in an 8 in. (203 mm) CMU, possibly too tight to maintain adequate cover under normal construction conditions. A limit on shear reinforcement diameter based on CMU size should be considered.

Figure 5-1 shows the experimental results and the predictions using the MSJC (2008) strength design provisions, the equations by Fattal (1993a and b), the New Zealand code, and the strut and tie model. As shown, the equations by Fattal (1993a and b) were unconservative for four of the specimens, i.e. PG085-48, PG120-48, PG169-48, and FG085-48, but was less unconservative than the MSJC (2008) except for FG085-00. For the remaining specimens, PG085-32 was predicted fairly well (-9% error) but PG085-24 was predicted at only 80% of the experimental strength, which is overly conservative. The equations, while more conservative than the MSJC (2008), were not judged to be adequate as a replacement. The New Zealand code was unconservative for four of the specimens, i.e. PG085-48, PG120-48, PG169-48, and FG085-48, and was reasonably close to the MSJC (2008) predictions for these specimens. Predictions for specimens PG085-32 and PG085-24 were conservative. The New Zealand code predictions

were judged to be generally similar to the MSJC (2008) and did not present a substantial improvement. The strut and tie model was a good predictor for all specimens except FG085-00. This was surprising in that the strut and tie was expected to be a reasonable predictor for the fully grouted wall. The partially grouted specimens were all predicted within 0.86 to 1.08 (ratio: V_n / V_{test}).

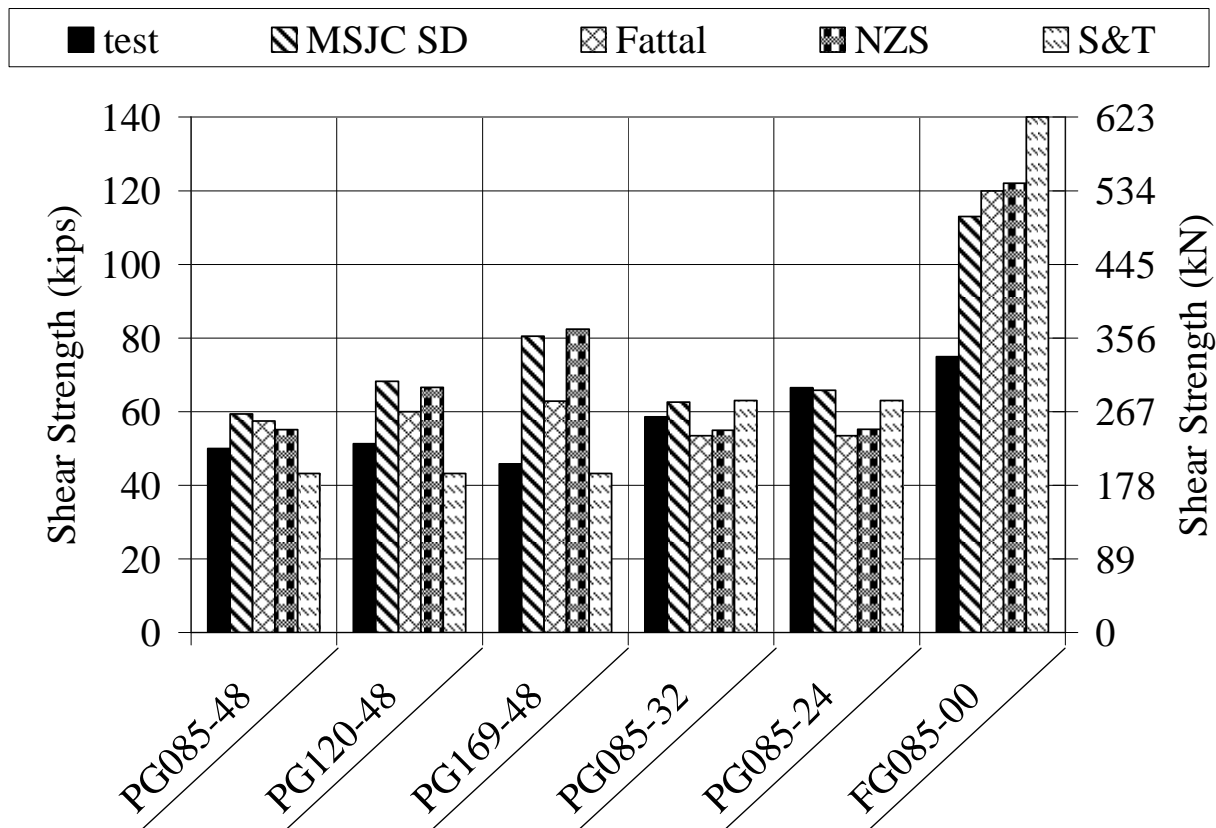


Figure 5-1: Experimental shear strength and shear strength predictions using MSJC (2008) Strength Design, Fattal equations, New Zealand code, and strut and tie model.

The failure behavior of the partially grouted walls does not conform to the assumption that plane sections remain plane. There was some evidence that the behavior may reflect a

reinforced concrete frame with masonry infill, but there is inadequate data to make a definitive statement.

5.3 Modifications To MSJC (2008) Strength Design Equations

The current MSJC equations may be improved with adjustments to the equation for nominal shear strength from the reinforcement, V_{ns} , as shown in Equation 4-8, presented here as Equation 5-1:

$$V_{ns} = \beta \cdot \left(\frac{1}{2} \right) \cdot (A_v \cdot f_y) \cdot \left(\frac{d_{45}}{s} \right) \quad (5-1)$$

where d_{45} = the lesser of $\{d_v, h_w\}$

where: $\beta = 1.0$ for $\rho_h \leq 0.001$, else

$$\beta = 1 - 2 \cdot \rho_h \quad (5-2)$$

where ρ_h is calculated as:

$$\rho_h = \frac{A_v}{s \cdot t} \quad (5-3)$$

Further improvement is possible with a modification to the nominal shear strength from the masonry, V_{nm} , as shown in Equation 4-6, presented here as Equation 5-4:

$$V_{nm} = \alpha \cdot \left[4.0 - 1.75 \left(\frac{M_u}{V_u \cdot d_v} \right) \right] \cdot A_n \cdot \sqrt{f_m} + 0.25 P_u \quad (5-4)$$

where: $\alpha = 1.0$ for $A_n / A_g \geq 0.5$, else

$$\alpha = 3.44 \left(\frac{A_n}{A_g} \right) - 0.8 \geq 0 \quad (5-5)$$

It is important to note that all of these modifications rely on using a value for the compressive strength of masonry, f_m , obtained from tests on *ungROUTED* masonry prisms when calculating the shear strength of partially grouted walls. The MSJC (2008) is silent on whether f_m should be calculated from ungrouted masonry prisms, grouted masonry prisms, or based on an average of ungrouted *and* grouted masonry prism tests. It is recommended that the MSJC provisions explicitly state that when calculating the shear strength of a partially grouted wall, the compressive strength of masonry, f_m , must be for *ungROUTED* masonry prisms.

5.4 Future Research

Additional specimens need to be tested to confirm the behavior observed during this research. Further research is needed to address some questions raised by this research. Among those questions are:

- There appears to be an upper limit to the horizontal reinforcement ratio, after which additional steel provides no additional strength. Tentatively, this limit appears to be in the range of 0.085% to 0.100% for 48 in. (1219 mm) grout horizontal spacing. If this limit exists, it may be different for varying grout horizontal spacings. This limit is probably best addressed through the use of a scaling factor applied to V_{ns} .
- As grout horizontal spacing decreases, the net cross sectional area of masonry increases as a power function. The behavior seen during this research suggests the strength increases linearly as grout horizontal spacing decreases. If this is correct, the current equation is addressing the increase in net area improperly.
- The current assumption that plane sections remain plane is questionable. This assumption needs to be examined in greater detail over a larger number of specimens.

REFERENCES

- American Concrete Institute: 2005, *Building Code Requirements for Structural Concrete (ACI 318-05) and Commentary (ACI 318R-05)*, Farmington Hills, MI.
- Brandow, G.E., Ekwueme, C.G., Hart G.C., 2006 *Design of Reinforced Masonry Structures*, Concrete Masonry Association of California and Nevada, Citrus Heights, CA, 2007.
- Davis, C.L. "Evaluation of Design Provisions For In-Plane Shear In Masonry Walls", Washington State University, Masters Thesis, Dec 2008.
- Elmapruk, J.H., ElGawady, M.A., "Evaluation of the MSJC 2008 Shear Strength Equations For Partially Grouted Masonry Shear Walls." 11th Canadian Masonry Symposium, Toronto, Ontario, May 31-June 3, 2009.
- Fattal, S. G. (1993a) "Strength of partially-grouted masonry shear walls under lateral loads," NISTIR 93-5147, Gaithersburg, MD.
- Fattal, S. G. (1993b) "The effect of critical parameters on the behavior of partially grouted masonry shear walls under lateral loads," NISTIR 93-5147, Gaithersburg, MD
- FEMA 356: Prestandard and Commentary for the Seismic Rehabilitation of Buildings, Federal Emergency Management Agency, Washington, D.C., Nov 2000
- Masonry Standards Joint Committee: 2008, *Building Code Requirements for Masonry Structures*, TMS 402-08, The Masonry Society, Boulder, CO, ACI 530-08, American Concrete Institute, Farmington Hills, MI, ASCE 5-08, American Society of Civil Engineers, Reston, VA.
- New Zealand Standard 4230:2004, *Design of Reinforced Concrete Masonry Structures*, Standards Association of New Zealand, Wellington.

- Priestley, M.J.N., Calvi, G.M., Kowalsky, M.J., *Displacement-Based Seismic Design of Structures*, IUSS Press, Italy, 978-88-6198-000-6, 2007.
- Priestley, M.J.N., Seible, F., Calvi, G.M., *Seismic Design and Retrofit of Bridges*, Wiley, New York, NY, 0-471-57998-X, 1996.
- Voon, K.C. "In-Plane Seismic Design of Concrete Masonry Structures", University of Auckland, PhD Thesis, June 2007.
- Wight, G.D., Kowalsky, M.J., Ingham, J.M., "Direct Displacement-Based Seismic Design of Unbonded Post-Tensioned Masonry Walls." *ACI Structural Journal*, Sept-Oct 2007, pp560-569.

NOTATION

A_n	net cross-sectional area of a member, in. ²
A_v	cross-sectional area of shear reinforcement, in. ²
d_v	actual depth of a member in direction of shear considered, in.
d_{45}	effective depth of a 45° shear crack, taken as the lesser of d_v and h_w
\hat{f}_m	specified compressive strength of masonry, psi
f_y	specified yield strength of steel for reinforcement and anchors, psi
h_w	height of the wall to the point V_u is applied, in.
M_u	factored moment, in.-lb
P_u	factored axial load, lb
s	spacing of reinforcement, in.
t	nominal thickness of member, in.
V_n	nominal shear strength, lb
V_{nm}	nominal shear strength provided by masonry, lb
V_{ns}	nominal shear strength provided by shear reinforcement, lb
V_u	factored shear force, lb
ρ_h	horizontal reinforcement ratio
ρ_{heff}	effective horizontal reinforcement ratio

APPENDIX A: CONSTRUCTION

A.1 Foundation Design And Construction

All foundations were constructed using the same reinforcement schedule and dimensions. Foundations were reinforced with 8 #9 rebars for flexural strength and 9 evenly spaced #4 stirrups for shear (Figure A-1). Foundation forms were made from plywood and lumber to nominal dimensions of 142 in. long by 25 in. wide by 19 in. high (3607 mm x 635 mm x 483 mm) (Figure A-2).

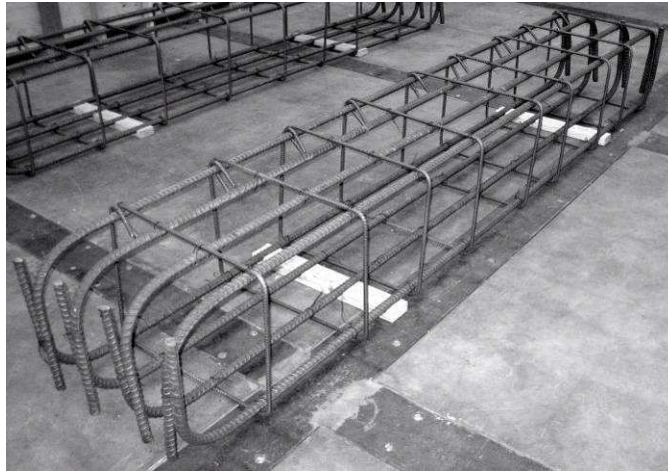


Figure A-1: Foundation reinforcement



Figure A-2: Foundation forms

All foundations were poured at the same time and from the same concrete batch. Figure A-3 shows the freshly poured foundations with flexural steel being held at the proper spacing by 2x4 lumber. Figure A-4 shows a foundation with the form stripped away.



Figure A-3: Freshly poured foundations



Figure A-4: Foundation with flexural reinforcement at 48 in. (1219 mm).

A.2 Wall Specimen Construction

See Chapter 2 for the primary details of wall construction. Presented here are photos of the walls at various stages of construction.

Figure A-5 shows three specimens During the second day of construction. The first six courses have been grouted and courses 7 through 12 are under construction. Figure A-6 shows a completed specimen. The OSB boards at the 12th course are a template holding the bolts at the correct spacing.



Figure A-5: Wall specimens at mid-construction



Figure A-6: Finished wall specimen

APPENDIX B: MATERIAL PROPERTIES SPECIMENS AND TESTING

B.1 Material Properties Specimens

B.1.1 Masonry Prisms

Masonry prisms were constructed from masonry units randomly selected from the shipment of units used to construct the wall specimens. Four ungrouted and four grouted prisms comprised of three CMU each were prepared. Prisms were prepared according to ASTM C1314-07. Gypsum caps were cast on the top and bottom of each prism as shown in Figure B-1.



Figure B-1: Station for applying gypsum caps.

B.1.2 Grout Prisms

Grout was collected from the second and third lifts and used to construct three prisms per grout lift. Prisms were prepared according to ASTM 1019-07 with the following exceptions:

1. Prisms were removed from the molds after 4 days (03 March 2009 prisms) and 3 days (04 March 2009 prisms), instead of within 24 to 48 hours.
2. Prisms were not placed in a water bath until the third day after removal from the molds, instead of within 8 hours after removal.

Gypsum caps were cast on the top and bottom of each prism as shown in Figure B-1. Table B-1 lists the dimensions of the grout prisms prepared.

Table B-1: Grout prism dimensions

Date	Prism #	height (in)	width1 (in)	width2 (in)	area (in ²)	average width	width1 off average by	width2 off average by	width as % of height
03 Mar 09	G3-3-1	7.67	4.15	4.06	16.84	4.10	-1.2%	1.2%	53.5%
03 Mar 09	G3-3-2	7.74	4.14	4.42	18.32	4.28	3.3%	-3.3%	55.4%
03 Mar 09	G3-3-3	7.67	3.99	4.25	16.95	4.12	3.1%	-3.1%	53.7%
04 Mar 09	G3-4-1	7.64	4.13	4.18	17.27	4.16	0.6%	-0.6%	54.4%
04 Mar 09	G3-4-2	7.63	4.28	4.35	18.60	4.31	0.9%	-0.9%	56.5%
04 Mar 09	G3-4-3	7.69	4.02	4.23	16.99	4.12	2.5%	-2.5%	53.6%

B.1.3 Mortar Prisms

Mortar prisms were not collected due to miscommunication.

B.1.4 CMU

Four full-block masonry units were randomly selected from the shipment of units used to construct the wall specimens. Gypsum caps were cast on the top and bottom of each prism as shown in Figure B-1.

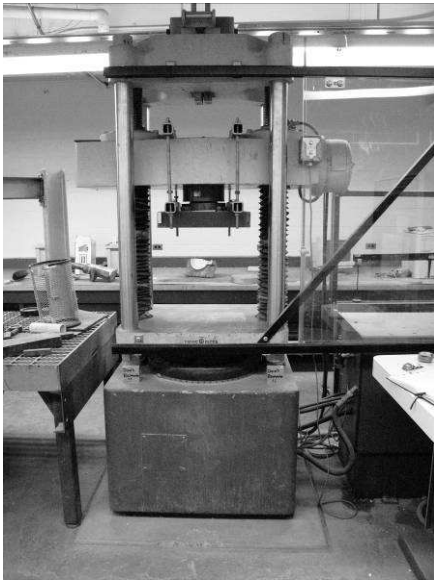
B.1.5 Rebar Coupons

Two coupons were prepared for each size of rebar to be tested. The coupons were 24 in. (610 mm) long and consisted of unworked rebar.

B.2 Testing

B.2.1 Test Equipment

All materials properties specimens were tested in a hydraulic tension/compression machine. Figure B-2(a) shows the press set up for compression testing. Figure B-2(b) shows the press controller and data collection system.



(a)



(b)

Figure B-2: Material properties testing equipment, (a) tension/compression press, and (b) controller and data acquisition system.

B.2.1 Masonry Prisms

Testing was carried out per ASTM C1314-07. One ungrouted prism (UG2) was destroyed due to operator error, leaving 3 valid specimens. All four grouted prisms were tested without problems.

B.2.2 Grout Prisms

Testing was carried out per ASTM 1019-07. One prism (G3-4-2) had to be discarded when the top plate of the hydraulic press engaged the top of the prism at an angle, thereby applying the load to only a portion of the prism cross section.

B.2.3 CMU

Testing was carried out per ASTM 1314-07. No problems were encountered during testing.

B.2.4 Rebar

Rebar coupons were tested under a direct tension pull. Only one #7 rebar was tested due to the first coupon becoming lodged in the testing machine. After examining the results for the #5, #6 and single #7, it was determined the data was consistent enough to justify not testing the second #7 coupon given the probability of the coupon becoming lodged in the testing machine.

B.3 Material Properties Test Results

B.3.1 Masonry Prisms

Table B-2 lists the results for the ungrouted prisms. The coefficient of variation for the compressive strength was 6.8%. The compressive strength was 1640 psi (11.3 MPa).

Table B-2: UngROUTed prism results

Prism #	lbf	area (in ²)	psi	correction factor	corrected psi	average psi	report as (psi)
UG1	86,436	61.93	1396	1.08	1507		
UG2	75,265	bad test - operator error					
UG3	97,527	61.93	1575	1.08	1701		
UG4	97,588	61.93	1576	1.08	1702	1637	1640
COV =						6.8%	

Table B-3 lists the results for the ungrouted prisms. The coefficient of variation for the compressive strength was 5.0%. The compressive strength was 2860 psi (19.7 MPa).

Table B-3: Grouted prism results

Prism #	lbf	length (in)	width (in)	area (in ²)	psi	correction factor	corrected psi	average psi	report as (psi)
FG1	317,946	15.5625	7.625	118.16	2691	1.08	2906		
FG2	290,314	15.5625	7.625	118.16	2457	1.08	2654		
FG3	320,651	15.5625	7.6875	118.16	2714	1.08	2931		
FG4	324,537	15.5625	7.625	118.16	2747	1.08	2966	2864	2860
COV =								5.0%	

B.3.2 Grout Prisms

Table B-4 lists the results for the grout prisms. The coefficient of variation for the compressive strength was 6.9%. The compressive strength was 4239 psi (29.2 MPa).

Table B-4: Grout prism results

Date	Prism #	lbf	area (in ²)	psi	average psi	report as (psi)
03 Mar 09	G3-3-1	68,973	16.84	4096		
03 Mar 09	G3-3-2	82,064	18.32	4480		
03 Mar 09	G3-3-3	65,502	16.95	3866		
04 Mar 09	G3-4-1	72,071	17.27	4174		
04 Mar 09	G3-4-2	bad test				
04 Mar 09	G3-4-3	77,835	16.99	4582	4239	4240
COV =						6.9%

B.3.3 CMU

Table B-5 lists the results for the CMU. The coefficient of variation for the compressive strength was 5.6%. The compressive strength was 2630 psi (18.1 MPa).

Table B-5: CMU test results

CMU #	lbf	area (in ²)	psi	average psi	report as (psi)
CMU1	168,951	61.93	2728		
CMU2	167,816	61.93	2710		
CMU3	149,451	61.93	2413		
CMU4	165,915	61.93	2679	2633	2630
			COV =	5.6%	

B.3.4 Rebar

Table B-6 lists the results for the rebar coupons. The coefficient of variation for the yield stress was 0.37%. The yield stress was 63.6 ksi (438.5 MPa).

Table B-6: Rebar coupon results

Sample	bar size	bar area (in ²)	force (lbf)	yield stress (psi)
5-A	#5	0.31	19600	63,226
5-B	#5	0.31	19700	63,548
6-A	#6	0.44	28100	63,864
6-B	#6	0.44	28000	63,636
7-A	#7	0.60	38200	63,667
		average yield stress		63,588
		standard deviation		233
		COV		0.37%

APPENDIX C: COORDINATES OF INSTRUMENTATION

All coordinates are for the point physically on the specimen where displacements are being recorded. When a rod length is listed, it is the length of the steel bolt from the face of the specimen to where the string pot is actually attached to the rod. The coordinate system used for all specimens is as follows:

- (0,0,0) is defined as the point where the vertical centerline of the wall on the south end-shell intersects the foundation.
- Negative z-values are to the east of the centerline, positive z-values are to the west of the centerline.
- Positive x-values are to the north, negative to the south.
- Positive y-values are above the foundation.

Strain gage coordinates are not provided, refer to Appendix D for approximate locations. All strain gage locations are approximations due to the constraints of construction. All coordinates are given in inches, conversion to SI units is not provided.

C.1 Specimen PG085-48

Table C-1: Coordinates of string pots on specimen PG085-48

pot #	x (in)	y (in)	z (in)	rod length (in)	Description
1	0	4	3.25	0.75	South end, 1 st CMU course
2	0	12	1	0.625	South end, 2 nd CMU course
3	0	19.75	-3	0.75	South end, 3 rd CMU course
4	104.25	3.875	3	0.5	North end, 1 st CMU course
5	104.25	12	0.75	0.625	North end, 2 nd CMU course
6	104.25	20	-3.25	0.625	North end, 3 rd CMU course
7	121	0.875	0		Sliding, foundation on floor
8	71.75	4.25	3.75	1.125	Sliding, wall on foundation
9	104.25	92	0	0	Top global displacement
10	100.25	3.75	3.75		Diagonal, from north toe
11	3.5	3.75	3.75		Diagonal, from south toe
12	104.25	92	-1.5	0.625	North end, 12 th CMU course
13	0	92.25	-1.25	0.625	South end, 12 th CMU course
14	77	12.375	3.75	1	West face, 2 nd CMU course
15	57.5	11.75	3.75	0.5	West face, 2 nd CMU course
16	47.25	12	3.75	0.5	West face, 2 nd CMU course
17	28	11.625	3.75	0.75	West face, 2 nd CMU course
10b	0	86.875	0	1.75	Anchor for diagonal from north toe
11b	104.25	86.875	0	1.625	Anchor for diagonal from south toe

C.2 Specimen PG120-48

Table C-2: Coordinates of string pots on specimen PG120-48

pot #	x (in)	y (in)	z (in)	rod length (in)	Description
1	0	4.5	1	0.875	South end, 1 st CMU course
2	0	12.5	2.875	0.875	South end, 2 nd CMU course
3	0	20.5	-3	1	South end, 3 rd CMU course
4	104.25	4	0.75	1.25	North end, 1 st CMU course
5	104.25	12.5	3	1	North end, 2 nd CMU course
6	104.25	20.125	-2.75	0.875	North end, 3 rd CMU course
7	119.5	0	0		Sliding, foundation on floor
8	71.5	4.25	3.75	0.875	Sliding, wall on foundation
9	104.25	92.5	0	0	Top global displacement
10	100.75	4.25	3.75		Diagonal, from north toe
11	4	4.25	3.75		Diagonal, from south toe
12	104.25	92.5	-1	0.75	North end, 12 th CMU course
13	0	92	-1	1	South end, 12 th CMU course
14	76.25	12.25	3.75	1.125	West face, 2 nd CMU course
15	57.5	12.25	3.75	0.875	West face, 2 nd CMU course
16	46.75	12.125	3.75	1	West face, 2 nd CMU course
17	28.25	12.25	3.75	0.875	West face, 2 nd CMU course
10b	0	86.5	3.75		Anchor for diagonal from north toe
11b	104.25	87	3.75		Anchor for diagonal from south toe

C.3 Specimen PG169-48

Table C-3: Coordinates of string pots on specimen PG169-48

pot #	x (in)	y (in)	z (in)	rod length (in)	Description
1	0	4	1.25	1.125	South end, 1 st CMU course
2	0	12.25	0.75	1.125	South end, 2 nd CMU course
3	0	20	-3.25	1.25	South end, 3 rd CMU course
4	103.5	4.125	1	1.125	North end, 1 st CMU course
5	103.5	12.5	3	1.25	North end, 2 nd CMU course
6	103.5	20.25	-2.75	1.25	North end, 3 rd CMU course
7	118.75	0	0		Sliding, foundation on floor
8	69.625	4.25	3.75	1.5	Sliding, wall on foundation
9	103.5	93	0	0	Top global displacement
10	100.25	3.875	3.75		Diagonal, from north toe
11	3.5	4.25	3.75		Diagonal, from south toe
12	103.5	92.75	-1	0.75	North end, 12 th CMU course
13	0	96.5	-1.25	1.25	South end, 12 th CMU course
14	76	12.5	3.75	1	West face, 2 nd CMU course
15	57.25	12.5	3.75	1.375	West face, 2 nd CMU course
16	46.25	12.25	3.75	1.125	West face, 2 nd CMU course
17	27.5	12.25	3.75	0.875	West face, 2 nd CMU course
10b	0	82	3.75		Anchor for diagonal from north toe
11b	103.5	87	3.75		Anchor for diagonal from south toe

C.4 Specimen PG085-32

Table C-4: Coordinates of string pots on specimen PG085-32

pot #	x (in)	y (in)	z (in)	rod length (in)	Description
1	0	4	1.25	1.125	South end, 1 st CMU course
2	0	12	2.75	1.375	South end, 2 nd CMU course
3	0	20	-3	1.25	South end, 3 rd CMU course
4	104.25	4.25	1.25	1.125	North end, 1 st CMU course
5	104.25	12.25	2.875	1.5	North end, 2 nd CMU course
6	104.25	20.375	-3.25	1.375	North end, 3 rd CMU course
7	120	0	0		Sliding, foundation on floor
8	57.5	4.5	3.75	1.25	Sliding, wall on foundation
9	104.25	92.875	0	0	Top global displacement
10	100.5	4	3.75		Diagonal, from north toe
11	3.5	3.5	3.75		Diagonal, from south toe
12	104.25	92.875	-1.125	1.5	North end, 12 th CMU course
13	0	92.125	-1.25	1.375	South end, 12 th CMU course
18	87	12.125	3.75	1.375	West face, 2 nd CMU course
19	73	12.25	3.75	1.25	West face, 2 nd CMU course
20	63.25	12.125	3.75	1.125	West face, 2 nd CMU course
21	41	12	3.75	1.375	West face, 2 nd CMU course
22	30.75	12	3.75	1.375	West face, 2 nd CMU course
23	16.75	12.125	3.75	1	West face, 2 nd CMU course
10b	0	86.125	3.75		Anchor for diagonal from north toe
11b	104.25	86.75	3.75		Anchor for diagonal from south toe

C.5 Specimen PG085-24

Table C-5: Coordinates of string pots on specimen PG085-24

pot #	x (in)	y (in)	z (in)	rod length (in)	Description
1	0	4.125	1	1.125	South end, 1 st CMU course
2	x	x	x	x	South end, 2 nd CMU course
3	0	20.5	-3	1.375	South end, 3 rd CMU course
4	104	4.125	1.25	1	North end, 1 st CMU course
5	x	x	x	x	North end, 2 nd CMU course
6	104	20.25	-3	1.25	North end, 3 rd CMU course
7	120.5	0	0		Sliding, foundation on floor
8	73	4.375	3.75	1.25	Sliding, wall on foundation
9	104	92.875	0	0	Top global displacement
10	100.25	3.625	3.75		Diagonal, from north toe
11	3.5	4	3.75		Diagonal, from south toe
12	104	92.875	-1	1.375	North end, 12 th CMU course
13	0	92.25	-0.75	1.25	South end, 12 th CMU course
15	57.25	12.25	3.75	1.125	West face, 2 nd CMU course
16	47.75	12	3.75	1.25	West face, 2 nd CMU course
24	89.5	12.125	3.75	1.125	West face, 2 nd CMU course
25	81.25	12.25	3.75	1.25	West face, 2 nd CMU course
26	x	x	x	x	West face, 2 nd CMU course
27	x	x	x	x	West face, 2 nd CMU course
28	23.25	12	3.75	1.375	West face, 2 nd CMU course
29	14.75	11.875	3.75	1.125	West face, 2 nd CMU course
10b	0	86.5	3.75		Anchor for diagonal from north toe
11b	104	86.375	3.75		Anchor for diagonal from south toe

C.6 Specimen FG085-00

Table C-6: Coordinates of string pots on specimen FG085-00

pot #	x (in)	y (in)	z (in)	rod length (in)	Description
1	0	4	1.25	1	South end, 1 st CMU course
2	0	12	2.5	1.125	South end, 2 nd CMU course
3	0	20.375	-3	1.25	South end, 3 rd CMU course
4	103.75	4	1	1.125	North end, 1 st CMU course
5	103.75	12	2.5	0.875	North end, 2 nd CMU course
6	103.75	20	-3	1.5	North end, 3 rd CMU course
7	119.25	1	0		Sliding, foundation on floor
8	70.75	4.5	3.75	1.125	Sliding, wall on foundation
9	103.75	92.5	0	0	Top global displacement
10	99.75	4.375	3.75		Diagonal, from north toe
11	3.75	3.625	3.75		Diagonal, from south toe
12	103.75	92.75	-1	1.125	North end, 12 th CMU course
13	0	91.75	-1	1.25	South end, 12 th CMU course
14	76	12.375	3.75	1.25	West face, 2 nd CMU course
15	56.875	12.25	3.75	1.125	West face, 2 nd CMU course
16	46.375	12.125	3.75	1.375	West face, 2 nd CMU course
17	27.75	12.125	3.75	1	West face, 2 nd CMU course
10b	103.75	86.75	3.75		Anchor for diagonal from north toe
11b	0	86.75	3.75		Anchor for diagonal from south toe

APPENDIX D: INSTRUMENTATION

D.1 Specimens PG085-48, PG120-48, PG169-48, And FG085-00

Specimens PG085-48, PG120-48, PG169-48 and FG085-00 were instrumented in the same pattern (Figure D-1).

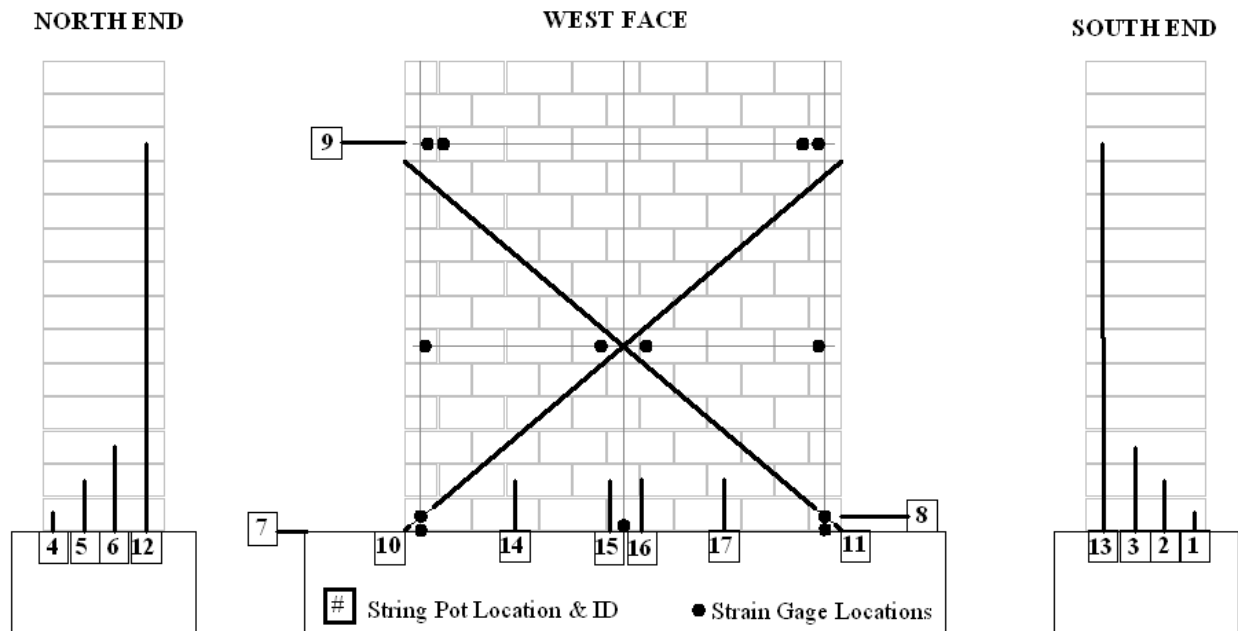


Figure D-1: Location of strain gages and location and identifier for string potentiometers on specimens PG085-48, PG120-48, PG169-48 and FG085-00

D.2 Specimen PG085-32

Specimen PG085-32 was instrumented as shown in Figure D-2.

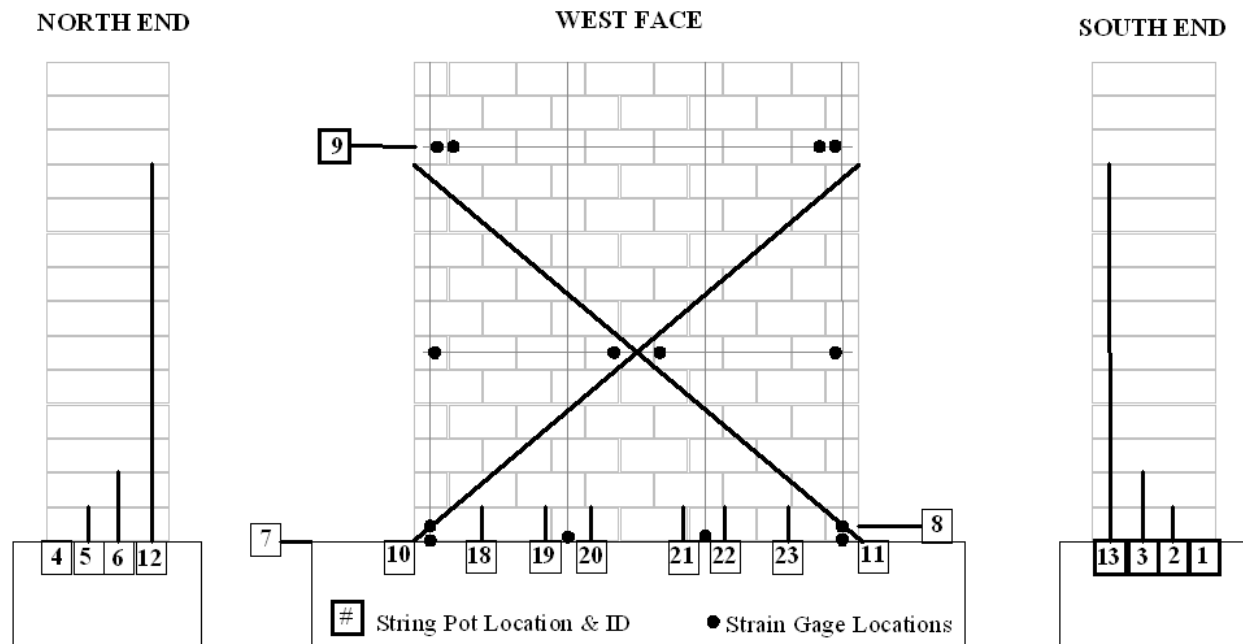


Figure D-2: Location of strain gages and location and identifier for string potentiometers on specimen PG085-32

D.3 Specimen PG085-24

Specimen PG085-24 was instrumented as shown in Figure D-3.

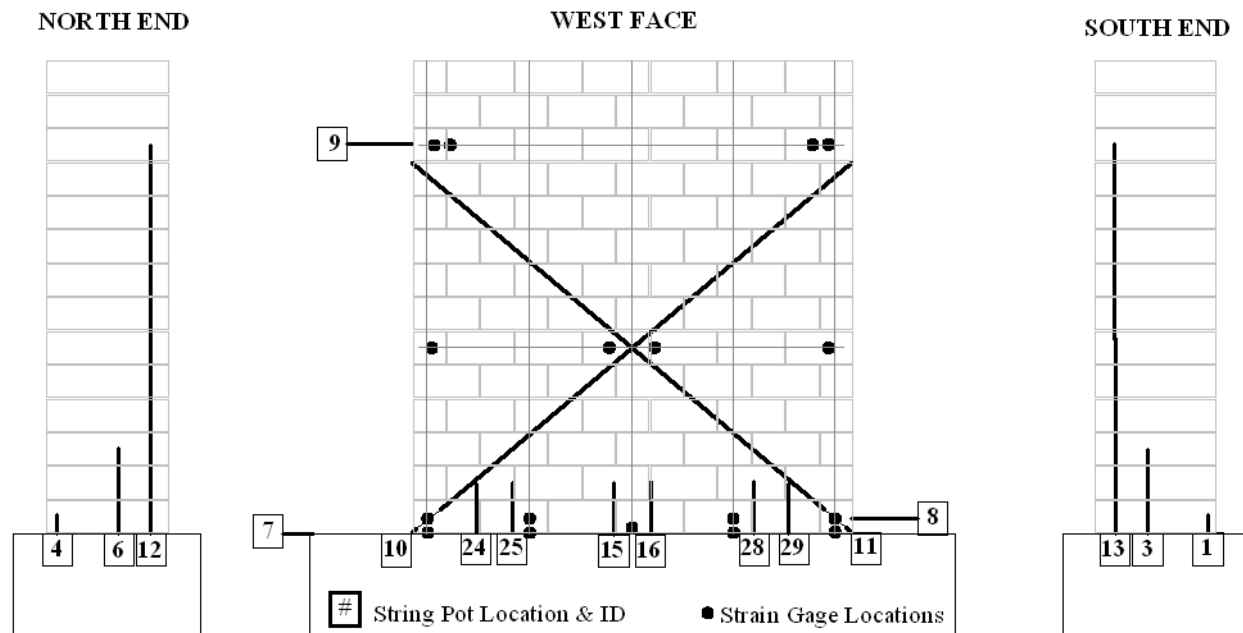


Figure D-3: Location of strain gages and location and identifier for string potentiometers on specimen PG085-24

APPENDIX E: STRAIN GAGE HYSTERETICS

E.1 Introduction

Strain gage hysteretics are presented in this appendix for each test sample. Hysteretics are presented in the same sequence, i.e. south to north / bottom to top, for all specimens with gages on flexural reinforcement presented first followed by gages on shear reinforcement. The location of the strain gage is indicated by the figure on each hysteretic graph.

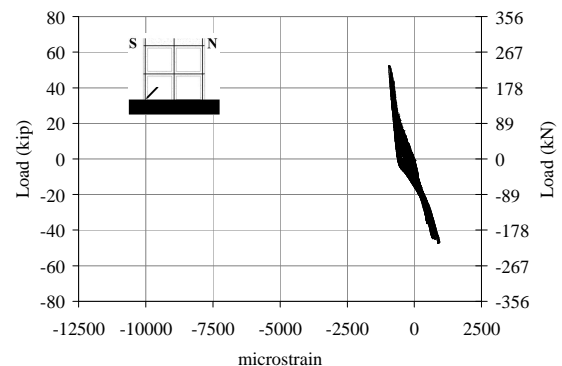
For specimens with a 48 in. (1219 mm) spacing between vertical reinforcement (PG085-48, PG120-48, PG169-48, FG085-00), the locations and numbers of strain gages at each location are identical. To aid comparisons, *the strain gages are presented in the same order for these specimens* with the remark of "no data" in place of a figure when the relevant strain gage failed. Failed gages for the remaining specimens (PG085-32, PG085-24) will be noted in the accompanying text.

Strain gages that did not reach yield strain do not have a yield strain line on the figure. Gages that closely approached or exceeded yield strain have a yield strain line presented.

E.2 Specimen PG085-48

NO
DATA

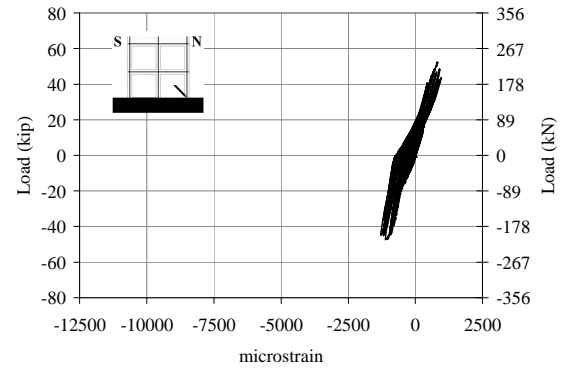
(a)



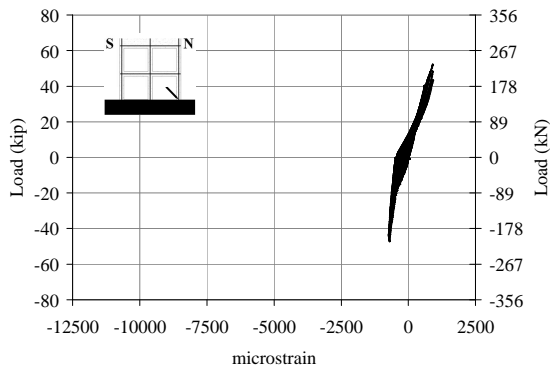
(b)

NO
DATA

(c)



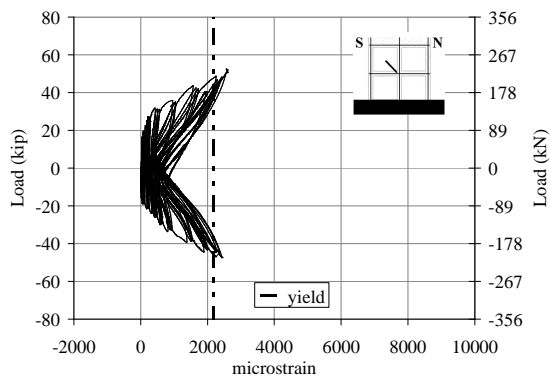
(d)



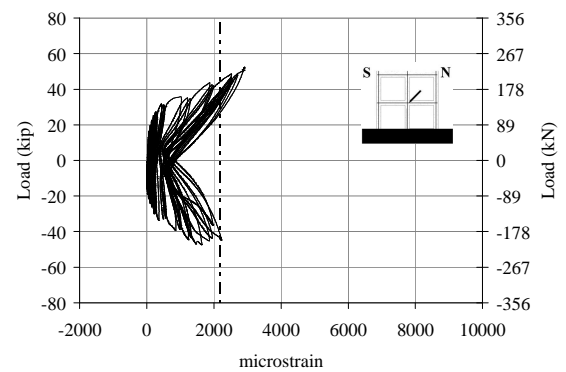
(e)

NO
DATA

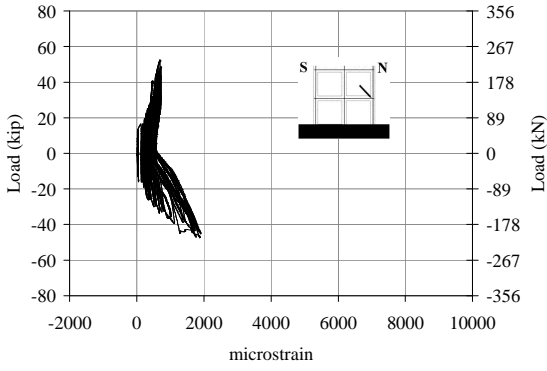
(f)



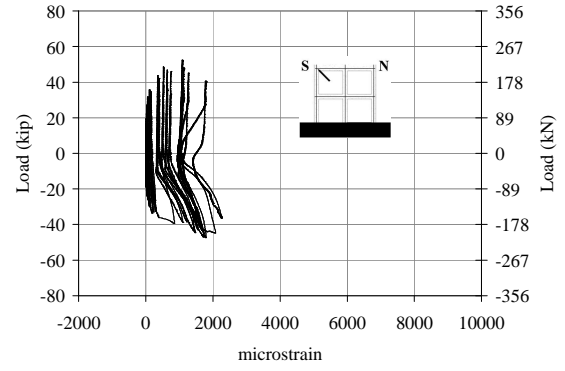
(g)



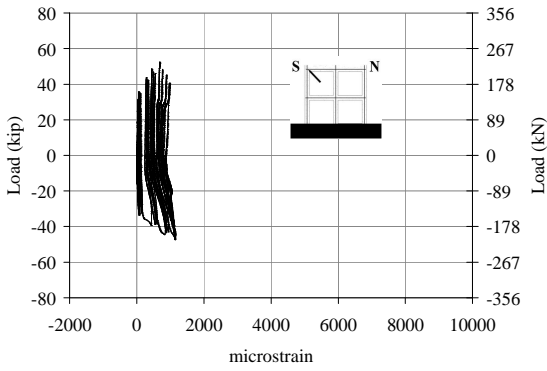
(h)



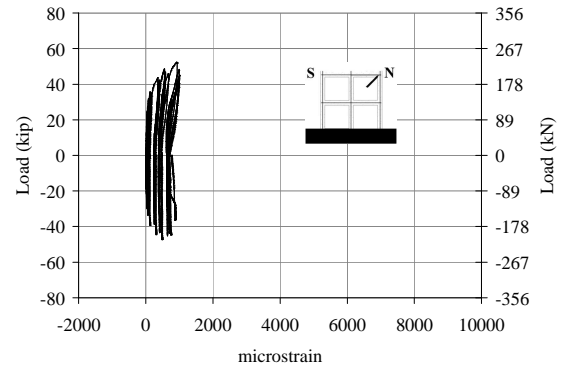
(i)



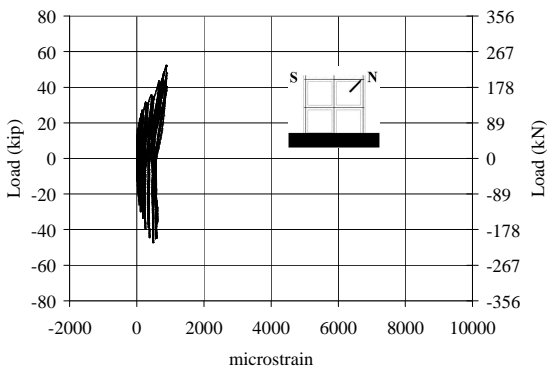
(j)



(k)



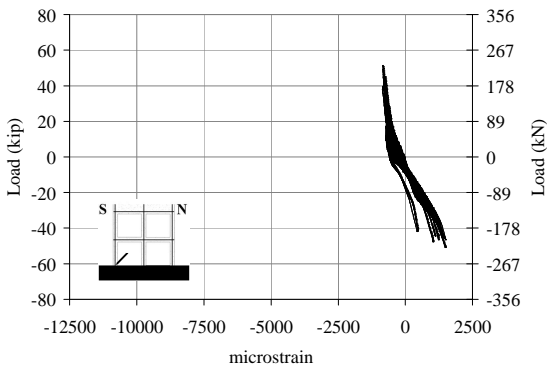
(l)



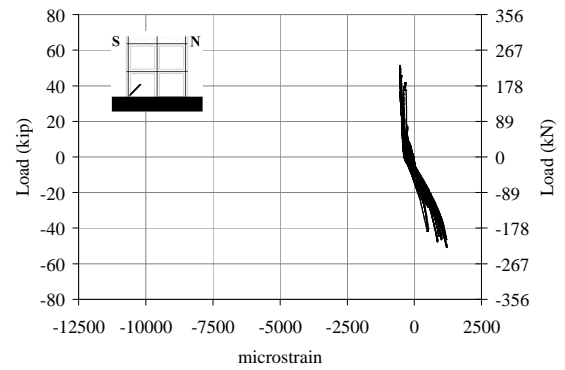
(m)

Figure E-1: Strain gage hysteretics for PG085-48

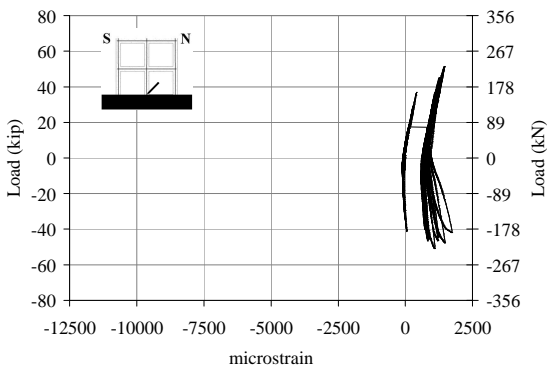
E.3 Specimen PG120-48



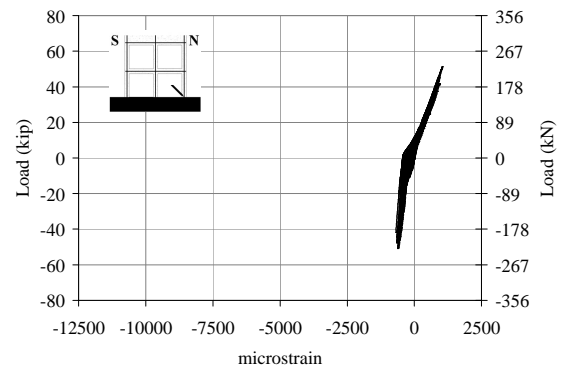
(a)



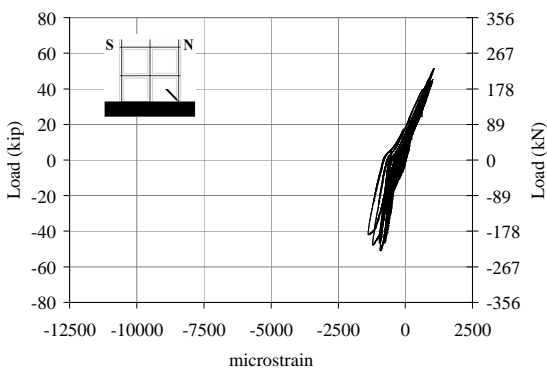
(b)



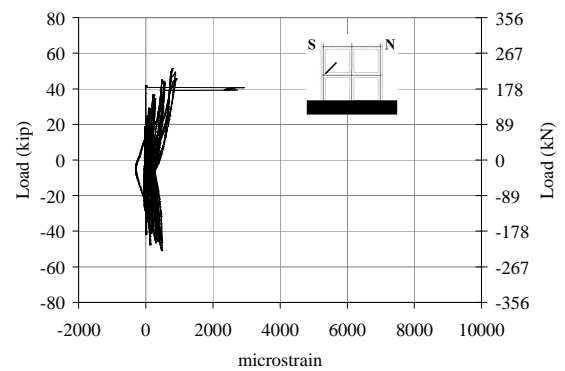
(c)



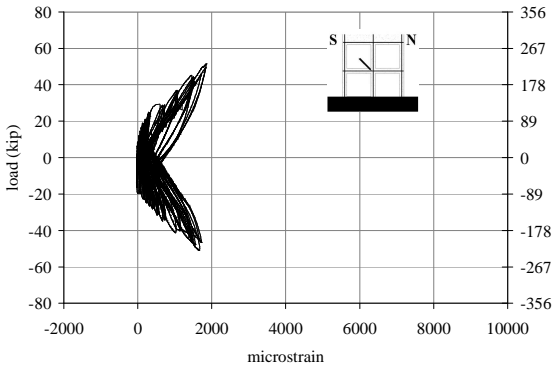
(d)



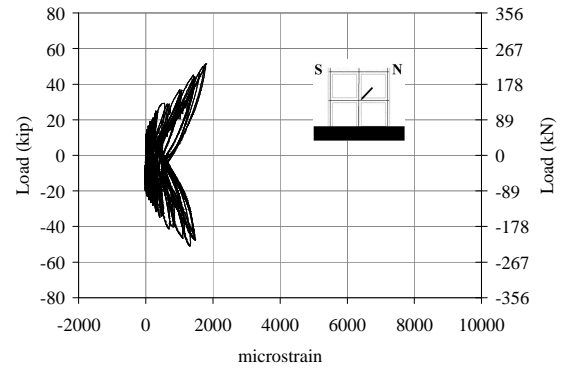
(e)



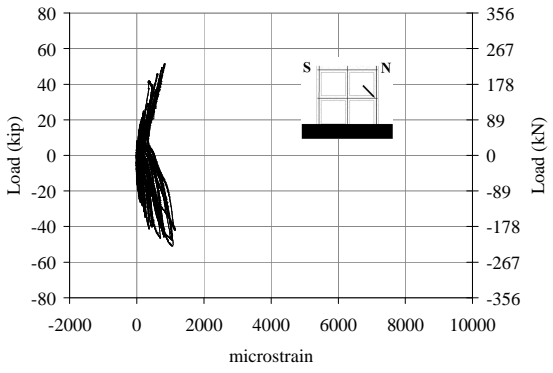
(f)



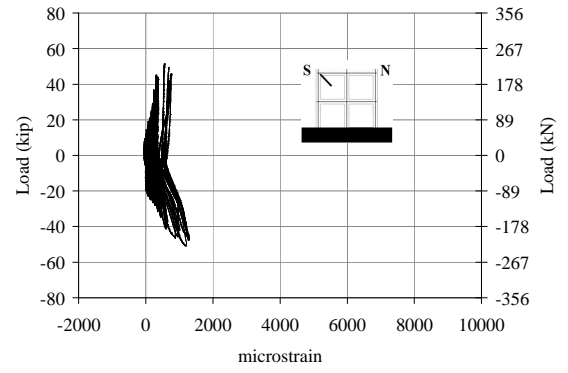
(g)



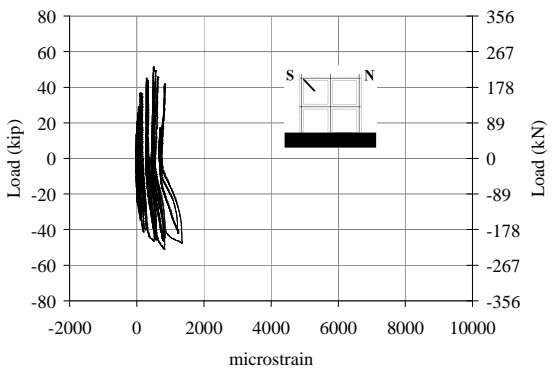
(h)



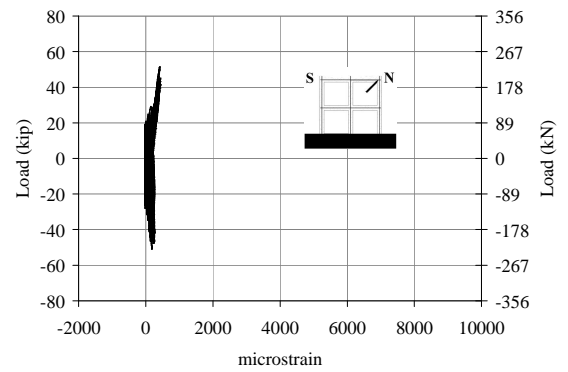
(i)



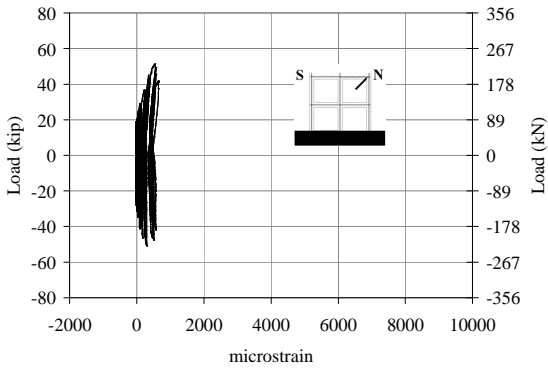
(j)



(k)



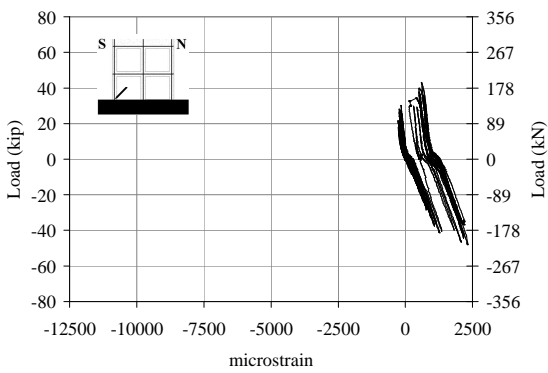
(l)



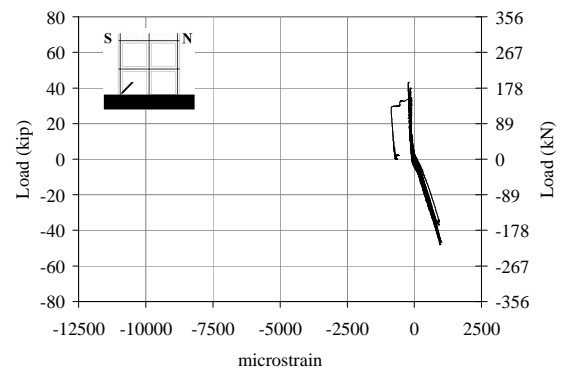
(m)

Figure E-2: Strain gage hysteretics for PG120-48

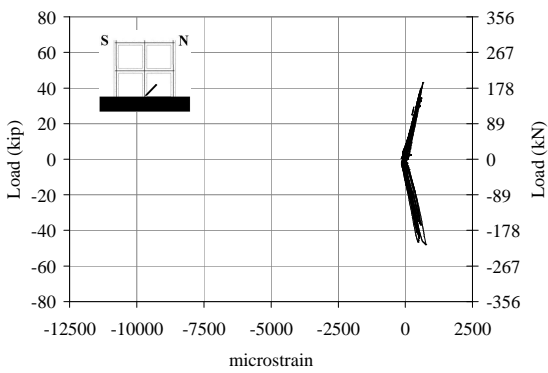
E.4 Specimen PG169-48



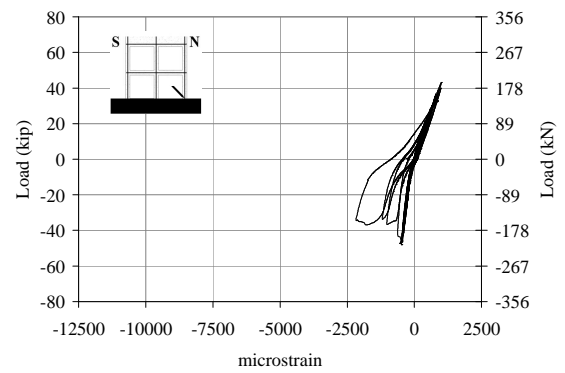
(a)



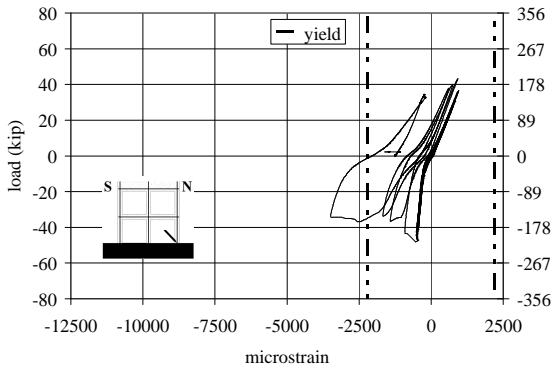
(b)



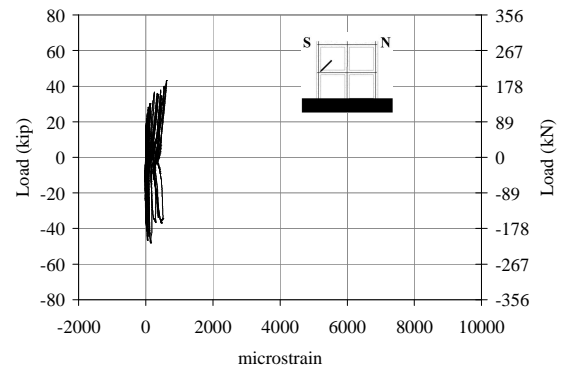
(c)



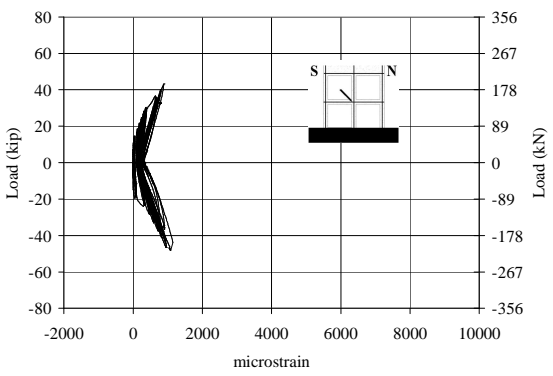
(d)



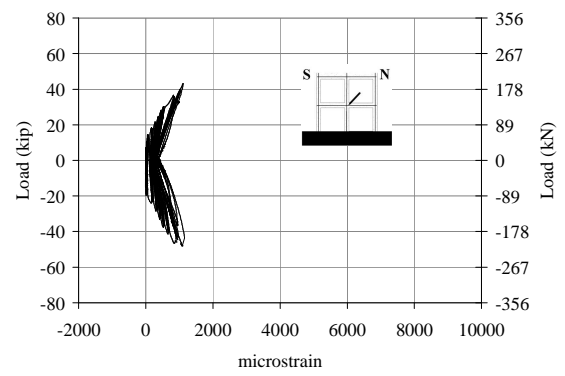
(e)



(f)



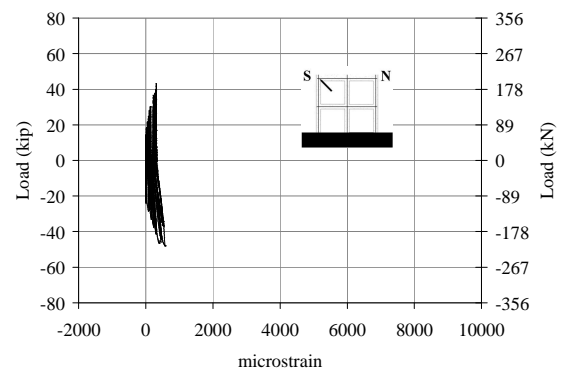
(g)



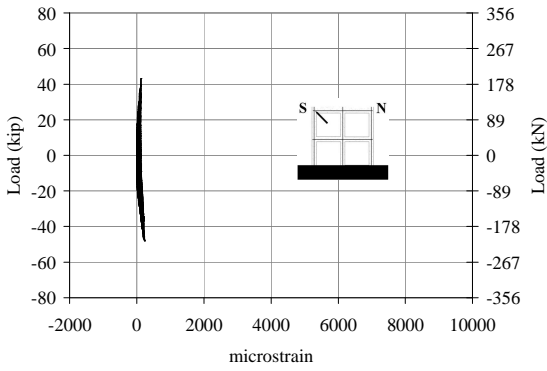
(h)

NO
DATA

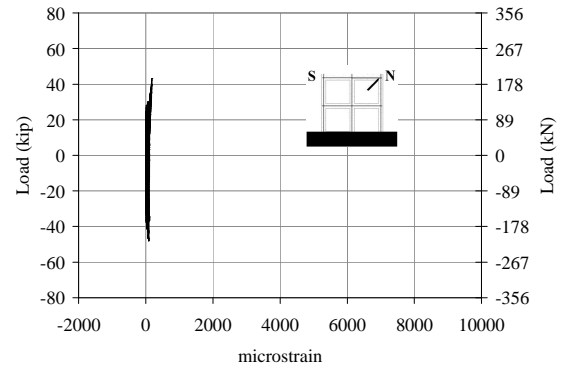
(i)



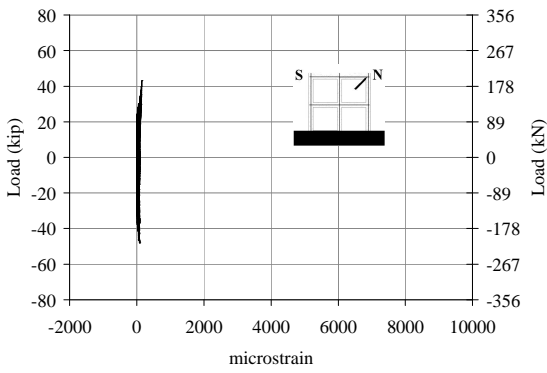
(j)



(k)



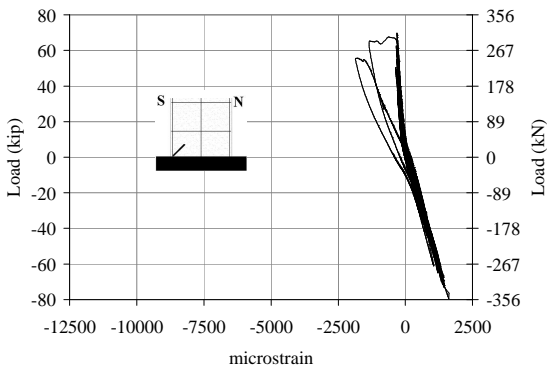
(l)



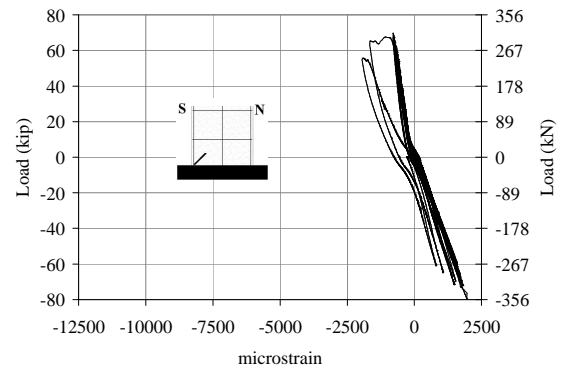
(m)

Figure E-3: Strain gage hysteretics for PG169-48

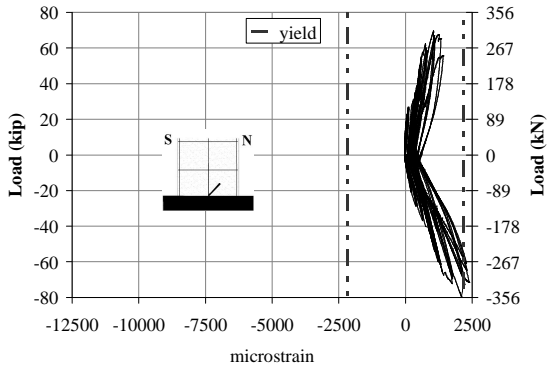
E.5 Specimen FG085-00



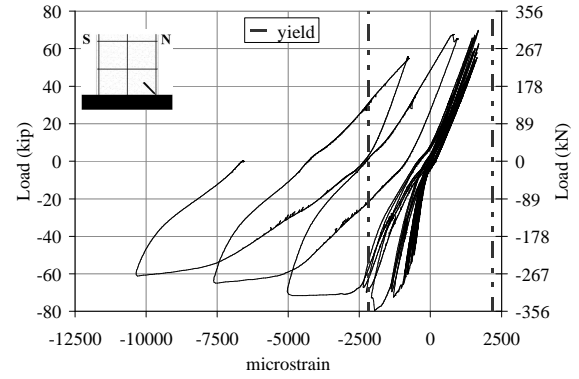
(a)



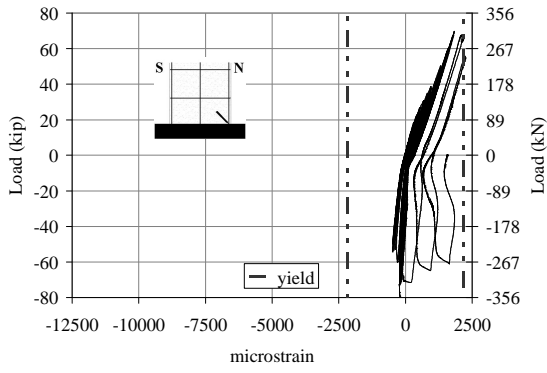
(b)



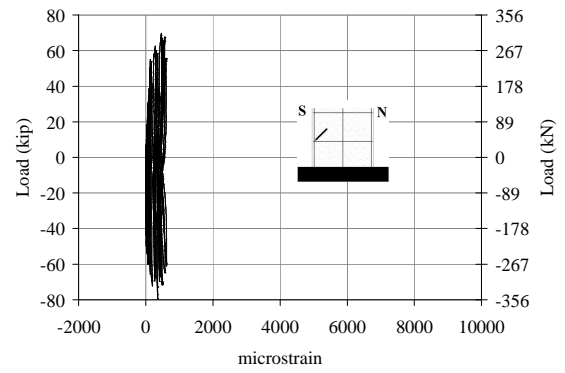
(c)



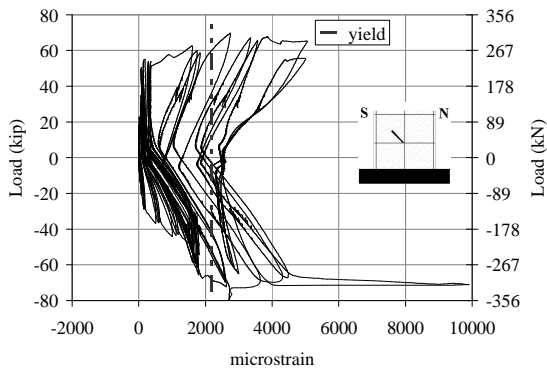
(d)



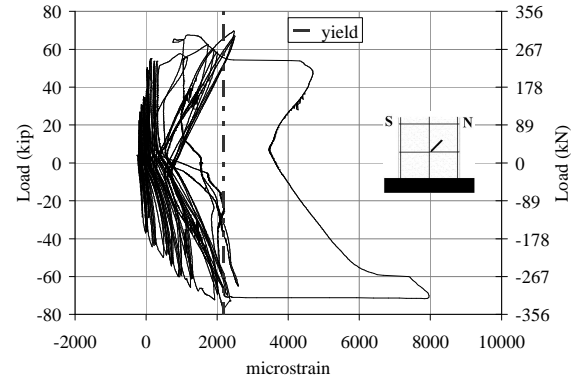
(e)



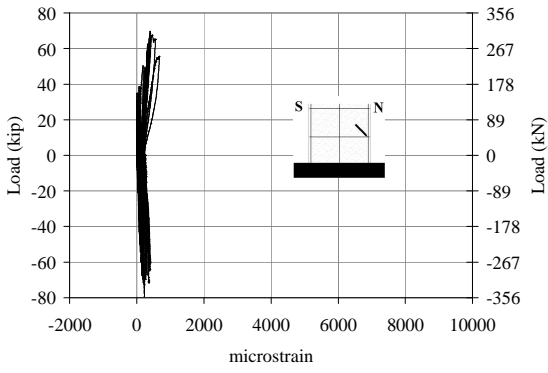
(f)



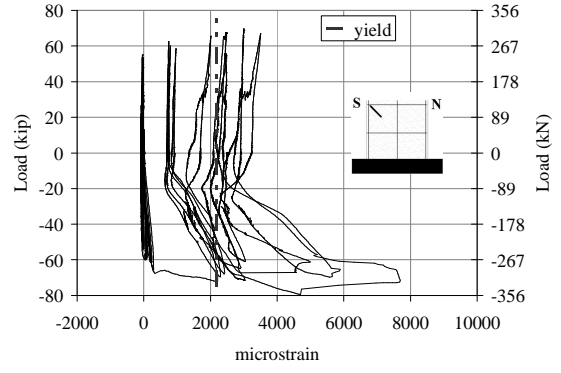
(g)



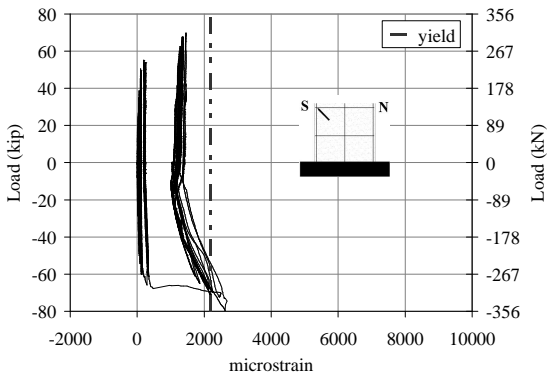
(h)



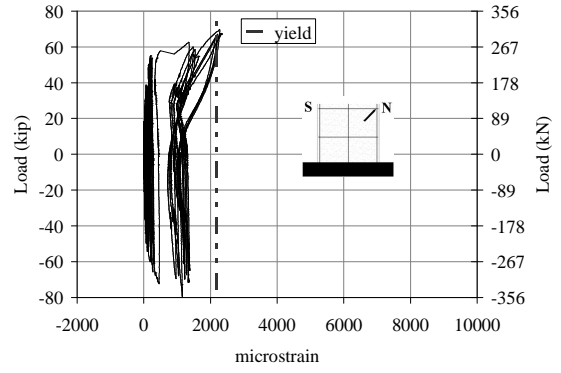
(i)



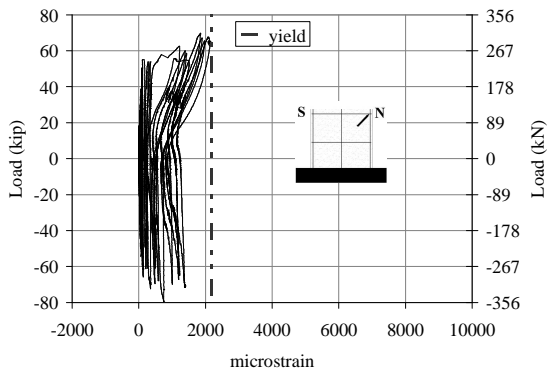
(j)



(k)



(l)

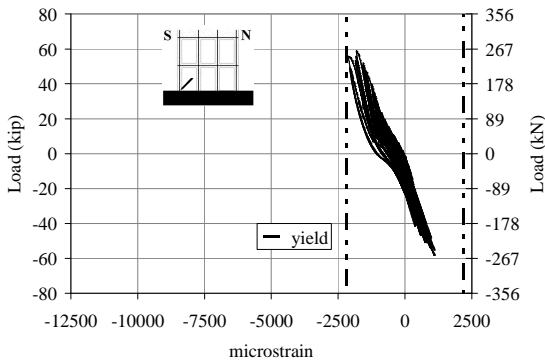


(m)

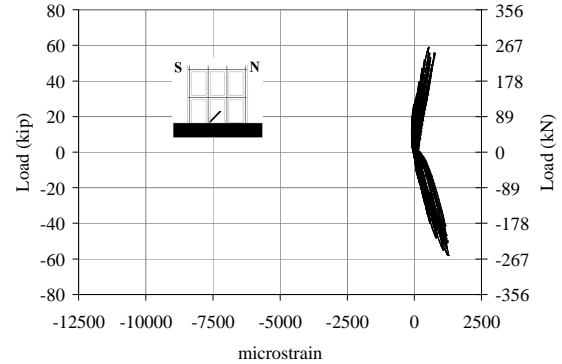
Figure E-4: Strain gage hysteretics for FG085-00

E.6 Specimen PG085-32

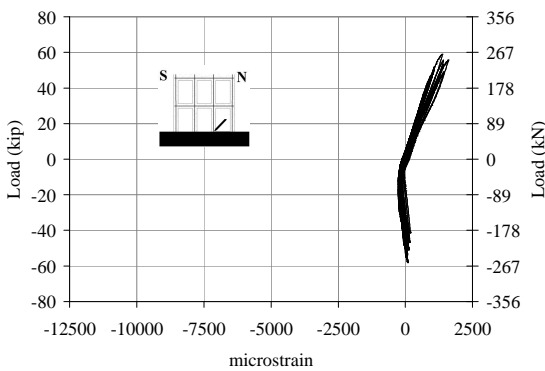
The following strain gages failed for this specimen: south flexural #1, north flexural #2, north mid-wall shear.



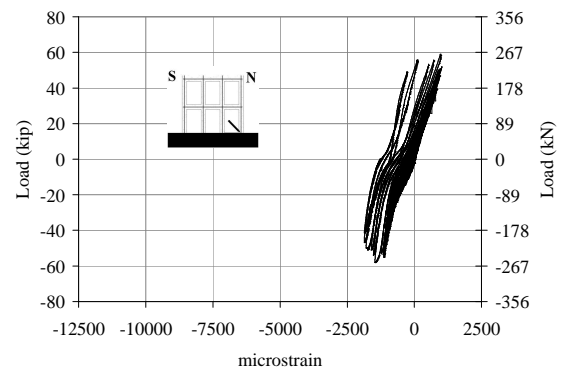
(a)



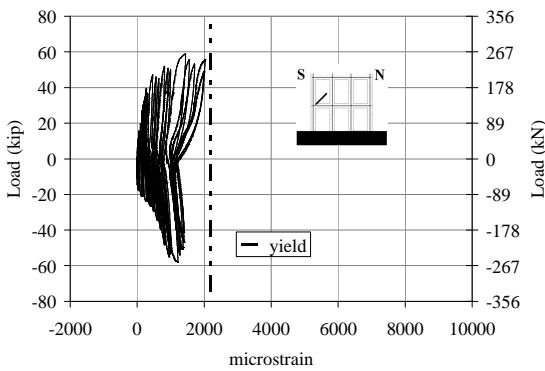
(b)



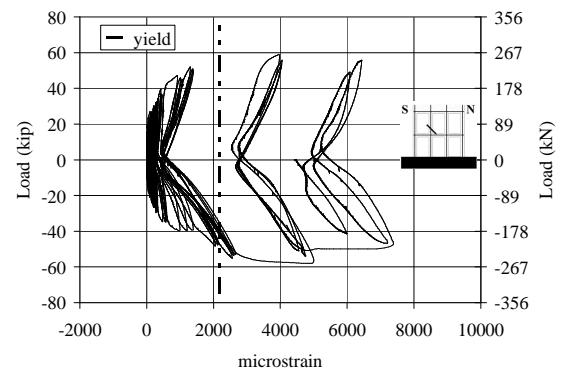
(c)



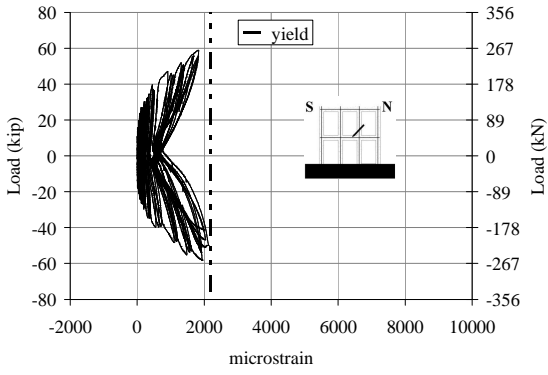
(d)



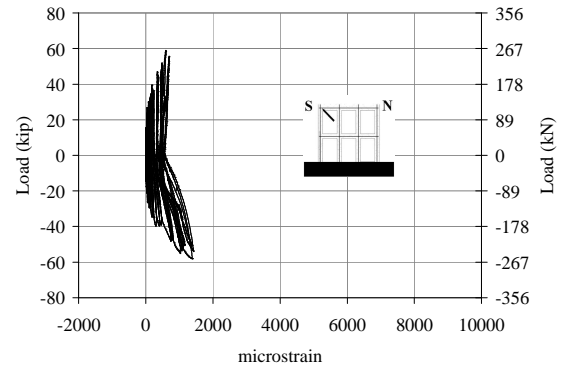
(e)



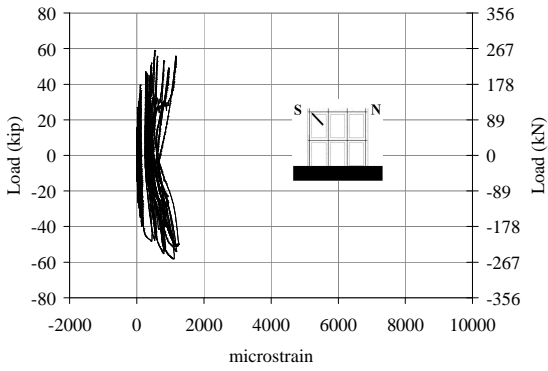
(f)



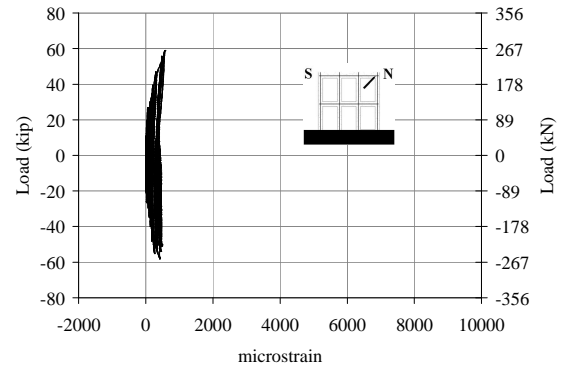
(g)



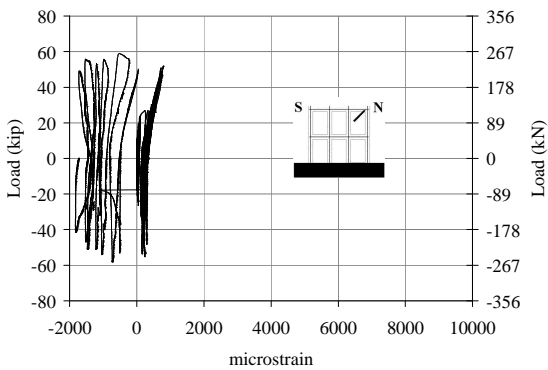
(h)



(i)



(j)

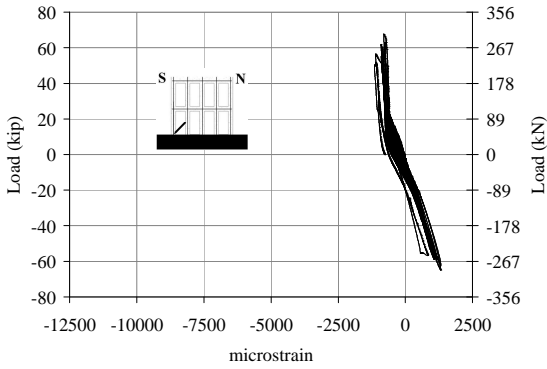


(k)

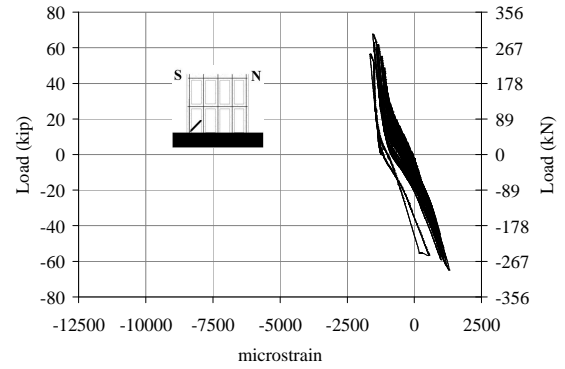
Figure E-5: Strain gage hysteretics for PG085-32

E.7 Specimen PG085-24

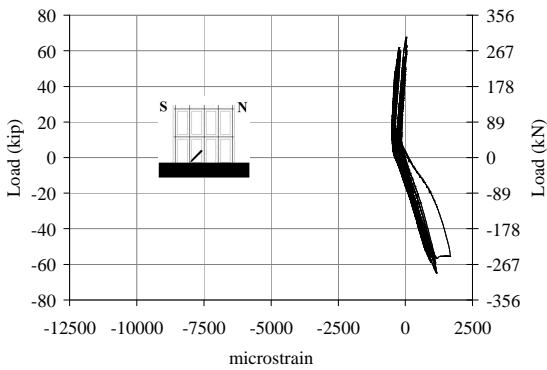
The following strain gages failed for this specimen: north flexural #1.



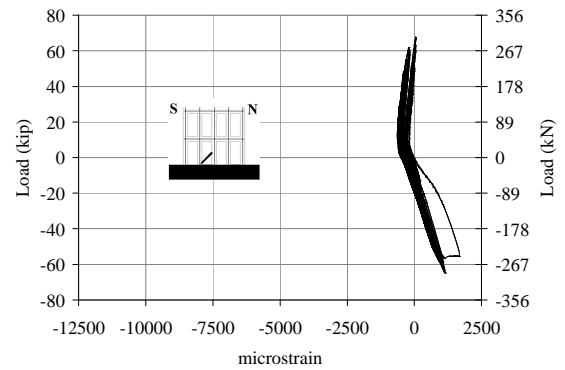
(a)



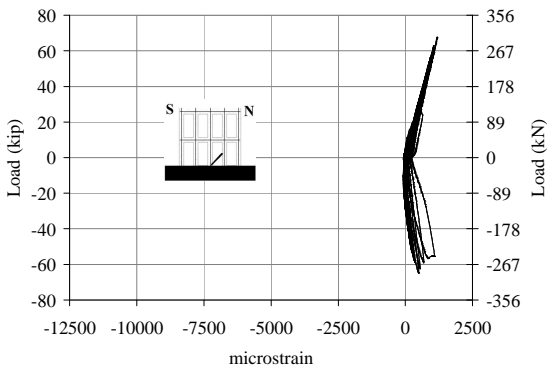
(b)



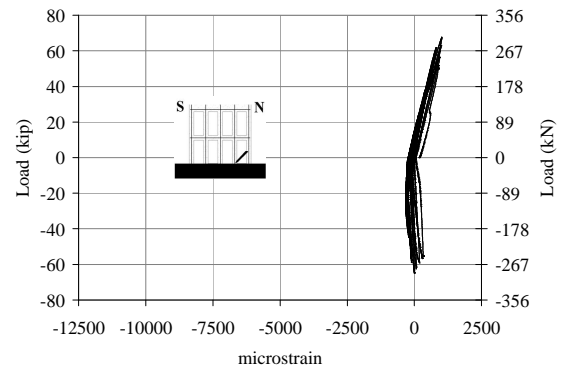
(c)



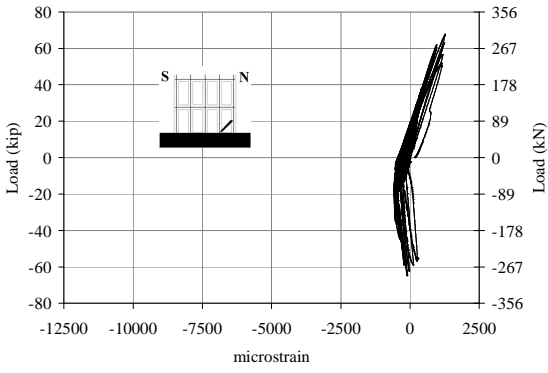
(d)



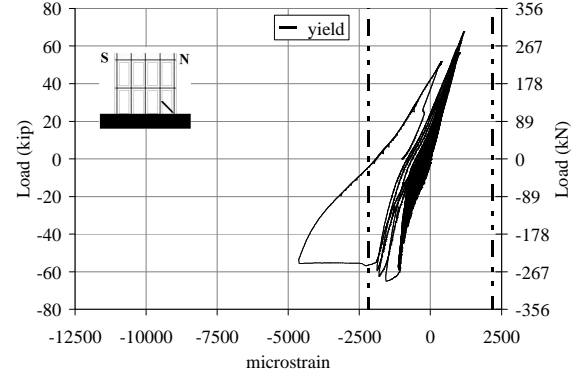
(e)



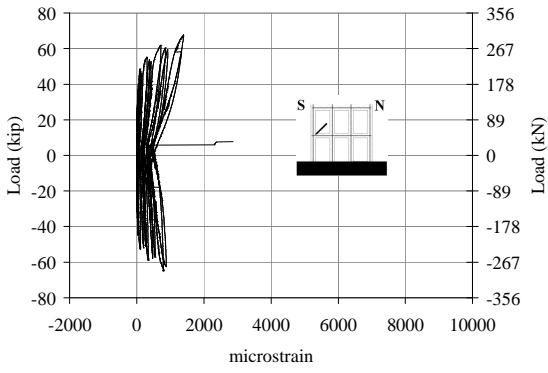
(f)



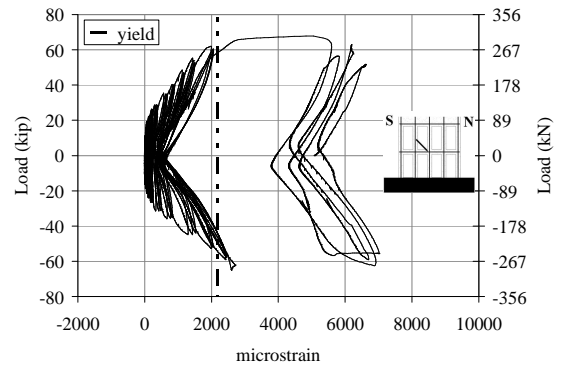
(g)



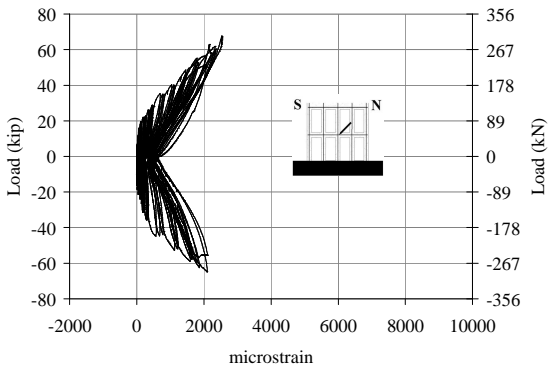
(h)



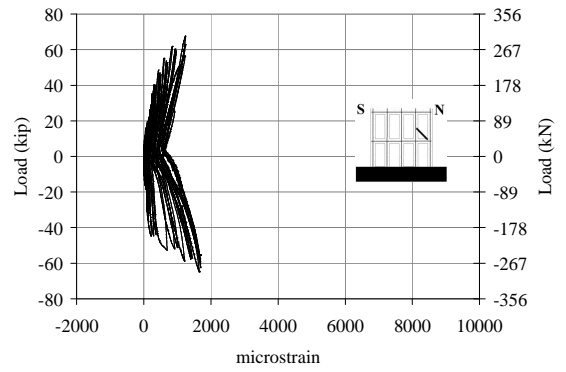
(i)



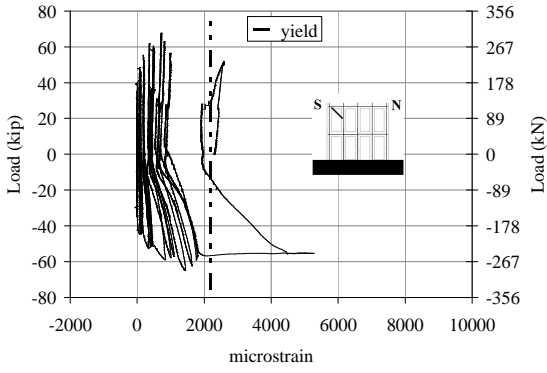
(j)



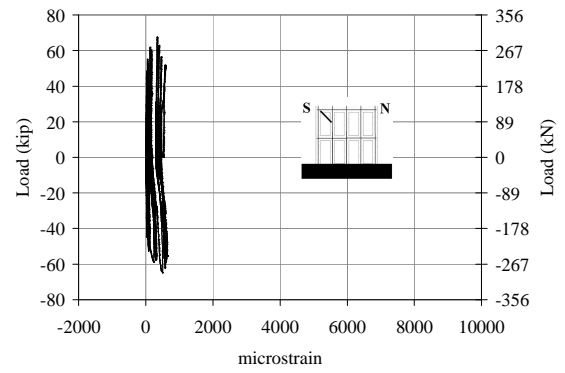
(k)



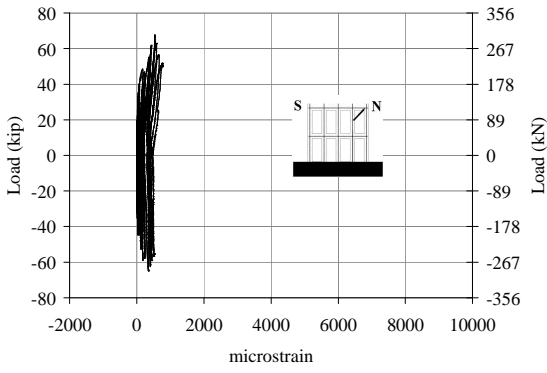
(l)



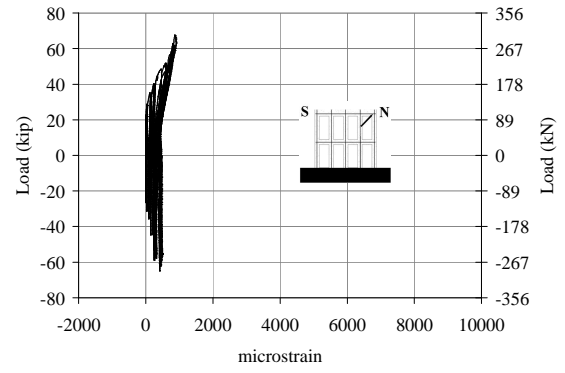
(m)



(n)



(o)

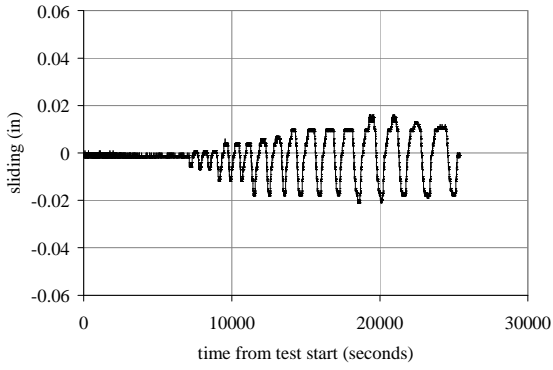


(p)

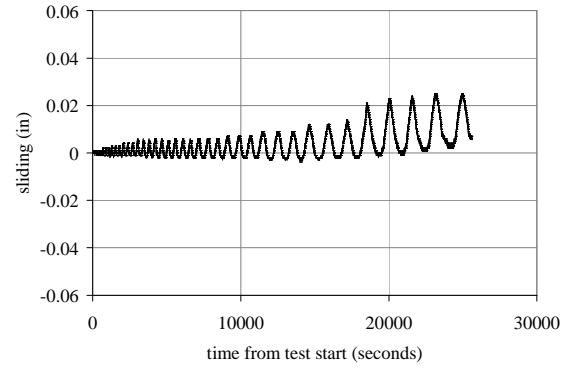
Figure E-6: Strain gage hysteretics for PG085-24

APPENDIX F: FOUNDATION SLIDING ON REACTION FLOOR

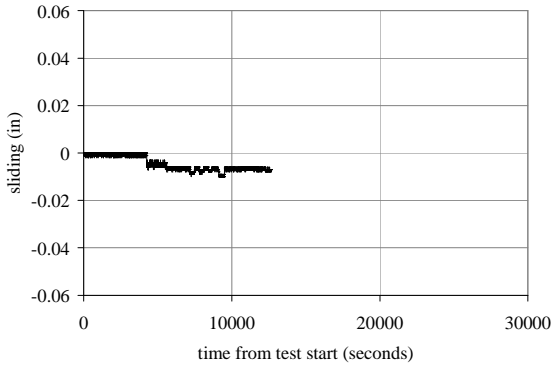
Sliding of the foundation on the reaction floor was minimal for all specimens. Typical values were on the order of 0.02 in. (0.51 mm). Specimen PG085-24 was the exception with 0.05 in. (1.3 mm) to the north. The string potentiometer for Specimen PG085-32 recorded sliding as high as 6 in. (152 mm), which is clearly not possible, and is therefore assumed to have failed for the entirety of the test. Figure F-1 shows the sliding over the duration of the test for all specimens.



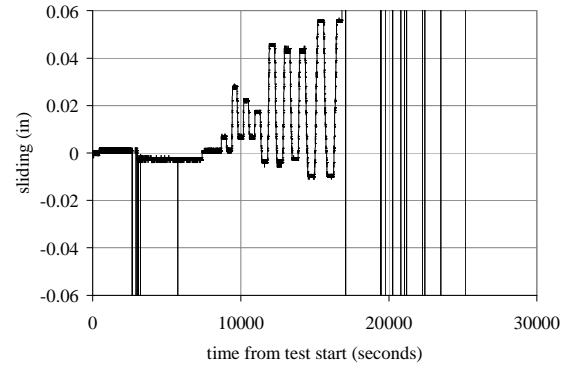
(a)



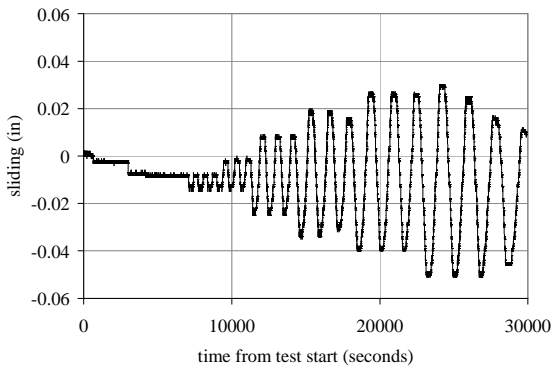
(b)



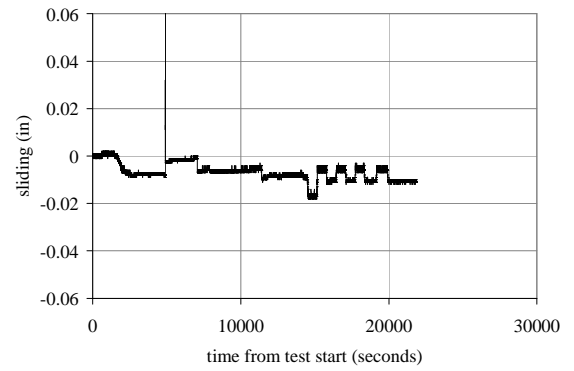
(c)



(d)



(e)



(f)

Figure F-1: Sliding of the foundation on the reaction floor as the test progresses, specimen (a) PG085-48, (b) PG120-48, (c) PG169-48, (d) PG085-32, (e) PG085-24, and (f) FG085-00.